AD-A068 470 NAVAL RESEARCH LAB WASHINGTON D C F/G 20/7
NRL INERTIAL CONFINEMENT FUSION THEORY PROGRAM 1978 ANNUAL REPO--ETC(U)
FEB 79

UNCLASSIFIED NRL-MR-3944 SBIE-AD-E000 293 NL

1 OF 2
AD
A068470

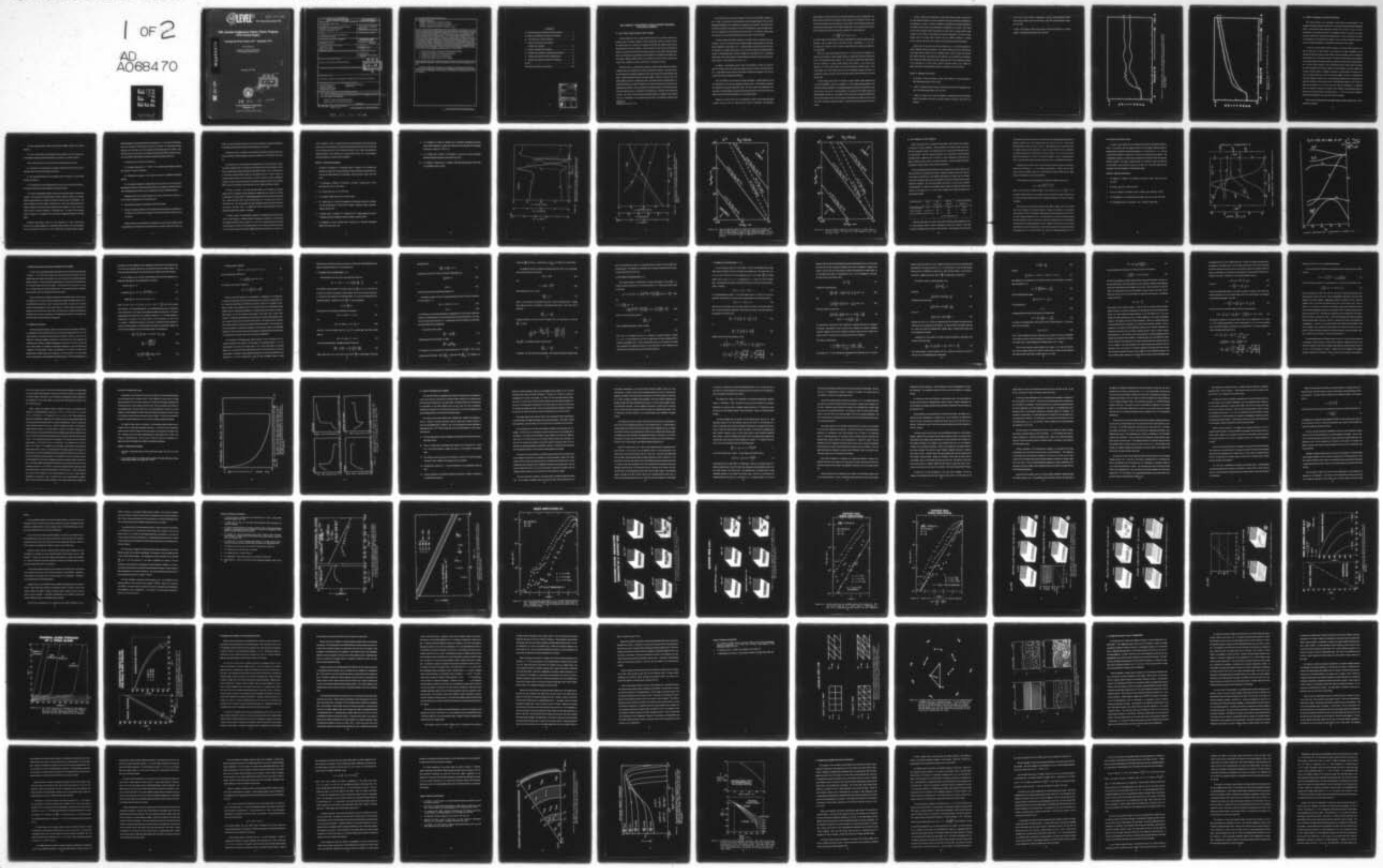

⑫ LEVEL III

Nu

ADE 000 293

NRL Memorandum Report 3944

NRL Inertial Confinement Fusion Theory Program 1978 Annual Report

Covering the Period October 1977 - September 1978

Work Performed by:

Laboratory for Computational Physics
and the Plasma Physics Division

February 26, 1979

NAVAL RESEARCH LABORATORY
Washington, D.C.

REPORT DOCUMENTATION PAGE

READ INSTRUCTIONS BEFORE COMPLETING FORM

1. REPORT NUMBER NRL Memorandum Report 3944	2. GOVT ACCESSION NO.
	3. RECIPIENT'S CATALOG NUMBER
4. TITLE (and Subtitle) NRL INERTIAL CONFINEMENT FUSION THEORY PROGRAM 1978 ANNUAL REPORT October 1977–September 1978	5. TYPE OF REPORT & PERIOD COVERED Interim report on a continuing NRL problem. 6. PERFORMING ORG. REPORT NUMBER
7. AUTHOR(s) The Laboratory for Computational Physics and The Plasma Physics Division	8. CONTRACT OR GRANT NUMBER(s)
9. PERFORMING ORGANIZATION NAME AND ADDRESS Naval Research Laboratory Washington, DC 20375	10. PROGRAM ELEMENT, PROJECT, TASK AREA & WORK UNIT NUMBERS NRL Problem 77H02-58 DOE Project No. NP-01-05-01; NP-02-01
11. CONTROLLING OFFICE NAME AND ADDRESS Department of Energy Office of Laser Fusion Washington, DC 20545	12. REPORT DATE February 26, 1979 13. NUMBER OF PAGES 110
14. MONITORING AGENCY NAME & ADDRESS(if different from Controlling Office)	15. SECURITY CLASS. (of this report) UNCLASSIFIED 15a. DECLASSIFICATION/DOWNGRADING SCHEDULE

16. DISTRIBUTION STATEMENT (of this Report)

Approved for public release; distribution unlimited.

DDC
RECEIVED
MAY 11 1979
B

17. DISTRIBUTION STATEMENT (of the abstract entered in Block 20, if different from Report)

18. SUPPLEMENTARY NOTES

This work was sponsored by the Department of Energy, Project No. NP-01-05-01; NP-02-01

19. KEY WORDS (Continue on reverse side if necessary and identify by block number)

Heavy Ion Beam Transport	Computational Fluid Dynamics
Ion Beam Channelling	Ablation Theory
Inertial Confinement Fusion	
Rayleigh–Taylor Instability	

20. ABSTRACT (Continue on reverse side if necessary and identify by block number)

This ~~is the 1978~~ annual report of the NRL Inertial Confinement Fusion Theory Program e ~~It~~ covers research performed ~~from October 1977 through September 1978. Research~~ in each of the following five current program areas ~~is reported~~.

Section A) Transport of Charged Particle Beams;

Section B) Laser and Particle Beam Absorption;

(Continued)

DD FORM 1 JAN 73 1473 EDITION OF 1 NOV 65 IS OBSOLETE
S/N 0102-LF-014-6601

79 03 15 046

20. ABSTRACT (Continued)

~~Section~~(C) Fluid Dynamics and Ablative Acceleration,
Section(D) Development of Computational Techniques; and
~~Section~~(E) Rayleigh-Taylor Stabilization Techniques.

Our work on the transport of charged particle beams has concentrated on two problems: (A1) determining computationally the emittance growth due to plasma effects from space charge forces in heavy ion beam transport through a quadrupole focussing lens system and (A2) ion beam transport and stability in preprepared plasma channels. In Section B we report our work on the absorption of laser light in the plasma blow off at material surfaces. The role of non-resonant absorption due to ion acoustic fluctuations has been studied in the presence of magnetic fields. The thrust of our work on fluid dynamics, laser ablative acceleration, ion deposition and computational techniques is focussed on the scoping and subsequent quantitative analysis of Rayleigh-Taylor instability problems and closely allied asymmetry problems. The occurrence or potential occurrence of growing R-T modes in pellet implosion is nearly universal. Nevertheless, four rather distinct environments can be identified where the operative physics and hence the required computational tools benefit from independent analysis. The organization of the remaining four sections of the annual report highlights these distinct environments. Each of these four segments combines elements of C, D and E above.

C. Ablation Layer Structure and Analysis of Rayleigh-Taylor Instability.
D. Rayleigh-Taylor Instability at Internal Material Interfaces.
E. Instability and Symmetry Issues in Colliding Shells.
F. Rayleigh-Taylor Stability and Central Core Dynamics.

Each of these four aspects differs enough from the others to make treating them separately worthwhile. The Rayleigh-Taylor Instability is an ideal unifying theme for much of the research which has to be done.

The report concludes with a small section on our plans for the extension and continuation of this research and an NRL Inertial Confinement Fusion bibliography encompassing recent contributions to ICF theory and understanding. Footnotes, figures, and references for each section below are compiled separately.

CONTENTS

NRL INERTIAL CONFINEMENT FUSION THEORY PROGRAM
1978 ANNUAL REPORT

A1. Space Charge Limited Transport of Heavy Ion Beams

Current proposals for heavy in beam ignited inertial fusion are attractive because they generally require only modest extensions of current technology. However, the ability to focus the required power onto a small spot at a distance from the final lens requires a beam not only with high power but also low emittance. It has been known for some time from the observed behavior in proton linacs and from the theoretical analysis of beam stability that high phase space current densities are accompanied by space-charge driven instabilities and possible emittance growth. Because emittance growth in turn limits the spot size to which a beam can be focused, these instabilities can create a major barrier to the ignition of a pellet.

When the current in a particle beam is pushed up towards its space-charge limit, collective oscillations that can be supported by the beam are plasma-like in behavior. This means that all the non-linearities and attendant complexities of the Vlasov equation can become important and render a detailed theoretical treatment extremely complex. Because the beam is only a few Debye lengths across and is transported for only a few plasma periods the detailed behavior is particularly amenable to computer simulation by the particle techniques well developed in the plasma physics community. Since the beams will be long compared to their transverse dimensions, the transverse behavior is simulated in two dimensions in a reference frame moving with the beam. The orbits of several thousand rod-shaped particles are followed as these particles move in the combination of lens focusing forces and their self-consistently calculated space charge forces.

Manuscript submitted January 4, 1979

Initial calculations have been done assuming a thin lens, alternate gradient transport system. In order to make contact with existing theory and the ongoing program at LBL, an initial Kapchinskij-Vladimirskij (K-V) distribution was assumed for the particles. The lens force are simulated by applying to each particle a ΔVx and ΔVy proportional to the lens strength and to the x and y displacement of each particle from the beam axis. In the absence of space charge this numerical system reproduces the idealized thin lens system to within roundoff.

To ensure accurate and reliable simulations, an extensive series of numerical tests were performed. A test case was chosen to be an alternate gradient transport system with 90° phase advance depressed by space charge to 30°. A numerical regime was identified where the results are insensitive to variations over factors of two in time step, numbers of simulation particles, number of computational grids, boundary condition and macroparticle size[1]. By extending these results, and by further testing, it was determined that simulation could accurately be performed down to a time depression of at least (7.5°.)

In addition, a comprehensive series of tests[2] was performed to examine the long term growth in emittance due to the smaller than physical number of particles in the simulation system. A major effect was seen only when the number of particles was decreased to far below the number which could be economically employed.

With the reliability of the numerical techniques established, a detailed parametric study was undertaken of a 90° thin lens quadrupole transport system. Good qualitative agreement was obtained with theoretical calculations at LBL. One case[3], with the tune depressed to 45°, was subject to detailed analysis and quantitative agreement obtained with the LBL theory with respect to growth rates and the detailed form of the unstable behavior.

Figure A1.1 is a plot of the x and y rms emittances of a beam, with enough space charge to depress the tune to 30°, as it evolves from the initial K-V equilibrium. The behavior is characterized by an initial constancy of the emittance followed by a period of rapid growth. The growth rapidly saturates and the emittance is then constant for the duration of the run. This saturation and steady state is also observed in other moments of the distribution function and the system does indeed appear to have reached a steady state. For any given equilibrium distribution, Maschke and Courant[4] have derived a scaling law for transportable power

$$P = C \left[\frac{A}{Z}\right]^{4/3} B_q^{2/3} \epsilon^{2/3} (\beta\gamma)^{7/3} (\gamma - 1) \qquad (1)$$

By using the figure of merit defined by Laslett and degrading it for emittance growth and beam spreading, it can be argued[5] that the case shown in Fig. 1 corresponds to $C = 1.2 \times 10^{15}$. This steady state, therefore turns out to yield a transportable power consistent with pellet ignition requirements.

When the current being transported results in a much greater tune depression, the behavior of the emittance evolution changes. Figure A1.2 shows the evolution in emittance for a tune of 90° depressed by space charge to 7.5°. The period of constancy and rapid growth in this case is followed by a period of slower growth in the emittance. A case with the tune depressed to 15° shows similar behavior but the long term growth is somewhat slower. These results suggest that a space charge limit does exist for quadrupole transport, and when it is exceeded the emittance will grow until the phase space density has been reduced to below this limiting value.

How this limiting value varies as a function of various transport system parameters has not yet been established. However, a simulation of a 130° transport system depressed to 50° verified the predicted instability in the envelope equations and showed a rapid growth in emittance by about a factor of five. This lends support to the assertion[6] that transport systems with advances greater than 90° are to be avoided. In fact recent work by Lasslett and Smith[6] indicate that 60° transport systems hold the promise of transporting even greater currents than the 90° systems. Preliminary simulations appear to support this conclusion at least for K-V distributions.

In order to determine the dependence of space-charge limited transport on the form of the initial distribution function, a series of simulations have been performed with different initial distributions. In order to overcome the difficulty of establishing self consistent equilibria in the presence of space charge, these distributions are established at low currents. The currents are then slowly increased so that the distribution can adjust itself in a manner similar to what would occur in the center of a beam being slowly bunched longitudinally. The form of the distribution does in fact effect both the growth rates and instability thresholds. In general however, behavior worse than the K-V results has not been observed in these simulations.

Progress thus far has shown that particle simulations are a very promising approach to reliably modelling intense beam behavior. The results summarized here have indicated that space charge collective effects can have a significant effect on beam transport and focusing. Since system economics, performance and even feasibility can be influenced by these effects, and the numerical model employed can easily incorporate many of the complications important to the performance of an actual system, computer simulation appears to be a highly cost effective approach in making intelligent decisions in the design of future experiments.

Section A1. References and Footnotes

1. Irving Haber, "Computer Simulation of Space Charge Effects in Particle Accelerators," NRL Memorandum Report 3705, Jan 1978.

2. I. Haber, "Collisional Emittance Growth in the Particle Simulation of Focused Beam Transport." NRL Memorandum Report 3817, July 1978.

3. I. Haber, L.J. Laslett, and L. Smith, "Comparison of Instability Theory with Simulation Results" Proceedings of the Heavy Ion Fusion Workshop, Argonne Il, Sept 1978, to be published.

4. E.D. Courant, "Power Transport in Quadrupole or Solenoid Focusing Systems", ERDA Summer Study of Heavy Ions for Inertial Fusion, LBL 5543, Lawrence Berkeley Laboratory, Dec 1976.

5. I. Haber, A.W. Maschke, "Steady State Transport of High Current Beams in a Focused Channel," NRL Memorandum Report 3787, May 1978.

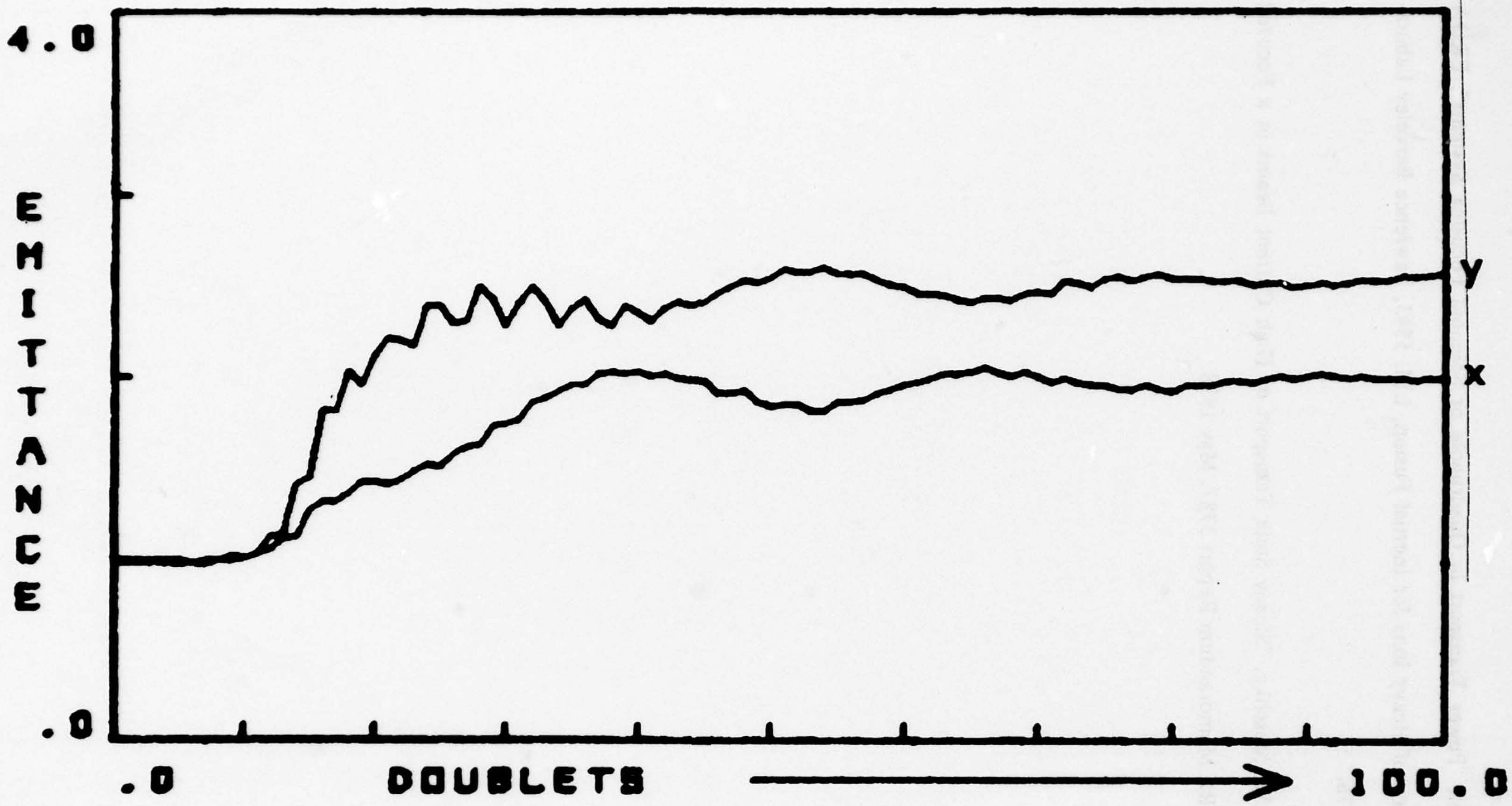

Figure A1.1 Evolution of the x and y rms emittances of an initially matched K-V distribution in a 90° transport system depressed to 30° by space charge.

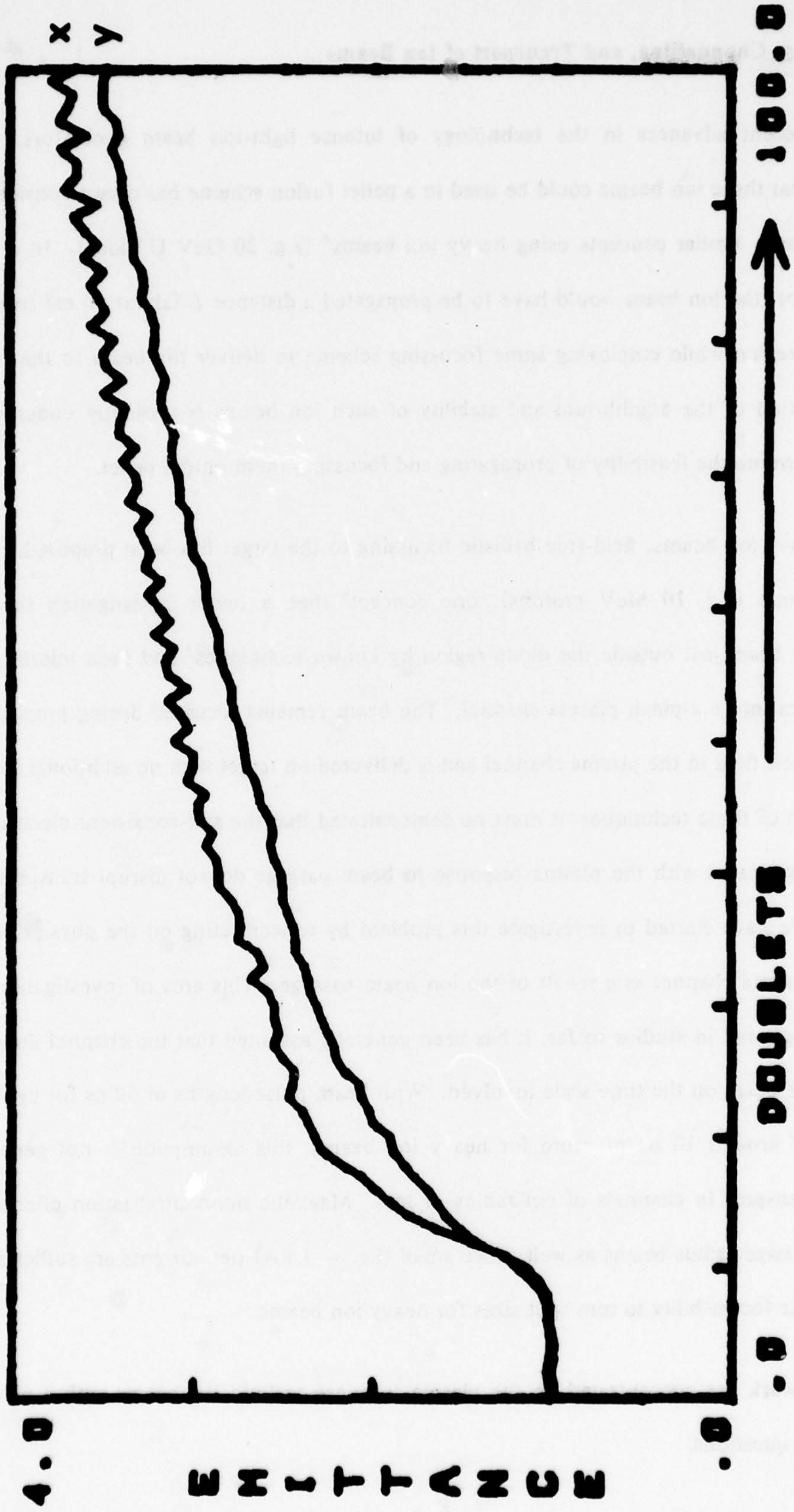

Figure A1.2 Evolution of the x and y rms emittance when the tune is initially depressed to 7.5°

A2. Stability, Channelling, and Transport of Ion Beams

With recent advances in the technology of intense light-ion beam generators,[1,2] the suggestion that these ion beams could be used in a pellet fusion scheme has drawn considerable interest[3] as have similar concepts using heavy ion beams[4] (e.g. 20 GeV U^+ ions). In a functioning reactor, the ion beam would have to be propagated a distance L (about 10 m) from the acceleration region while employing some focussing scheme to deliver the beam to the target. An investigation of the equilibrium and stability of such ion beams is presently underway in order to determine the feasibility of propagating and focussing them onto a pellet.

For heavy ion beams, field-free ballistic focussing to the target has been proposed.[4,5] For light ion beams (e.g. 10 MeV protons), one concept[6] that is under investigation involves focussing the beam just outside the diode region by known techniques[1] and then injecting the focussed beam into a z-pinch plasma channel. The beam remains focussed during propagation by the magnetic field in the plasma channel and is delivered on target with no additional focussing. For both of these techniques, it must be demonstrated that the self-consistent electromagnetic fields associated with the plasma response to beam passage do not disrupt transport and focussing. We have started to investigate this problem by concentrating on the physics occurring in the plasma channel as a result of the ion beam passage. This area of investigation has been largely ignored in studies so far; it has been generally assumed that the channel does not respond to the beam on the time scale involved. With beam pulse lengths of 50 ns for light ion beams and of around 10 ns or more for heavy ion beams, this assumption is not generally correct for transport in channels of cm radius or less. Magnetic nonneutralization effects are important for large radius beams as well, since small (i.e. $\sim$ 1 kA) net currents are sufficient to destroy ballistic focussibility to mm spot sizes for heavy ion beams.

Recent work has concentrated on the plasma response to light-ion beams with a view to answering the questions:

(a) Does a plasma-parameter window exist which allows efficient transport over 10 meter distances?

(b) Do the self-consistent electromagnetic fields associated with beam heating, net current effects and plasma hydrodynamics disrupt beam transport or its ability to bunch?

Some constraints which have to be satisfied by the beam plasma system include:

(a) The density in the hole bored by the applied z-discharge and beam currents must be sufficiently high to permit complete charge-neutralization.

(b) The beam-heated plasma must be sufficiently high in temperature to provide good magnetic neutralization.

(c) The temperature must be sufficiently high to reduce return-current electric fields to a level which neither slows the beam appreciably nor disrupts bunching.

A 1-D radial, time-dependent, Eulerian code has been developed recently to answer these questions. The code solves the plasma moment equations, Maxwell equations, and transport equations using coefficients for electrical and thermal conduction taken from Braginskii.[7] The beam is specified by its current density in space and time. Direct beam energy deposition and radiation cooling as well as return-current heating have been included in the code. Initial conditions consist of a plasma z-discharge in a high-density gas[8]. The density of the discharge channel is typically .01-.1 atmosphere of low-z gas while the background density may be much higher.

Preliminary results appear in Fig. A2.1. They correspond to a 1 MA, 10 MeV proton beam, 0.6 cm in radius propagating in a preformed hydrogen channel of the same dimension with an initial density on the axis of 2×10^{18}. Results shown are radial profiles for density, azimuthal-magnetic and axial-electric fields, and temperature at $t = 40$ ns into the beam pulse. These are the conditions which develop near the tail of the beam. No impurities have been included in this calculation so that only hydrogen bremsstrahlung losses are included. Time histories through any point fixed in the chamber of the maximum B-field, maximum temperature, central electric-field strength and minimum channel density appear in Fig. A2.2.

Conclusions which can be drawn at this point are:

(1) Hydrogen backgrounds of 1-3 × 10^{18}cm^{-3} in the channel allow propagation satisfying all constraints to transport and bunching.

(2) Hydrodynamic expansion at lower densities may result in insufficient neutralizing densities.

(3) Low plasma temperatures at higher densities cause excessive return-current electric field strengths which slow the beam and perturb bunching. Line-radiation cooling from impurities in the background may result in too low temperatures *if present in sufficient densities.*

Phenomena which have not been included in the code yet and which are important to a more complete understanding of the channel physics are:

- Non-equilibrium ionization of the plasma at the head of the beam.
- Values for electrical conductivity at low temperatures which determines the penetration of the B-field into the plasma and the degree of current non-neutralization achieved late on in the pulse.

These phenomena plus comparison with experiments at lower current intensities (with correspondingly lower temperatures and ionization levels), extension of this work to heavy ion beams, and a more consistent treatment of the ion-current distribution in position and time due to self fields and bunching will constitute future developments of this work.

During the past year, an analysis of microinstabilities associated with light and heavy ion beams traversing the plasma-background conditions established by the MHD code was carried out.

The linear growth of two electrostatic microinstabilities, the e-b mode and the e-i mode, have been investigated under the conditions of good charge and current neutralization for both heavy ion beam-plasma systems[9] and light ion beam-plasma systems.[10] The e-b mode is driven by the relative streaming between beam ions and electrons and the e-i mode is driven by streaming between plasma ions and electrons. If either of these two modes is sufficiently unstable to create strong microturbulence, the resulting anomalous resistivity could seriously affect the current neutralization of the beam which, in turn, might disrupt beam transport.

For heavy ion beams,[9] it was found that both modes can be stabilized in parameter regimes which are consistent with the conditions for charge and current neutrality and which are appropriate for a fusion reactor. Typical marginal stability curves for both the e-b mode and the e-i mode are shown in Fig. A2.3 for a 40 GeV beam of U^{+1} ions and in Fig. A2.4 for a 7 GeV beam of Xe^{+1} ions. If occurring at all, these instabilities can grow only when the beam is quite close to the pellet. Thus, it is unlikely that either of these electrostatic modes will significantly degrade beam transport or focussing.

For light ion beams,[6] the high densities required for the background z-pinch plasma provide for a high frequency of collisions between the electrons and plasma ions. This results in the collisional damping of the e-b mode for $T_e \leqslant 50$ eV in a typical system with the z-pinch current flowing on the surface of the plasma channel. If the z-pinch current flows in the interior of the plasma channel, the azimuthal magnetic field further stabilizes the e-b mode ($T_e \leqslant$

1 keV for stability). Since it is expected that the current distribution will be between these extreme forms, and hydrodynamic computer-code calculations demonstrate that the electrons will not be heated above 50 eV, the e-b mode will be stable. The e-i mode is also stabilized by collisional damping. Other generally more slowly growing modes, such as electromagnetic pinching instabilities, are presently under investigation.

Section A2. References and Footnotes

1. D. Mosher, G. Cooperstein, S. J. Stephanakis, Shyke A. Goldstein, D. G. Colombant and Roswell Lee, presented at the 2nd International Topical Conference on High Power Electron and Ion Beam Research and Technology, Cornell University, Ithaca, New York (1977).

2. S. J. Stephanakis, D. Mosher, G. Cooperstein, J. R. Boller, J. Golden and S. A. Goldstein, Phys. Rev. Lett. **37**, 1543 (1976).

3. M. J. Clauser, Phys. Rev. Lett. **34**, 570 (1975).

4. A. W. Maschke, IEEE Trans. Nucl. Sci. **22**, 1825 (1975).

5. R. L. Martin and R. C. Arnold in Proceedings of the Conference on Heavy Ion Acceleration and Storage Rings for Pellet Fusion Reactors, Argonnne National Laboratory, Argonne, Illinois (1976).

6. D. Mosher, Shyke A. Goldstein, P. F. Ottinger and W. W. Hsing, presented at the Topical Meeting on Inertial Confinement Fusion, San Diego, California (1978).

7. S. I. Braginskii, in *Reviews of Plasma Physics,* edited by M. A. Leontovich (Consultants Bureau, New York, 1965) p. 205.

8. S. A. Goldstein, D. P. Bacon, D. Mosher and G. Cooperstein, Proceedings 2nd International Topical Conference on High Power Electron and Ion Research and Technology, Cornell Univ., Ithaca, N.Y. (1977), p.71.

9. P. J. Ottinger and D. Mosher, in Proceedings of the Heavy Ion Fusion Workshop, Brookhaven National Laboratory, Upton, New York (1977).

10. P. F. Ottinger, D. Mosher and S. A. Goldstein, NRL Memorandum Report 3784 (1978); to be published in Phys. of Fluids.

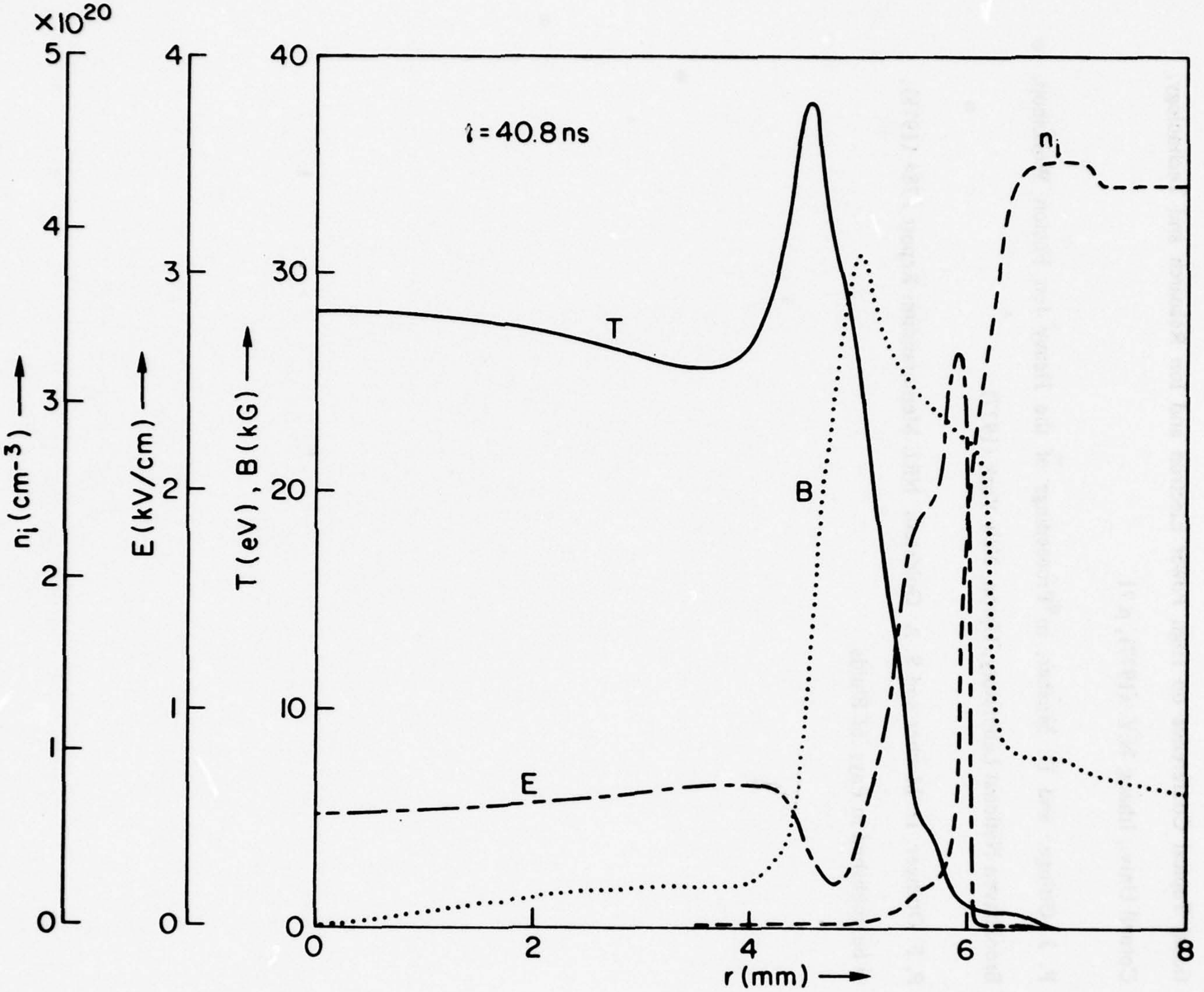

Figure A2.1. Radial profiles of density, azimuthal magnetic field, axial electric field, and temperature at $t = 40$ ns.

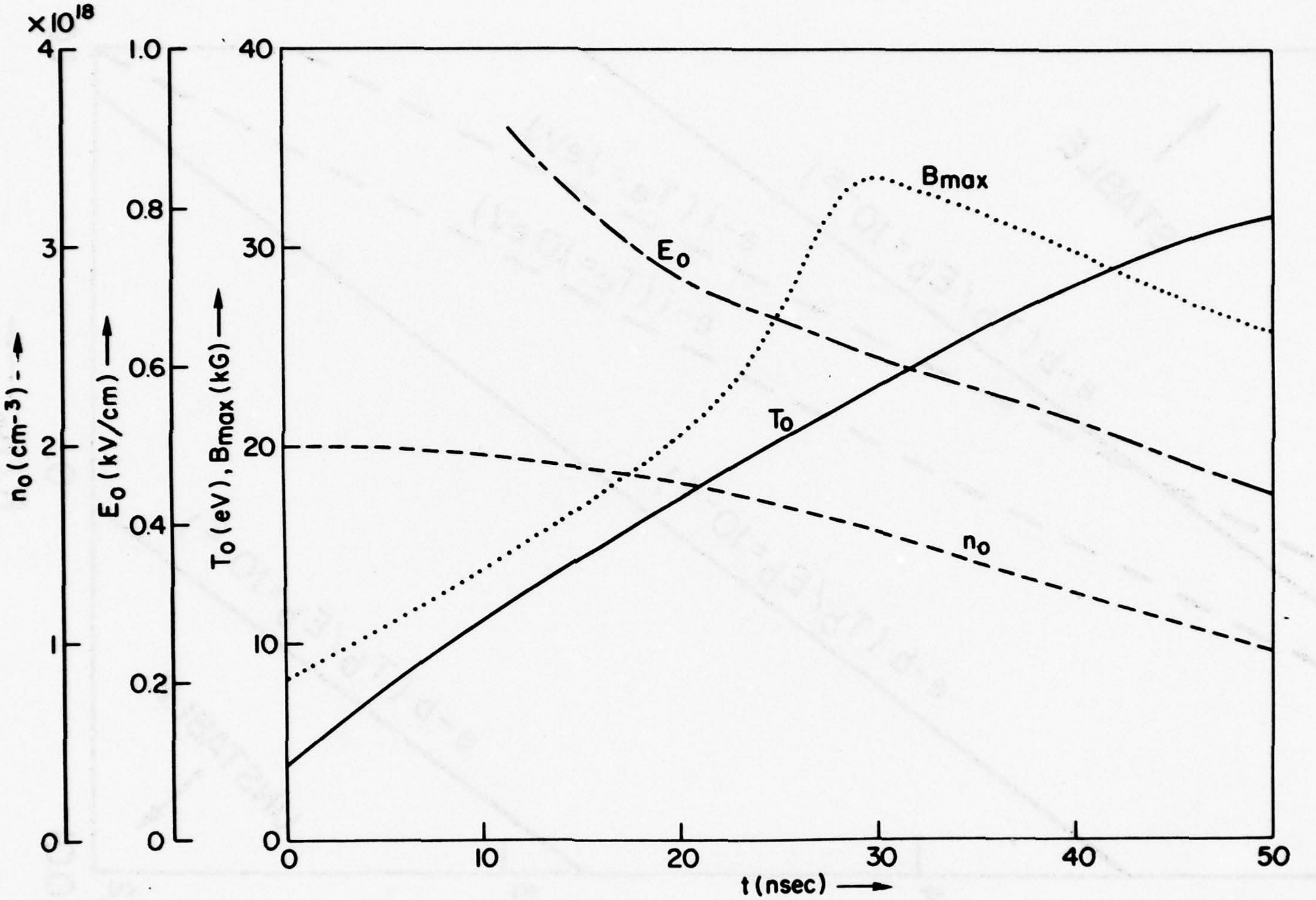

Figure A2.2. Time histories of the maximum B field, maximum temperature, central electric field strength and minimum channel density.

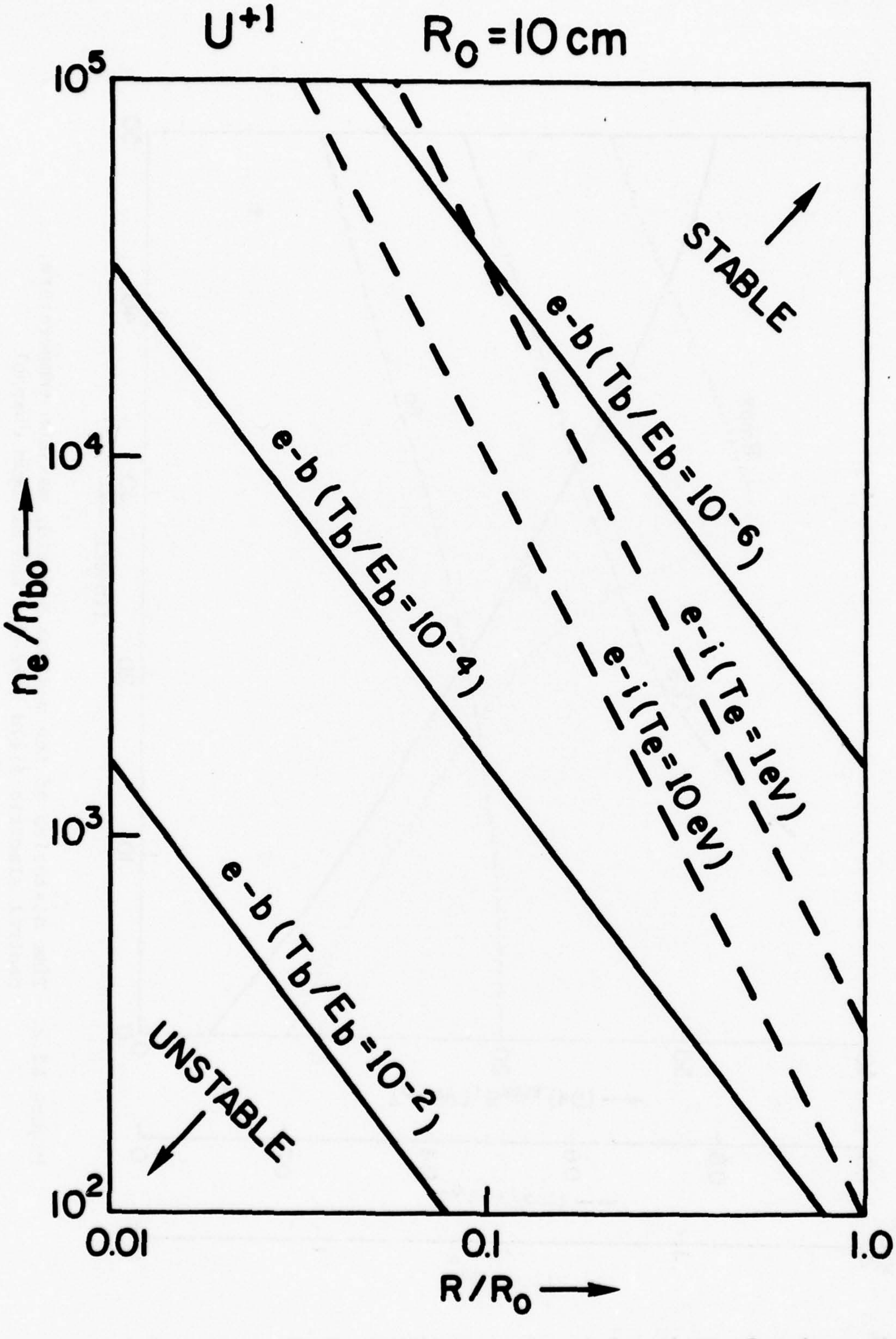

Figure A2.3 Typical marginal stability curves as functions of n_e/n_{bo}, the ratio of beam radius to initial beam radius, and T_b/E_b, the ratio of beam thermal energy to beam streaming energy. In this case R_o = 10 cm and the beam is composed of V^{+1} ions with E_b = 40 GeV.

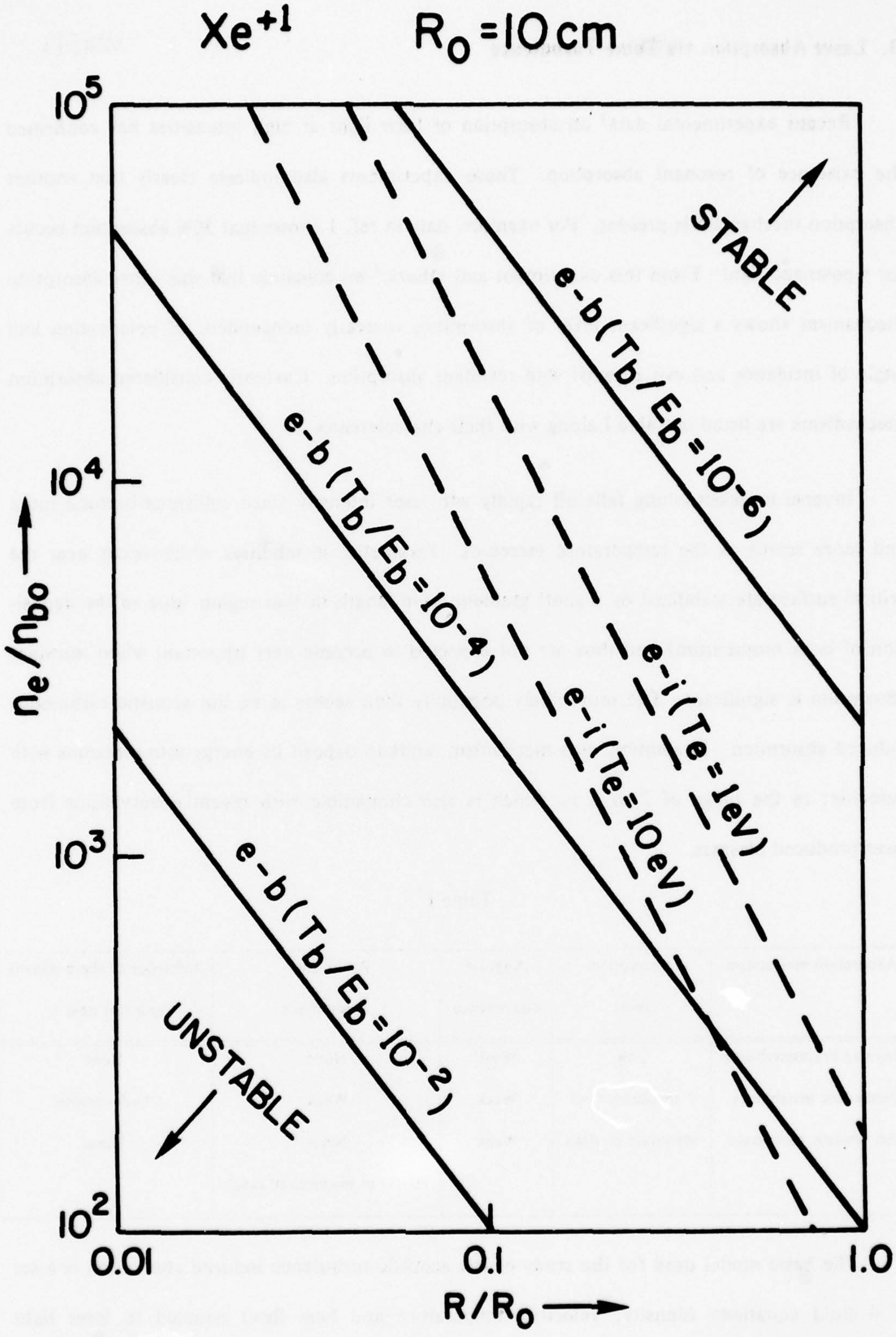

Figure A2.4 Typical marginal stability curves similar to those shown in Fig. A2.4, but in this case for a beam composed of X_e^{+1} ions with E_b = 7 GeV

B. Laser Absorption via Tame Turbulence

Recent experimental data[1] on absorption of laser light at high intensities has confirmed the existence of resonant absorption. These experiments also indicate clearly that another absorption mechanism is present. For example, data in ref. 1 shows that 30% absorption occurs for s-polarized light. From this experiment and others,[2] we conclude that this other absorption mechanism shows a significant level of absorption, is nearly independent of polarization and angle of incidence and can co-exist with resonant absorption. Currently considered absorption mechanisms are listed in Table I along with their characteristics.

Inverse bremsstrahlung falls off rapidly wth laser intensity since collisions become more and more scarce as the temperature increases. Parametric instabilities which occur near the critical surface are stabilized by a short gradient scale length in that region (due to the deposition of laser momentum) and thus are not expected to become very important when resonant absorption is significant. The most likely possibility then seems to be ion acoustic turbulence induced absorption. In addition, this mechanism tends to deposit its energy into electrons with velocities in the range of 2 to 4 v_{th} which is also compatible with recent observations from laser-produced plasmas.

Table I

Absorption mechanism	Absorption level	Angular dependence	Polarization dependence	Influence of sharp density gradient near n_c
Inverse bremsstrahlung	Low	Weak	None	None
Parametric instabilities	? (Probably low)	Weak	Weak	Unfavorable
Ion acoustic turbulence	Moderate to High	Weak	None (Some in magnetized case)	None

The basic model used for the study of ion acoustic turbulence induced absorption is a set of 4 fluid equations (density, velocity, temperature and heat flux) coupled to laser light (incident and reflected) and ion acoustic modes equations. These equations have been solved in the steady state starting from below the critical density and integrating back toward the laser[4] Boundary conditions have been determined from the work by Lee et al.[3]. Typical results obtained from this model are shown in Fig. B1. A high absorption level is found which does not depend strongly on either polarization or target tilt angle. However, the main problem is the absorption length which reaches 60μ in the case of Fig. B1. It is not at all clear that the plasma can expand that far in case of a short pulse experiment. Even in a long pulse experiment, a long underdense region could almost certainly give rise to strong Brillouin backscatter.

Although there are many ways in which this length could be reduced (by assuming a higher level of turbulence at $x = 0$, by reducing the absorption), a similar study was undertaken in presence of magnetic field.[5] It is well established that magnetic fields of order a megagauss can be generated in a laser-produced plasma.

In the magnetized case, the anomalous heat conduction coefficient takes the form

$$K_{\text{anom}} \approx \sum_k \left| \frac{e\,\phi\,(k)}{T_e} \right|^2 \frac{Ve^2\,\omega_{pe}}{\omega_{ce}^2}$$

where k is the ion acoustic mode wave number. So for a given Q $(= K_{\text{anom}}\, N\, \frac{dT_e}{dx})$ at $x = 0$, the smaller the fluctuation level is, the larger dT_e/dx is and therefore the larger the growth rate is. Thus, the transient region of small $e\phi/T_e$ is effectively eliminated in the case of a magnetized plasma.

Also, the wave vector of the ion acoustic modes might be aligned with the electric field vector and this geometry will enhance absorption. Results corresponding to the magnetized case are shown in Fig. B2. In that figure, 20% absorption has been assumed at the critical density (due to resonant absorption, for ex.) From these results, we see that the absorption length has been reduced by a factor of more than 6 and that the absorption level is still significant. The polarization and angular dependence are more complex to determine than in the unmagnetized case but are not as strong as in the case of resonant absorption. Other results show that the temperaure ratio T_e/T_i can be lowered to 5 in the case of a magnetized plasma for $Z = 2.7$

(corresponding to polyethylene targets).

In summary, these results look very promising and satisfy the characteristics outlined in Table I. One problem with this approach however is the boundary conditions which are imposed somewhat arbitrarily on most fluid quantities at $x = 0$ and on Q at $x = -\infty$. The way to specify these quantities in a physical way is to solve for the dynamics of the interaction. This time-dependent approach is currently being undertaken and should yield fully self-consistent boundary conditions. The range of integration needs to be increased in order to include both the solid target on one side and the vacuum on the other one. This model might also shed some light on the time-dependence of this absorption process.

Section B. References and Footnotes

1. K. R. Manes, V. C. Rupert, J. M. Auerback, P. Lee and J. E. Swain, *Phys. Rev. Lett.* **39**, 281 (1977).

2. B. H. Ripin, *Appl. Phys. Lett.* **30**, 136 (1977).

3. K. Lee, D. Forslund, J. M. Kindel, and E. M. Lindman, *Phys. Fluids*, **20**, 51 (1977).

4. W. M. Manheimer, D. G. Colombant and B. H. Ripin, *Phys. Rev. Lett.* **38**, 1135 (1977).

5. W. M. Manheimer and D. G. Colombant , *Phys. of Fluids*, **21**, 1818 (1978).

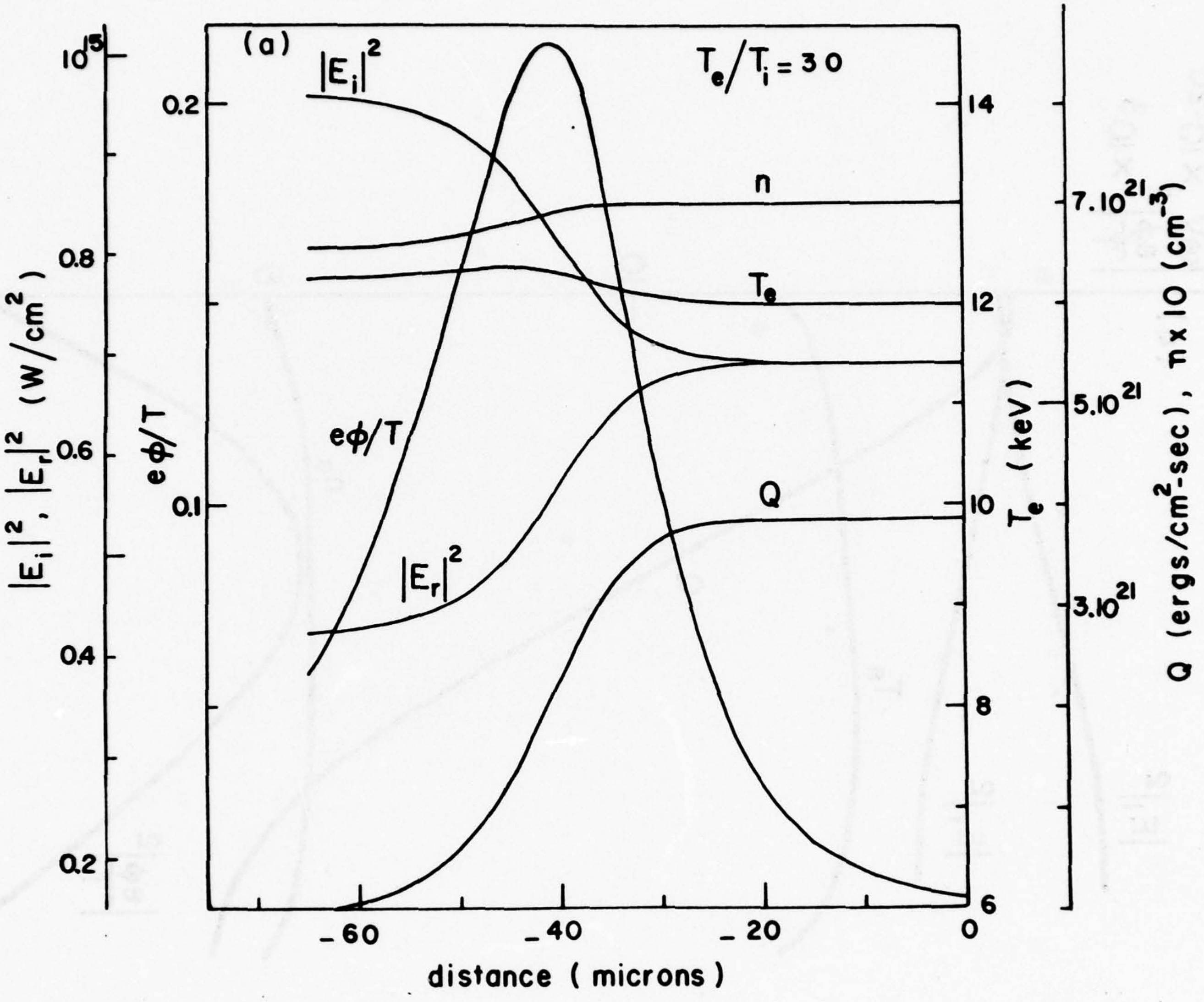

Figure B1 Unmagnetized case - fluid quantities as a function of x

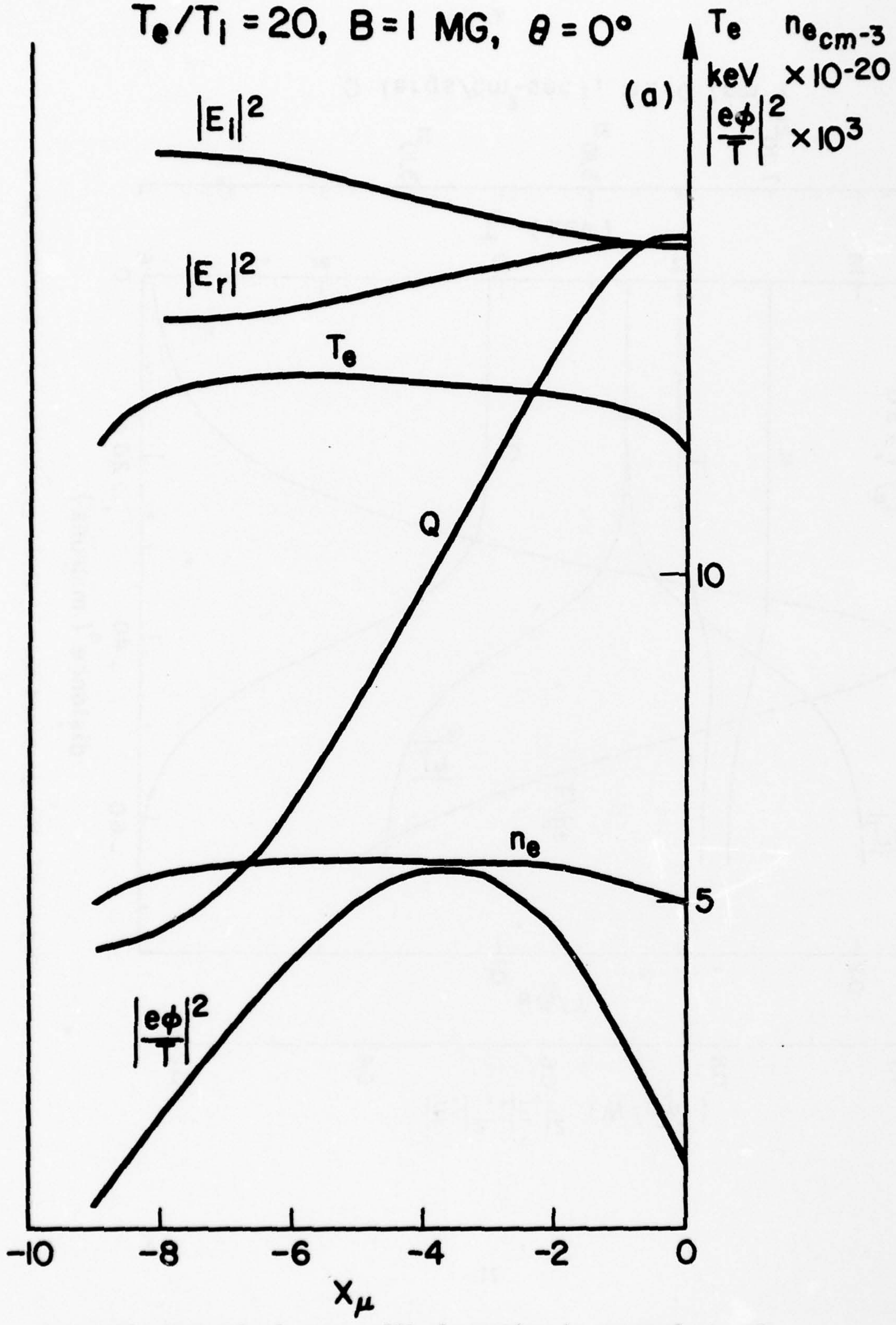

Figure B2 Magnetized case - 20% absorption is assumed at x=0

C. Ablation Layer Structure and Analysis of Rayleigh-Taylor Instability

The NRL inertial confinement program emphasis has moved toward pellet concepts which use longer (~ 3 to 10 nsec) lower intensity driver pulses than previously assumed. For laser-coupled targets, this change was motivated by our recent experiments with enhanced stimulated Brillouin backscatter. For electron and ion coupled targets, our motivation is the possibility that 10-15 nsec pulse lengths may soon be available. To accept these 10-15 nsec pulses, it is necessary to consider larger radius, thinner shelled pellets. The computational studies of Rayleigh-Taylor instability at NRL are being directed toward this regime.

There are essentially four different circumstances where Rayleigh-Taylor modes can grow: in the ablation layer, at internal material interfaces where materials of different density abut, at the buffer-shell interfaces which occur in multiple shell pellets, and where the core shocks interact with density gradients and the pusher interface. At NRL research has proceeded on aspects of all four of these cases. This section of the annual report is directed toward studies of the ablation layer structure and calculations of Rayleigh-Taylor instability in the ablation layer which have been performed during the preceding year.

C1. Ablation Layer Structure

Previous numerical simulations at NRL have shown that density and pressure profiles for an accelerating D-T shell and ablation layer can be temporally superimposed with very little scatter. Because of the presence of these long lived "quasi-static" profiles, we felt that it was important to model the equilibrium solutions for a laser ablation layer both analytically and numerically and to develop a detailed understanding of the nature of this flow. Facility with such a model enables us to calculate the quantitative dependence of the shell thickness and acceleration, the peak density, velocity, and temperature of the shell, the width of the Rayleigh-Taylor unstable region, and the distance to the critical surface on the total plasma mass, the critical density, and the absorbed and reflected laser flux. This "quasi-equilibrium", as determined by the input parameters of the configuration, can be used as an inexpensive input or driver for other numerical studies and as an equilibrium solution for stability analyses. Following is the detailed description of the laser ablation layer included in the numerical model.

For our analyses we use the basic one-dimensional steady state fluid equations for a plasma slab transformed into an accelerating frame of reference

$$\text{continuity: } \frac{d}{dx}(\rho v) = 0 \tag{1a}$$

$$\text{momentum: } \frac{d}{dx}(\rho v^2 + P) = \rho g - \left(\frac{I_a + 2I_r}{c}\right)\delta(x - x_c) \tag{1b}$$

$$\text{energy: } \frac{d}{dx}(Pv + Ev + q) = \rho g v + I_a\,\delta(x - x_c). \tag{1c}$$

where $\tau \equiv T/m_i$, $P = \rho\tau$, $E = \frac{1}{2}(3P + \rho v^2)$, $q = -Km_i^{7/2}\tau^{5/2}\frac{d\tau}{dx}$, and g is the acceleration of the slab. I_a is the absorbed laser flux, I_r is the reflected laser flux, and x_c is the location of the critical surface. As is evident, we are treating the plasma as a fluid with a γ of 5/3 and a classical plasma heat conductivity with a coefficient variation of $T^{5/2}$. The laser deposition is represented as a δ-function at the critical surface. Note that equation (1a) tells us that $\rho v =$ constant. To facilitate the analysis it is convenient to transform the basic equations (1), except at the critical surface, into a dimensionless form where the normalization variables, subscript 0, are those defined at the point of maximum density in the plasma slab.

$$\frac{d\beta}{d\zeta} = \frac{N_o}{2}\frac{1}{\beta^{5/2}}\left[5(\beta - 1) + M_o^2(\eta - 1) - 2\zeta\right] + \frac{1}{\beta^{5/2}} \tag{2a}$$

$$\frac{d\eta}{d\zeta} = -\frac{2\eta\left(\frac{d\beta}{d\zeta} - 1\right)}{M_o^2\eta - \beta} \tag{2b}$$

or

$$\frac{2}{N_o}\frac{d}{d\zeta}\left(\beta^{5/2}\frac{d\beta}{d\zeta}\right) = \beta\frac{d}{d\zeta}\,ln\,(\eta\beta^3). \tag{2c}$$

The dimensionless variables are

$$\beta(\zeta) = \tau/\tau_o, \quad \eta(\zeta) = (\rho_o/\rho)^2, \quad \zeta = g/\tau_o \, x, \tag{3}$$

and the dimensionless coefficients are

$$N_o = \frac{\rho_o v_o}{k m_i^{7/2} g \tau_o^{3/2}} \text{ and } M_o^2 = v_o^2/\tau_o. \tag{4}$$

The isothermal mach number is defined by

$$M^2 \equiv \frac{v^2}{\tau} = \left(\frac{\rho_o}{\rho}\right)^2 \frac{v_o^2}{\tau} = \frac{\eta M_o^2}{\beta} \tag{5}$$

Only two of the three equations (2) are independent. Depending on the circumstances, we found that various pairs of the three equations were more convenient to analyze than others. Under this transformation the problem was reduced to solving for two dependent, dimensionless variables β (the temperature) and η (the density) based on one independent spatial variable ζ and two dimensionless coefficients N_o (primarily the thermal conductivity usually a large number), and M_o (the isothermal mach number at the density peak, usually a small number). We utilized this dimensionless set of equations (2) to generate either general numerical or analytic solutions and then matched these solutions to the specific physical constraints and boundary conditions to determine the desired self-consistent profiles. The numerical solutions were obtained by a Runge-Kutta integration of the non-linear coupled set of differential equations (2) while the analytic solutions were obtained by making appropriate approximations to the equations in the various regions and then solving the simplified set.

For the purpose of obtaining general analytic solutions, the set of equations (2) is conveniently divided into three regions. The first region is the accelerating shell ($\zeta < 0$). the second region is the vicinity of the density peak ($\zeta \approx 0$), and the third region is the blowoff plasma ($\zeta > 0$). Because of certain basic physical trends for the solutions β and η in each of these regions, it is possible to make simplifying assumptions that allow analytic solutions to the equations (2). As will be discussed later, there are other admissible solutions to these equations with counterintuitive physical trends but as yet these have not been sufficiently investigated to determine whether they, too are physically real.

a. The Region of the Accelerating Shell ($\zeta < 0$)

Rewriting equation (2a) into a more convenient form we find that:

$$5(\beta - 1) + M_o^2(\eta - 1) - 2\zeta = \frac{2}{N_o}\left|\beta^{5/2}\frac{d\beta}{d\zeta} - 1\right|. \tag{6}$$

The traditional physical profiles for this region require that $\frac{d\eta}{d\zeta} \leqslant 0$, $\beta \leqslant 1$, and $\eta M_o^2 \leqslant \beta$. In words, the density and temperature should decrease away from the density maximum at $\zeta = 0$ toward the inner regions of the accelerating shell ($\zeta < 0$), and for this region the flow is isothermally subsonic. Therefore from (2b) $\frac{d\beta}{d\zeta} \leqslant 1$ and correspondingly

$$0 \leqslant \beta^{5/2}\frac{d\beta}{d\zeta} \leqslant 1. \tag{7}$$

From (6) and (7) we then obtain the following two inequalities

$$5(\beta - 1) + M_o^2(\eta - 1) - 2\zeta \leqslant 0 \tag{8a}$$

and

$$5(\beta - 1) + M_o^2(\eta - 1) - 2\zeta + \frac{2}{N_o} > 0. \tag{8b}$$

Except for a very narrow region where $|\zeta| \approx \frac{1}{N_o}$ (N_o is usually large), Eqs. (8a) and (8b) imply that

$$5(\beta - 1) + M_o^2(\eta - 1) - 2\zeta \approx 0 \tag{9}$$

is quite a good approximation. By differentiating (2a) we find that

$$5\frac{d\beta}{d\zeta} + M_o^2\frac{d\eta}{d\zeta} - 2 = \frac{2}{N_o}\frac{d}{d\zeta}\left|\beta^{5/2}\frac{d\beta}{d\zeta}\right|. \tag{10}$$

Again, except where $|\zeta|$ is on the order of $\frac{1}{N_o}$ and $\beta^{5/2}\frac{d\beta}{d\zeta}$ is varying rapidly, we have the approximation that

$$5\frac{d\beta}{d\zeta} + M_o^2\,\frac{d\eta}{d\zeta} - 2 \approx 0. \tag{11}$$

Combining Eqs. (2b) and (11) gives us the further approximation that

$$\frac{d}{d\zeta}\,(\eta\beta^3) \approx 0 \tag{12a}$$

or

$$\eta\beta^3 \approx 1. \tag{12b}$$

This latter result can also be obtained from equation (2c).

Collecting our results, we have as a general approximate solution to the set of equations (2) for the region $\zeta < 0$,

$$5(\beta - 1) + M_o^2(\eta - 1) - 2\zeta \approx 0 \tag{13a}$$

$$\eta\beta^3 \approx 1. \tag{13b}$$

It is interesting to note that this approximation is independent of N_o and therefore the flow and profiles in the accelerating shell are not basically governed by thermal conductivity. Also equation (13b) states that the entropy P/ρ^γ is approximately constant throughout the accelerating shell which behaves like an adiabatic gas.

From equation (13b) we obtain

$$\frac{d\eta}{d\zeta} \approx -\,\frac{3}{\beta^4}\,\frac{d\beta}{d\zeta}. \tag{14}$$

Combining this result with equation (11) yields

$$\frac{d\beta}{d\zeta} \approx \frac{2\beta^4}{5\beta^4 - 3M_o^2} \tag{15}$$

It is important to note that equation (15) does not hold when $\zeta = 0$ and $\frac{d\beta}{d\zeta} = 1$ $\left[\zeta = 0\right.$ is the turning point for the density. There $\left.\frac{d\eta}{d\zeta}\right|_{\zeta=0} = 0$ and from (2b) $\left.\frac{d\beta}{d\zeta}\right|_{\zeta=0} = \left.1\right]$. Therefore it is evident that $\frac{d\beta}{d\zeta}$ varies from 1 to approximately $\frac{2}{5 - 3M_o^2}$ very quickly over a narrow region.

It is possible for the flow to approach an isothermal sonic point $(M_o^2\,\eta = \beta)$ in this region. From (13a) and (13b) this occurs when.

$$\beta(\zeta_s) \approx \sqrt{M_o} \tag{16a}$$

and

$$\zeta_s \approx 3\sqrt{M_o} - \frac{5 + M_o^2}{2}. \tag{16b}$$

Substituting (16a) into (15), we have

$$\left.\frac{d\beta}{d\zeta}\right|_{\zeta = \zeta_s} \approx 1 \tag{17}$$

where ζ_s is the location of the isothermal sonic point. This is an important result. It implies that equation (2b) may not be singular at the isothermal sonic point. In fact, from (14) we expect that

$$\left.\frac{d\eta}{d\zeta}\right|_{\zeta = \zeta_s} \approx -\frac{3}{M_o^2}$$

Applying L'Hospital's rule to the full set of equations (2) in the limit where $\beta \rightarrow M_o^2\eta$ and $\frac{d\beta}{d\zeta} \rightarrow 1$ yields:

$$\lim_{\substack{\beta \rightarrow M_o^2\eta \\ \frac{d\beta}{d\zeta} \rightarrow 1}} \frac{d\eta}{d\zeta} = -\frac{\left(\frac{N_o}{\beta^{3/2}} - 1\right)}{2M_o^2}\left[1 - \quad 1 - \frac{4\left(\frac{3N_o}{\beta^{3/2}} - 5\right)}{\left(\frac{N_o}{\beta^{3/2}} - 1\right)^2}\right]. \tag{18}$$

Since $\frac{N_o}{\beta^{3/2}} >> 1$ generally, Equation (18) tells us that

$$\left.\frac{d\eta}{d\zeta}\right|_{\zeta \rightarrow \zeta_s} \rightarrow -\frac{3}{M_o^2} \tag{19}$$

as expected. The fact that the flow approaches a well behaved, continuous isothermal sonic point is very helpful since it gives us a convenient position to define as the inner edge of the accelerating shell. This definition is reasonable since no physical information about the flow could be transmitted across this point.

b. The Vicinity of the Density Peak ($\zeta \approx 0$)

The simplest approach to determining an analytic approximation in this region is to expand the system of equations (2) in a Taylor series about $\zeta = 0$. Doing this for small ζ yields to third order

$$\beta \approx 1+\zeta+\frac{\zeta^2}{4}(3N_o-5)+\frac{\zeta^3}{12}\left[\frac{N_o(3N_o-5)}{2}\left(\frac{5-3M_o^2}{1-M_o^2}\right)-5(3N_o-5)-\frac{15}{2}\right] \tag{20a}$$

and

$$\eta \approx 1+\frac{\zeta^2/2}{1-M_o^2}(3N_o-5)$$
$$+\frac{\zeta^3/6}{1-M_o^2}\left[\frac{N_o(3N_o-5)}{2}\left(\frac{5-3M_o^2}{1-M_o^2}\right)-(3N_o-5)\left(\frac{7-5M_o^2}{1-M_o^2}\right)-\frac{15}{2}\right]. \tag{20b}$$

Since $\zeta = 0$ is to be a density maximum

$$\left.\frac{d^2\eta}{d\zeta^2}\right|_{\zeta=0} > 0 \tag{21}$$

which by differentiating equation (20b) twice yields

$$N_o > \frac{5}{3} \tag{22}$$

This is not a very stringent criteria for N_o. Generally for physical problems of interest $N_o >> 5/3$. It is also important to note that the region where the Taylor expansions (20) are accurate is exceedingly narrow. Trying to utilize these results for even a distance on the order of the thickness of the ablation layer does not yield valid results. In fact, equations (2) are included more for completeness than for their practical importance.

c. The Region of the Blowoff Plasma ($\zeta > 0$).

Two very important regions lie in the blowoff. The first is the Rayleigh-Taylor unstable region where the gradients of density and pressure have opposite sign. The second is the vicinity of the critical surface where the laser deposition occurs. In this region $\frac{d\beta}{d\zeta}$ is increasing rapidly from its value of 1 at $\zeta = 0$. Corresponding, $\beta >> 1$ except very near the density peak. It is expected that this region be isothermally subsonic at least until the critical surface is reached. Therefore,

$$| M_o^2(\eta - 1) - 2\zeta | << 5(\beta - 1) \tag{23}$$

is a valid approximation except in a very narrow region about $\zeta = 0$ where it is in error by about 40%. Here retaining ζ is important and the approximation is more properly written as

$$M_o^2(\eta - 1) << 5(\beta - 1) - 2\zeta \tag{24}$$

The error in (23) potentially could be as great as 20% in the vicinity of the critical surface as well. In practice (numerical integrations) it never becomes that large. Under these approximations equation (2a) becomes either

$$\frac{d\beta}{d\zeta} \approx \frac{N_o}{2} \frac{5}{\beta^{5/2}} \left[\beta - \left(1 - \frac{2}{5N_o}\right) - \frac{2}{5}\zeta\right] \tag{25a}$$

or

$$\frac{d\beta}{d\zeta} \approx \frac{N_o}{2} \frac{5}{\beta^{5/2}} \left[\beta - \left(1 - \frac{2}{5N_o}\right)\right] \tag{25b}$$

Equation (25b) can be solved analytically to yield:

$$\zeta = \frac{4}{5N_o}\left[\frac{1}{5}(\beta^{5/2} - 1) + \frac{\left(1 - \frac{2}{5N_o}\right)}{3}(\beta^{3/2} - 1) + \left(1 - \frac{2}{5N_o}\right)(\beta^{1/2} - 1)\right.$$
$$\left. - \frac{1}{2}\left(1 - \frac{2}{5N_o}\right)^{5/2} ln\left[\frac{\beta^{1/2} + \sqrt{1 - \frac{2}{5N_o}}}{1 + \sqrt{1 - \frac{2}{5N_o}}} \; \frac{1 - \sqrt{1 - \frac{2}{5N_o}}}{\beta^{1/2} - \sqrt{1 - \frac{2}{5N_o}}}\right]\right] \tag{26}$$

Equation (25a) can also be solved analytically to yield an approximation near $\zeta = 0$ that is more exact than (26), but little is gained by including it here due to its complexity. Though it is not crucial to use this more exact approximation to define the Rayleigh-Taylor unstable region, its use does improve the results in a measurable way. For $\zeta > 0$ it is advantageous to write equation (2b) in terms of the pressure where

$$\frac{P}{P_o} = \frac{\beta}{\sqrt{\eta}}. \tag{27}$$

This gives two interesting forms.

$$\frac{d}{d\zeta}\left[ln\ \frac{\eta}{\beta^2}\right] = -2\frac{d}{d\zeta}\left[ln\ P/P_o\right] = \frac{1}{\beta}\ \frac{d}{d\zeta}\ (M_o^2\,\eta - 2\zeta) \tag{28a}$$

and

$$2\frac{d}{d\zeta}\left[\frac{\beta}{\sqrt{\eta}}\right] = 2\frac{d}{d\zeta}\left[P/P_o\right] = -\frac{1}{\sqrt{\eta}}\ \frac{d}{d\zeta}\ (M_o^2\,\eta - 2\zeta) \tag{28b}$$

Subtracting (28b) from (28a) yields

$$\frac{d}{d\zeta}\left\{ln\ \frac{\eta}{\beta^2}\right\} = \frac{d}{d\zeta}\left\{[2\beta + M_o^2(\eta-1) - 2\zeta]\left\{\frac{1}{\beta} - \frac{1}{\sqrt{\eta}}\right\}\right\} \tag{29}$$

$$- [M_o^2(\eta-1) - 2\zeta]\ \frac{d}{d\zeta}\left\{\frac{1}{\beta} - \frac{1}{\sqrt{\eta}}\right\}$$

The second term on the R.H.S. of (29) is effectively a coefficient times the rate of change of the pressure. Conveniently it turns out that the rate of change of the pressure is significant where the coefficient is small and the coefficient is significant where the rate of change of the pressure is small. Therefore the term is always small and may be neglected.

We obtain as an approximation

$$\frac{\eta - \beta^2 \exp\left\{[2\beta + M_o^2(\eta-1) - 2\zeta]\left\{\frac{1}{\beta} - \frac{1}{\sqrt{\eta}}\right\}\right\}}{\eta - \beta^2} = 0 \tag{30}$$

The presence of $\eta - \beta^2$ in the denominator compensates for the additional root at $\eta = \beta^2$ introduced by subtracting (28b) from (28a). Equations (26) and (30) are then an extremely good approximation to the general solution for $\zeta > 0$. It is also relevant to note that these analytic solutions with the modifications included due to (25a) will hold around $\zeta \approx 0$ and even be valid when ζ is slightly less than zero and $\beta^{5/2}\frac{d\beta}{d\zeta}$ is varying rapidly as noted earlier.

From (28b) we obtain two interesting results. First

$$\frac{d}{d\zeta}\left[P/P_o\right]\Big|_{\zeta=0} = 1 \tag{31}$$

and second

$$\frac{d}{d\zeta}\left[P/P_o\right] = 0 \text{ when } \frac{d\eta}{d\zeta} = \frac{2}{M_o^2} \tag{32}$$

Combining (32) and (2b) yields

$$\frac{d}{d\zeta}\left[P/P_o\right] = 0 \text{ when } \frac{d\beta}{d\zeta} = \frac{\beta}{M_o^2\eta} \tag{33}$$

or from (5)

$$\frac{d}{d\zeta}\left[P/P_o\right] = 0 \text{ when } M^2\frac{d\beta}{d\zeta} = 1 \tag{34}$$

Equations (32) and (33) or (34) give us respectively the rate of change of the density and the temperature at the turning point of the pressure. It is just this offset of the density and pressure peaks that bounds the Rayleigh-Taylor unstable region, so-called because density and pressure gradients are opposed.

Combining (33) with equation (2a) yields an equation defining the relationship of the variables at the pressure peak

$$\frac{\beta}{M_o^2\eta} = \frac{N_o}{2}\,\frac{1}{\beta^{5/2}}\left[5(\beta-1)+\frac{2}{N_o}+M_o^2(\eta-1)-2\zeta\right]. \tag{35}$$

The relevant question is whether equation (35) has a solution for all values of M_o and N_o. From Eq. (32), in the Rayleigh-Taylor unstable region

$$0 \leqslant \frac{d\eta}{d\zeta} \leqslant \frac{2}{M_o^2}. \tag{36}$$

Therefore

$$\frac{d}{d\zeta}\,[M_o^2(\eta-1) - 2\zeta] \leqslant 0 \quad \text{or} \quad M_o^2(\eta-1) - 2\zeta \leqslant 0 \tag{37}$$

there applying (37) to equation (35) we obtain the condition for the existence of a pressure peak not located at $\zeta = 0$,

$$\beta < \frac{N_o}{2}\,\frac{M_o^2\eta}{\beta^{5/2}}\left[5(\beta-1) + \frac{2}{N_o}\right]. \tag{38}$$

also in the Rayleigh-Taylor region

$$\frac{d}{d\zeta}\,[P/Po] \geqslant 0 \quad \text{or} \quad \frac{P}{P_o} \geqslant 1 \tag{39}$$

or from equation (27)

$$\eta \leqslant \beta^2. \tag{40}$$

Combining inequalities (38) and (40) requires at the pressure peak

$$\beta^{3/2} < \frac{N_o}{2}\,M_o^2\left[5(\beta-1) + \frac{2}{N_o}\right]. \tag{41}$$

It is tedious, but straightforward to show that there can be no regime where $\beta - 1 \geqslant 0$ and inequality (41) can hold when

$$N_oM_o^2 \leqslant \frac{2}{5}\sqrt{3}. \tag{42}$$

This is a rather significant result since it shows that not all values of M_o and N_o are admissible if one requires a solution to the set of equations (2) where there is a turning point in the pressure profile. Figure 1 displays graphically the allowable region of $M_o - N_o$ space.

The only other important modeling necessary for the region $\zeta > 0$ is near the critical surface. Here we integrate equations (1) across the critical surface to obtain the jump conditions and utilize the density shelf criteria of Felber[1] and *Lee at al.*[2] where

$$\sqrt{\eta_-} = 2\sqrt{\eta_c}\,\frac{(1-M_-)^2}{M_-^2 - \ln(M_-^2) - 1} \qquad (43)$$

with the subscript minus referring to the values just interior to the jump and

$$\eta_c = \left(\frac{\rho_o}{\rho_c}\right)^2 \; (\rho_c \textit{ is the critical density}). \qquad (44)$$

We force the temperature to remain constant across the jump and the heat flux to be zero outside the critical surface. We did not believe that it was important to model the underdense gas outside the critical surface since the density is so low there. Felber[1] has chosen to model this region as an adiabatic gas and that would probably be as good a choice as any other. We do require that the flow out of the critical surface be supersonic and that gives us an additional constraint on M_o that

$$M_o^2 < M_-^2 < \frac{3}{5} \qquad (45)$$

This constraint is also included in Figure 1. When M_o and N_o are chosen within the bounds depicted in Figure 1 the solutions to equations (2) are profiles that can be given physical explaināations. For values outside that regime equations (2) are still solvable, but it is not clear whether the profiles generated also have a physical significance or are merely mathematical curiosities. This question is worthy of further investigation. There are two possible approaches to obtain profile solutions to equations (2) for given specific boundary conditions. First the coupled set of non-linear first order differential equations can be integrated numerically by a Runge-Kutta method and then the boundary conditions matched. Second, the general analytic approximations (13), (26), and (30) can be utilized instead of a numerical integration and then matched to the specific boundary condition. Conceptually there is not much difference in either method. Because of the complexity of the analytic approximations both methods require the use of a computer. The major advantage of the analytic approximation approach is that, by allowing an error in the results of a few percent, significant computational time can be saved. Also the analytic approach often gives a better insight into what is physically occurring. The three available boundary conditions not previously taken into account are the total plasma mass, the absorbed laser flux, and the reflected laser flux. Certainly the original slab mass must be encompassed by the density profile. For our model we assume that all the mass lies between the interior isothermal sonic point and the critical surface. Because the densities outside this region are exceedingly small compared to the peak density, this approximation should have little effect on the results. Therefore, if m is the total slab mass per unit area,

$$m = \int_{x_s}^{x_c} \rho dx = \frac{\rho_o \tau_o}{g} \int_{\zeta_s}^{\zeta_c} \frac{1}{\sqrt{\eta}} d\zeta \tag{46}$$

or from (4)

$$m = \frac{km_i^{7/2}}{M_o} N_o \tau_o^2 \int_{\zeta s}^{\zeta c} \frac{1}{\sqrt{\eta}} d\zeta . \tag{47}$$

In either the Runge-Kulta method or the analytic method this integration (46) could be performed numerically, but for the analytic method, with certain approximations, the integration can be performed analytically. From (46)

$$m = \frac{km_i^{7/2}}{M_o} N_o \tau_o^2 \left[\int_{\zeta s}^{o} \frac{1}{\sqrt{\eta}} d\zeta + \int_{o}^{\zeta c} \frac{1}{\sqrt{\eta}} d\zeta \right] \tag{48}$$

Now from (13b) and (15) the first integral in (48) can be approximated by

$$I_s(M_o) = \int_{\zeta_s}^{0} \frac{1}{\sqrt{\eta}} d\zeta = \int_{\sqrt{m_o}}^{1} \left(\frac{5}{2} \beta^{3/2} - \frac{3}{2} \frac{M_o^2}{\beta^{5/2}} \right) d\beta = 1 + M_o^2 - 2M_o^{5/4} \tag{49}$$

The dominant contribution to the second integral in (48) is in the neighborhood of $\zeta = 0$ where $\eta \approx \beta^2$ is a reasonable approximation (*N.B.* the approximation $\eta \approx \beta^2$ is only of any practical use for this specific integration and should not be used elsewhere). The second integration in (48) can be approximated using (25b) as

$$\begin{aligned} I_c(N_o) &= \int_{0}^{\zeta_c} \frac{1}{\sqrt{\eta}} d\zeta = \frac{2}{5N_o} \int_{1}^{\beta_c} \frac{\beta^{3/2}}{\beta - \left(1 - \frac{2}{5N_o}\right)} d\beta \\ &= \frac{4}{5N_o} \left[\frac{1}{3} \left(\beta_c^{3/2} - 1\right) + \left(1 - \frac{2}{5N_o}\right) \left(\beta_c^{1/2} - 1\right) \right. \\ &\quad \left. - \frac{1}{2} \left(1 - \frac{2}{5N_o}\right)^{3/2} ln \left(\frac{\beta_c^{1/2} + \sqrt{1 - \frac{2}{5N_o}}}{1 + \sqrt{1 - \frac{2}{5N_o}}} \, \frac{1 - \sqrt{1 - \frac{2}{5N_o}}}{\beta_c^{1/2} - \sqrt{1 - \frac{2}{5N_o}}} \right) \right] \end{aligned} \tag{50}$$

Of course, in (50) β_c is, as yet, an undetermined parameter.

At the critical surface we handle the jump conditions and laser deposition much as Felber[1] did where

$$\phi^2 \equiv 1 + 2\frac{I_a - \Delta q}{\rho_- v_-^3} = 1 + 2\frac{I_a - \Delta q}{\rho_o M_o \tau_o^{3/2} \beta_c M_-^2} \tag{51}$$

and we have used the constancy of ρv, and equation (5). It is also true from reference 2 that

$$\frac{I_a + 2I_r}{c\rho_o \tau_o \beta_c}\sqrt{\eta_-} = (1 - M_-^2 \phi)\left(1 - \frac{1}{\phi}\right) \tag{52}$$

By use of equations (43), (48), (51), and (52), we are able to determine the position of the critical surface for a given M_o and N_o. This is accomplished by obtaining the value of the first integral in (48) either through a Runge-Kutta solution of equations (2) and a numerical integration from $\zeta = 0$ toward the isothermal sonic point or from equation (49). Then we begin at $\zeta = 0$ and move in the direction of increasing ζ again using a Runge-Kutta solution and numerically integrating to obtain the second integral in (48) or using the analytic approximations and equation (50). We assume that at each point we have reached the critical surface. Then from (48) we can obtain the value τ_o such that all the plasma mass would be contained within the density profile to that point. With the τ_o equations (51) and (52) will determine the corresponding ρ_o. This value of ρ_o may then be used to see if equation (43) is satisfied. When (43) is satisfied, we have reached the critical surface. Also we have the values of ρ_o and τ_o needed to transform the general profiles into the specific profiles for the given boundary conditions. The other values of interest v_o and g can be found from (4).

The preceeding discussion has masked a rather curious fact. Even with all the criteria we have specified, we cannot determine a unique solution based on a single pair of M_o and N_o but rather have obtained a whole family of possible "quasi-equilibrium" solutions based on values of M_o and N_o only constrained as in Figure 1. Maybe we have not specified all the available boundary conditions but it is difficult to think of another two, only based on the equilibrium, that we are at liberty to specify. More likely, what the results are telling us is that there really are various possible "quasi-equilibrium" states and just which one would occur in a given physical situation might be determined by the neccessarily time-dependent evolution leading up to that equilibrium. Such an effect might be an initial shock which impacts an entropy to the shell. Others may exist.

Figure 2 displays the profiles of density, temperature, pressure, and isothermal mach number for the "quasi-equilibrium" where $Km_i^{7/2} = 10^{-33}$, $\rho_c = 4\times10^{-3}\ g/\mathrm{cm}^3$, $I_a = 10.2$ TW $/cm^2$, $I_r = 10.2 TW/\mathrm{cm}^2$, $m = .773 mg/\mathrm{cm}^2$ $M_o \approx .07$, and $N_o \approx 700$. These profiles were obtained by a Runge-Kutta integration of the equations (2), but curves generated through the analytic approximations discussed earlier are virtually indistinguishable. These are rather typical results and while variation of M_o and N_o, within the constraints of Figure 1, does change the profiles quantitatively there is not much qualitative variation. The density, temperature, and pressure are seen to decrease smoothly away from the density peak toward the isothermal sonic point. For this case the thickness of the shell is about 35 microns and the peak density is about .3g/cm^3. The corresponding temperatures and pressures at the density peak are respectively approximately 8×10^{12} cm^2/sec^2 and 2.5×10^{12} dyne/cm^2. The acceleration for the shell is about 4×10^{15} cm/sec^2. It is impossible to see in the figure, but the offset of the pressure and density peaks is about .1 micron. The peak pressure is only slightly greater than the pressure at the density peak. In the blowoff plasma the density drops sharply while due to the thermal conductivity the temperature increases rapidly. It is interesting to note that the decrease in density is nearly balanced by the increase in temperature such that the pressure remains relatively constant. The critical surface is approximately 100 microns from the density peak and the critical temperature is about 4.5×10^{14} cm^2/sec^2. The density and isothermal mach number just inside the critical surface are respectively approximately 4.5×10^3 g/cm^3 and .6. These profiles have been used as initial conditions for time varying models and are seen to remain relatively unchanged for long periods of time. Therefore they are truly "quasi-equilibrium" solutions. Further, since the density and pressure gradients in the constant adiabat shell are aligned, the shell interior is Rayleigh-Taylor stable.

Development of this "steady-state" model is still continuing. The most important question yet to be resolved is how to choose M_o and N_o. What is desired is to relate M_o and N_o to some physical properties that would remain constant for the solutions while external parameters like the plasma mass or the laser intensity are slowly varied. One such possibility is the entropy of the accelerating shell. We have utilized one of our "quasi-equilibrium" solutions as an initial condition to a time dependent simulation model and followed the burning of the shell. During the evolution, the shell entropy did remain relatively constant. We have also examined the constancy of the shell momentum, but, as yet, have not reached any definite conclusions.

Our model has been used as an initializer to time dependent ablation models and as a pressure driver for a laser-target compression simulation. For this latter case the "steady-state" model was used to relate the variation of the laser intensity to the pressure at the surface of the shell. Generally we used the analytic approximations for these studies, since it entails a vast savings in computational time. We also plan to utilize our model as an equilibrium for a piggy-back analysis of Rayleigh-Taylor stability in the ablation layer plasma.

Section C1 . References and Footnotes

1. F.S. Felber, "Steady-State Model of a Flat Laser-Driven Target," *Phys. Rev. Lett. 39*, 84 (1977).

2. K. Lee, D.W. Forslund, J.M. Kindel, and E.L. Lindman, "Theoretical Derivation of Laser Induced Plasma Profiles," *Phys. Fluids 20*, 51 (1977).

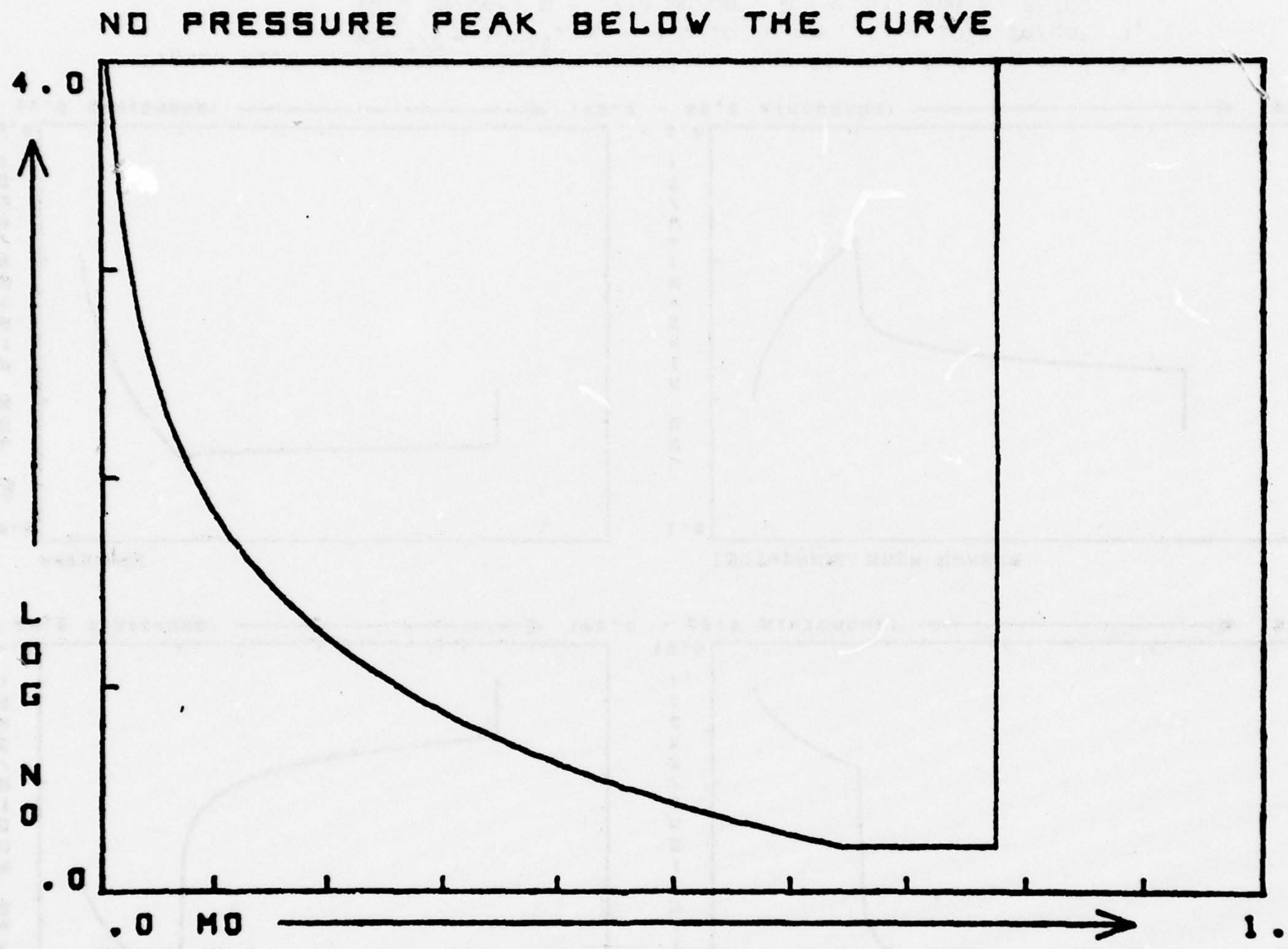

Figure C1.1 The region of M_o-N_o space that yields physically intuitive solutions. For the region below the curve there is no turning point in the pressure profile. For the region to the right of the curve the flow out of the critical surface is not supersonic.

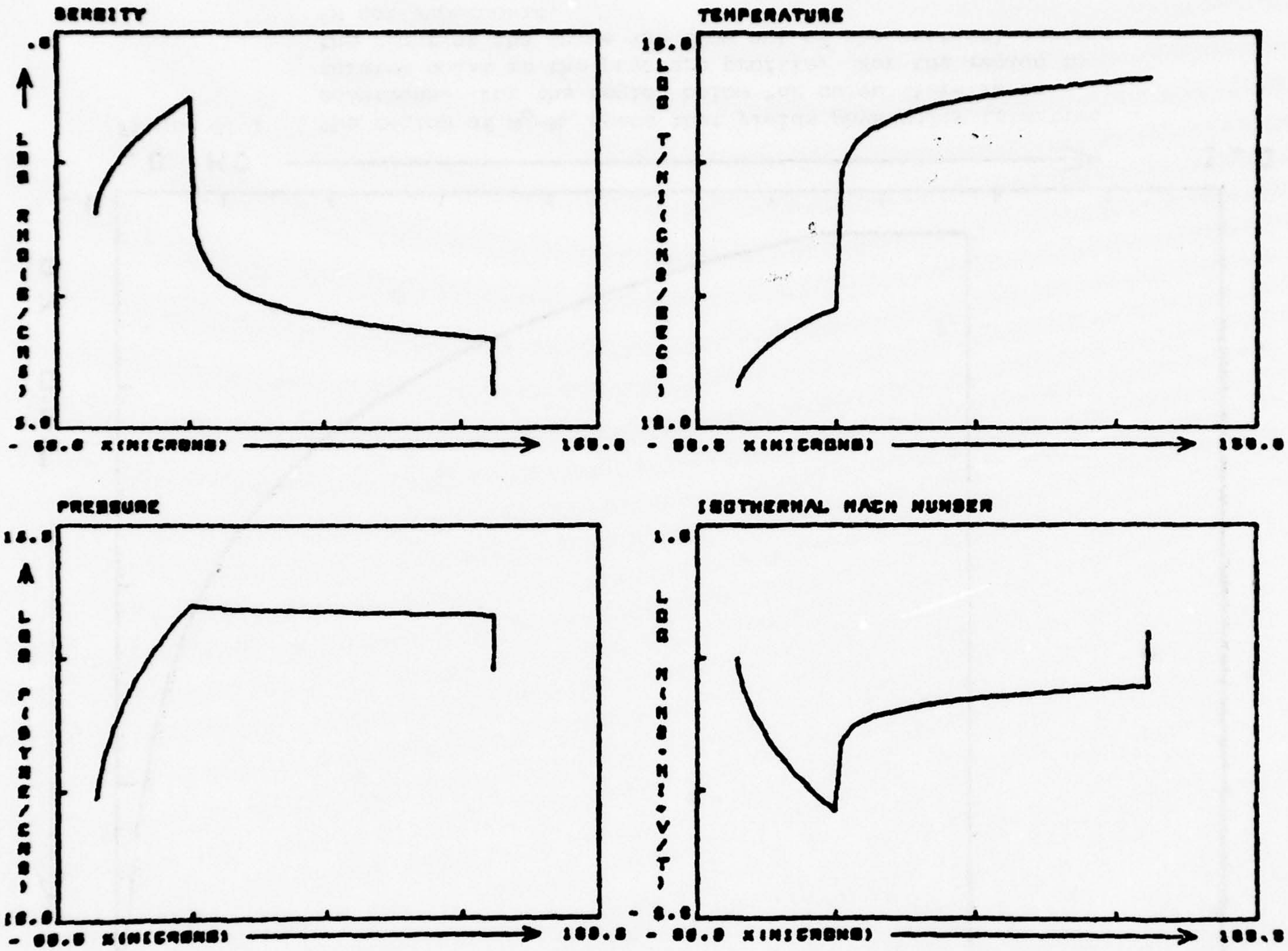

Figure C1.2 Typical solution profiles. Results are for the case where $K m_i^{7/2} = 10^{-33}$, $\rho_c = 4 \times 10^{-3}$ g/cm , $I_a = 10.2$ TW/cm^2, I_r = 10.2 TW/cm^2, m = .773 mg/cm^2, $M_o \approx .07$, and $N_o \approx 700$.

C2. Analysis of Rayleigh-Taylor Instability

The theoretical treatment of Rayleigh-Taylor modes in the ablation layer is complicated so much by the convection, conduction and acceleration effects attendant in the ablation process itself that analytic treatments are at best approximate. Numerical treatments are complicated by the requirement to treat widely disparate time and space scales with nasty nonlinearities. Therefore little quantitative is known about the linear phase in laser pellet configurations and almost nothing qualitative is known about the nonlinear phases.

Our picture of the external (ablation layer) Rayleigh-Taylor instability was obtained as a result of a number of numerical simulations using the sliding rezone Eulerian FAST2D[1,2,3] code in an accelerating frame of reference. Our current calculations have been performed in slab geometry with a $K_o T^{5/2}$ thermal conduction law and ideal hydrodynamics. These calculations show that:

A) The initial linear growth for long wavelengths occurs qualitatively as predicted by the simplest linear theories.

B) There is a cutoff at short wavelengths which appears to force the growth rate γ toward zero. The cutoff wavelength is roughly $2\pi\Delta$ where Δ is the thickness of the ablation region.

C) The nonlinear evolution observed is the formation of a droplet at the location classically occupied by a spike. Bubbles of hot plasma can form in the ablator.

D) Rayleigh-Taylor modes with $\lambda \sim h$ (the shell thickness) do not immediately fracture the shell.

E) Dynamic stabilization by oscillating the ablation layer appears to stabilize a wide band of the Rayleigh-Taylor spectrum.

Figure C2.1 presents dispersion relations for the Rayleigh-Taylor instability of a $D-T$ ice shell determined from a series of FAST2D calculations.[4,5] Growth rate γ is shown as a function of wavelength λ for two cases. On the right, $K_o = 5.88 \times 10^{49}$, the usual plasma thermal conduction for $D-T$, is used. On the left the thermal conduction has been increased artificially by a factor of 10. For both cases the temperature at the critical region was forced to be 280 ev and the cold shell was initially 20μ thick. The size of the plotting symbols indicates an estimate of the accuracy with which the growth rates could be determined from the numerical results.

The symbols indicate which transverse mode in the computational system is being studied. ⊙is the first mode, the longest wavelength that the system will support. The symbol x denotes the second mode, Δ the third mode, and □ the mode with four wavelengths across the system.

In the standard case on the right, three separate calculations were performed with 1μ x gridding. This was done to get information on both the long and the short wavelength ends of the spectrum. The cutoff at short wavelength is clearly indicated in the data but is difficult to follow down to zero growth because of the timestep limitations which result. Timesteps, coupled with the extensive grid needed for much finer resolution calculations made the cost of exploring the convergence prohibitive. Nonetheless, Figure C2.2 contains data from simulations with varying spatial resolution in both directions showing apparent convergence.

The system for these calculations was initialized using the steady-state, semi-analytic solutions developed by Joe Orens for proscribing the starting temperature, density, and velocity profiles.[6] We have verified that these solutions are compatible with FAST2D except for minor discrepancies when the ablation layer is insufficiently resolved in the simulation code. Thus the transient radial shocks driven by our previous approximate initialization are largely absent and negligible growth is observed when no perturbation of the equilibrium is applied.

The initial perturbation is applied to the density profile at its peak just behind the ablation layer. The ten longest wavelength modes are excited with equal (small) amplitudes and ran-

dom phases corresponding to a total initial density perturbation (RMS) of about .1% of the shell thickness. In order to study the mode amplitude growths at later times, a relatively clean diagnostic was needed. Some characteristic of the slab had to be Fourier analyzed as a function of *y* in order to measure the different mode amplitudes. We are now using the integrated mass through the shell rather than the ablation layer location or a time and space averaged vorticity as had been done previously. This new diagnostic is insensitive to acoustic waves in particular which are always observed rattling back and forth through our accelerating ablator shell. Thus the fluctuations previously observed in the Fourier-analyzed mode amplitudes are greatly reduced.

The integrated mass from the inside of the shell to the ablation layer is determined for each of the rows of computational cells, that is, for each discrete value of *y*. Where the laser is burning through more quickly the shell will be thinner and the integrated mass less. In regions where ablator "droplets" are forming the shell is thicker and the integrated mass relatively large. To determine the mode amplitudes the integrated mass values as a function of *y* were Fourier transformed. The growth rates were then determined by plotting a given mode amplitude as a function of time on semi-log paper and making an estimated straight line fit.

Figure C2.3 displays such a plot. After an initial transient period an exponential growth period develops. As can be seen, this new diagnostic allows for a clean measurement of the growth rates, say for the time interval from two to four nsec. The growth rates determined from this figure, along with others based on similar calculations, is shown in Figure C2.2. The growth rates for the first three modes in each of four different numerical simulations are plotted as a function of the mode wavelength. Error bars are estimated from fluctuations in the mode amplitude versus time plots. In the first three runs the *x* resolution in the vicinity of the ablation layer was 1.0μ and stretched zones were used in the low density regions. The periodicity length L_y was taken to be 20μ (Δ points), 40μ (● points), and 80μ (□points) for three runs. In each case 20 equally spaced cells were used. The fourth run had the number of *x* cells doubled

to 120 and the x resolution in the shell correspondingly halved to 0.5μ. The idea here was to see if the 0.1μ structure predicted for the steady state must be resolved in the computations to achieve convergence of Rayleigh-Taylor behavior.

The shaded area in Figure C2.2 corresponds to the classical Rayleigh-Taylor dispersion relation $\gamma = \sqrt{kg}$ where $k = \frac{2\pi}{\lambda}$. The width of the bar is due to the variation of g, the system acceleration, as a function of time. Although a constant laser flux of 10^{13} watts/cm^2 was used, the mass of the shell decreases because of the steady ablation. Hence the acceleration slowly increases.

At long wavelengths the runs become very long because growth rates are low. Thus appreciable reduction of the shell thickness occurs and the notion of a fixed growth rate is suspect. Nevertheless some evidence of accelerative stabilization can be argued from the deviations of γ below the $\sqrt{kg}$ limit shown clearly in the figures. This deviation is apparently quite small, however, compared to what we would expect based on recent theoretical predictions which attempt to relate the Rayleigh-Taylor growth rate to the thickness and strength of the unstable region where pressure and density gradients are opposed.[2,7] An analysis of the problem in terms of vorticity generation gives the following equation

$$\frac{\partial \xi}{\partial t} + \underline{V} \cdot \underline{\nabla} \xi + \xi \, \underline{\nabla} \cdot \underline{V} = \frac{\underline{\nabla} \rho \times \underline{\nabla} P}{\rho^2} \tag{1}$$

for the time evolution of the vorticity. A simple estimate of the growth rates is

$$\gamma^2 \int_o^\Delta \xi^2 dx \cong - \int_o^\Delta kL\xi^2 dx \; \frac{\nabla \rho_o \nabla P_o}{\rho_o^2} \tag{2}$$

which assumes that the major effect of unstable shear (vorticity in the ablation layer) is to change the angle between $\underline{\nabla}\rho$ and $\underline{\nabla}P$ rather than changing the profiles themselves when measured locally normal to the ablation layer. This approximation is obviously better for long wavelength variations as is the neglect of convective terms. In Eq. (2) Δ is the width of the unstable region from the peak of ρ_o to the peak of P_o. L is a length of order Δ ($L \equiv \Delta/2$ for the classical incompressible problem) which can absorb the geometric complications. The function $\xi(x)$ is the eigenfunction, unknown in general but assumed to be constant when the wavenumber k is small and the unstable region narrow.

Growth rates calculated using this formula and realistic $\rho_o(x)$, $P_o(x)$ profiles predict that low power-low acceleration systems should be more stable in reaching a given implosion velocity than a high-power system because the thickness of the Rayleigh-Taylor unstable region goes to zero as the acceleration decreases. The numerical evidence for this accelerative stabilization is not all that clear cut for long wavelengths. There are two possible explanations. The first is that the theory is wrong because the strong convection of fluid through the ablation layer is not properly accounted for.

The second explanation, that simulation code calculations are wrong, can also be argued for the low power ablations under discussion. Ablation layer analyses of varying sophistication performed on homogeneous, rather ideal situations such as treated in the simulations above,[6,8,9] generally agree that 0.1μ resolution or better is needed to resolve the details of the Rayleigh-Taylor unstable region for the low temperature-low z ablations of interest. The time dependent 2D and 1D piggy-back simulation models currently used to calculate the Rayleigh-Taylor growth do not resolve these scales effectively because the cost is prohibitive. This view might also explain the ambiguous no growth results of Brueckner, Jorna, and Janda[9] as situations where the growth was much smaller than expected.

Since neither explanation is compelling, the experimental guidance is lacking, and a definitive theory has so far eluded us, the next steps are to quantify the theory and remove the numerical restrictions which hamper time-dependent computations with the necessary resolution.

Another potential cause of instabilities on the surface of the shell arises because of the use of multi-shell targets. In order to suspend the inner shells from the outer ones, support membranes (webs) are being used. These membranes can cause inhomogeneities in the density distributions. The instabilities arising from these have also been studied in an idealized situation.

As a first step, we have used FAST2D in a slab geometry mode. Our initial profiles are the same as was used for our Rayleigh-Taylor studies.[6] In order to model the membrane, we have introduced an osculating, Gaussian density perturbation consisting of the same material as the slab (here, D-T).

All the FAST2D runs were performed on a 60 cell by 20 cell mesh. The length in the y-direction was 40μ corresponding to a resolution of 2μ. In the x-direction a 1μ resolution was used for the slab, and the grid was stretched both behind and in front of the slab in the x-direction. The laser flux was 10^{13} w/cm^2 and the slab and membrane were both composed of a 50-50 $D-T$ mixture.

A uniform amount of mass for each y-cell was distributed between two x-cells along the gaussian. Because of finite resolution and the grid stretching for large x, this uniform membrane appears as the irregular density perturbation in the upper left-hand corner of Figure C2.4. The density was chosen to be 0.125g/cc in the unstretched cells ($\Delta x = 1\mu$) as compared to 0.315g/cc for the maximum slab density. The five other profiles show the density surface at later times as labelled. One sees that a large "T-shaped" irregularity develops in a relatively short amount of time. A detailed study of the early timesteps shows that this mass flow arises from thermal conduction effects. Initially, the membrane is both colder and denser than its surroundings. Hence, the membrane heats and also loses mass. The heating is much more rapid, and this leads to a pressure profile that forces mass in towards the center in the y-direction and out away from the slab in the x-direction. This forms the characteristic "T-shape".

In Figure C2.5, the time development of two other cases is displayed. For the top sequence, the membrane density has been reduced by a factor of five. For the lower one, the

original density was used, but the membrane has been moved 5μ away from the slab. As can be seen, the prominent "T-shape" still develops, albeit, more slowly.

The first three mode amplitudes for two of the support web simulations are displayed in the next two figures (C2.6 and C2.7). The first is for the standard case where a maximum density of 0.125gm/cc was employed. Note that the growth rate is essentially exponential and that the relative magnitudes of the three amplitudes are very similar to our Raleigh-Taylor (R-T) simulations where an initial density perturbation is introduced instead of a membrane. For comparison, the approximate $k=1$ mode amplitude for our standard R-T case (see Figure C2.3) is represented by the solid line. The second figure is the same as the first except that it is for the reduced density ($\rho_{mem} = \rho_{mem}/5$) simulation. Here the magnitude of the mode amplitudes are comparable to our R-T ones.

We have shown in our simulations that the use of thin membranes (webs) to support inner shells of multi-shell pellets can lead to large deformations of the ablation layer which are certainly undesirable for acheiving thermonuclear burn. Hence, more detailed simulations, along with experimental studies, should be undertaken before a commitment to web-supported multi-shell targets is made.

Dynamic stabilization of the Rayleigh-Taylor instability in the ablation layer has been demonstrated for the case where the laser intensity is varied periodically.[1,2] The combination of this phenomenon with accelerative stabilization (if it turns out to be real) and the natural cutoff at short wavelengths should permit successful implosion of shells with a dynamic aspect ratio of 20 or 30 to 1. We are currently beginning investigations of dynamic stabilization of layered ablators where thin, higher-z layers temporarily interrupt the heat flow to produce the controlled oscillating acceleration.

Figures C2.8-10 summarize some of our recent dynamic stabilization calculations using the FAST2D computer code. The unstabilized control calculation is shown in the upper half of

each figure; the dynamically stabilized system is shown evolving in the lower half. The shell is composed of D-T treated as an ideal gas with $\gamma = 5/3$. The initial thickness of the shell was 20μ and the initial fluid (plasma) profiles were chosen close to quasi-static ID equilibrium to minimize initial transients. The outer surface of the shell was rippled with a linear combination of the 10 longest wavelength modes. This perturbation amounted to a 3.4% RMS thickness variation of the shell. The system was driven by specifying the temperature of the blowoff plasma at the critical density 0.004 gm/cm^3 to be 250 ev in the control case and to oscillate about this value at 1.25 cycles per nanosecond with an amplitude of 125 ev in the dynamically stabilized case.

The small plot in the lower left of Figure C2.8 shows the spatially averaged temperature at the grid points on the high density side of the average critical layer location plotted as a function of time. It also shows average shell velocities for the two cases versus time. The stabilizing oscillation was started at 1.37 nsec, a time just before the unstabilized case began to show organized linear growth. The unstabilizated case is shown as the dashed line. The unstabilized calculation was terminated at 7.2 nsec, as shown but the average shell velocity becomes a meaningless quantity somewhat earlier. The stabilized calculation ran somewhat longer and before shell breakup achieved a higher velocity by almost a factor of two. The laser finally breaks through in the longest wavelength mode supported by the system (40μ) in the "stabilized" case when most of the ablator has been burned away.

The upper part of Figure C2.10 displays the Fourier mode amplitudes of the mass integral through the shell. The + data refer to the mode of wavelength 40μ in the stabilized case. ΔM_k is the amplitude of the kth harmonic so 10^{-5} corresponds to a sinusoidal variation of ± 0.1μ when the shell density is 1 gm/cc. The 0 and data points refer to the first and second modes in the unstabilized case. Here the growth has continued unabated until mode amplitudes of $\Delta M > 10^{-4}$ are obtained. The corresponding deformation of the shell is shown at 5.8 nsec and 7.2 nsec in the upper portion of Figure C2.9.

The calculation was performed using 1μ resolution along the shell and 1μ resolution through the shell. The runs required $\sim$ 2500 timesteps and ran for about 14 minutes in the case of the $40 \times 40 = 1600$ grid point calculations shown.

To perform these dynamic stabilization calculations and to resolve the ablation layer structure well enough to study accelerative stabilization, our 1D plus piggyback model is being built on a fuly implicit hydrodynamics module called ADINC which allows timesteps much longer than the CFL condition would permit. Thus 0.1μ cells with sound speeds of order 10^7 cm/sec can be integrated stably with $\delta t \sim 10^{-11}$ sec. The model currently lacks an adequate treatment of strong shocks but is otherwise ideal for the purpose of investigating the dynamics and stability of quasi-static ablation profiles. A multi-material, many-layer shell is easily treated because of the Lagrangian description embodied for the shell and layer interfaces.

ADINC has been included in a 1D package that is presently being used to study our quasi-static ablation profiles.[6] Along with ADINC, this package contains a plasma thermal conduction routine, DIFFU1, and an initializer that allows for multi-material, many-layer shells. The thermal conduction for the mixture is handled correctly, and it's charge dependence is included.[10]

One of the most important aspects of the design of a successful laser-powered thermonuclear energy source is the ablation layer. This region must absorb and conduct the laser energy. This must be done efficiently and in a stable manner in order to allow for maximal heating of the fuel. The thickness of the ablation region, its shape, and its composition must be determined by simulation and experiment.

As a first step in simulating burn through of the ablation region, a one-dimensional, multi-material, plasma thermal conduction code DIFFU1, has been written. This has been coupled with a one-dimensional hydrodynamics code for detailed analyses of laser burn through of thin membranes.

DIFFU1 was first tested by comparing our numerical results for a simple case that has an analytical solution. This was done for the case of constant density, initial temperature and thermal conductivity. The right boundary temperature was specified according to the analytical solution:

$$T = T_o \left[\frac{r + V_o t}{r_o} \right]^{2/5} . \tag{3}$$

The thermal "shock" that is driven by this temperature profile has a constant velocity given by:

$$V = \frac{4 K_o T_o^{5/2}}{15 \rho r_o} . \tag{4}$$

A comparison of the numerical results generated by DIFFU1 and the analytical ones of Eqs. (3) and (4) are shown in Fig. C2.11 along with the parameters used. Both the "shock" position and temperature profiles are reproduced accurately.

In order to test the multi-material capabilities of this code we have repeated the thermal "shock" test, but with the introduction of a 1μ thick membrane in the plasma. As seen in Figure C2.12 this has been done for glass (S_iO_2), copper, and gold, all materials under active consideration for use. We have assumed that all materials are fully ionized. As expected, the highest Z material, gold, causes the greatest change from the pure D-T (no membrane) case that is also shown.

Although no simple analytical solution now exists for this problem, the numerical results certainly appear reasonable. Since the velocity is proportional to $K_o / \hat{N}$ which goes like $1/Z^2$ the burn through is slowest for gold. However, at large distances from the slab all the results seem to display approximately the same velocity with a time delay based on the material and the slab thickness.

We have shown in Figure C2.12 how the burn through delay of a thin plasma slab is dependent on its composition. A new series of runs was performed on glass to see how the burn through rate depended on slab thickness, and to study the effects of the slab at large distances.

In the accompanying Figures C2.13 both the "shock" position as a function of time, and temperature profiles are plotted for three cases as denoted. As expected, thickening the slab enhanced the retarding effects on the burn through. Also, for both slab thicknesses, it can be seen that the differences persist at large times and distances.

As can be seen from simple analytical arguments, the velocity of the thermal "shock" should approach the no-slab value far away from the slab. This can be seen to be verified by comparing the slopes of the three "shock" position curves at large times. However, neither the "shock" position nor the temperature profiles ever return to their no-slab values.

Preliminary results using the combined DIFFU1-ADINC implicit package have been encouraging. For example, one of our quasi-static profiles[6] has been shown to survive 1,000 timesteps (~ 10nsec) with very minor changes when simulated in a realistic time dependent way. Thus the simulation model and the analysis are consistent, the model is accurate, and the quasi-static approximation seems very appropriate.

A direct energy deposition algorithm has been added to the FAST2D code. This has been done by adding a source term into the thermal conductivity routine DIFFUT. Specifically, a time-dependent two dimensional flux has been introduced. The *x*-dependence, *y*-dependence, and time-dependence are all handled separately.

Presently, there are several different options available for generating the time evolution of the flux. These include linear, gaussian, and exponential growths. Of course, any more complicated evolution that might be needed to simulate realistic situations (such as a pre-burn pulse) can also be handled. A sinusoidal time-dependence can be utilized to further study dynamic stabilization effects on the Rayleigh-Taylor instabilities.

We have been performing all of our simulations with uniform illumination in the *y*-

direction. However, a more realistic Gaussian profile is available. Also, the region of illumination can be limited to simulate the plug burn-out experiments currently being performed at NRL. Finally, controlled perturbations of the laser intensity can simulate inhomogeneities that exist in all laser pulses, and the instabilities arising from them can be studied.

It is assumed that all of the flux absorption occurs in a region around the critical density, ρ_{crit}, (0.004 gm/cc for D-T). We distribute the flux linearly in the x-direction in the two cells between which $\rho = \rho_{crit}$. When he critical density goes across a cell boundary, a very steep rise occurs in the flux of the newly illuminated cell. A special algorithm has been written to smooth out this transition and hence dampen any thermal shocks that develop in non-physically due to the code resolution.

The multi-material capability of FAST2D has been partially implemented. Up to three different materials can be utilized simultaneously. The equation of state can handle both the ion and electron partial pressures. The temperature has been converted from the awkward $\frac{\text{cm}^2}{\text{sec}^2}$ unit to the more standard e.V. unit which is appropriate for mixtures. We have developed a simple formula for calculating the thermal conduction coefficient of a mixture. The derivation starts from the ion-electron Coulomb collisions and leads to a simple charge and density dependence for the thermal conductivity. This has been implemented, along with the charge dependence discussed, for example, in Spitzer.[10]

The major modification remaining involves allowing for the x- and y-dependence of the thermal conductivity when solving the heat equation in DIFFUT. Based on our experience with DIFFU1, a 1D plasma thermal conduction code where this change has been implemented, this modification will be straightforward. An example of the multi-material capability of DIFFU1 can be seen in Fig. C2.12.

Section C2. References and Footnotes

1. J. P. Boris, *Comments on Plasma Physics and Controlled Fusion* **3** 1 (1977) 1, also see NRL Memorandum Report 3427, 1976.

2. J. P. Boris, *Bull. Am. Phys. Soc.* **22** 4 (1977) 608, also Eastern Audio Association, Inc. Cassette Proceedings.

3. J. P. Boris, "Numerical Solution of Continuity Equations," Proc. of the Second European Conference on Computational Physics, Garching, 27-30 April 1976, (Published by North-Holland), also NRL Memorandum 3327 (1976).

4. S. E. Bodner et al., "Inertial Confinement Fusion at NRL," Paper B3, IAEA 7th International Conference on Plasma Physics and Controlled Nuclear Fusion Research, Innsbruck, Austria, 23-30 August 1978.

5. J. P. Boris and J. H. Orens, "Rayleigh-Taylor Stability in the Pellet Ablation Layer," Conference on Laser and Electro-Optical Systems, San Diego, CA, 609 February 1978.

6. J. H. Orens, et al., *Bull. Am. Phys. Soc.* **22** 9 (1977) 1180, and **23** 7 (1978) 750.

7. Y. F. Afansa'ev, et al., *JETP Lett.* **23** 11 (1976) 506.

8. F. S. Felber, *Phys. Rev. Lett* **39** 2 (1977) 84.

9. K. A. Brueckner, S. Jorna, and R. Janda, *Phys. of Fluids* **17** 8 (1974) 1554.

10. Lyman Spitzer, Jr., *Physics of Fully Ionized Gases,* Interscience Publishers, 1967, pp 144-145.

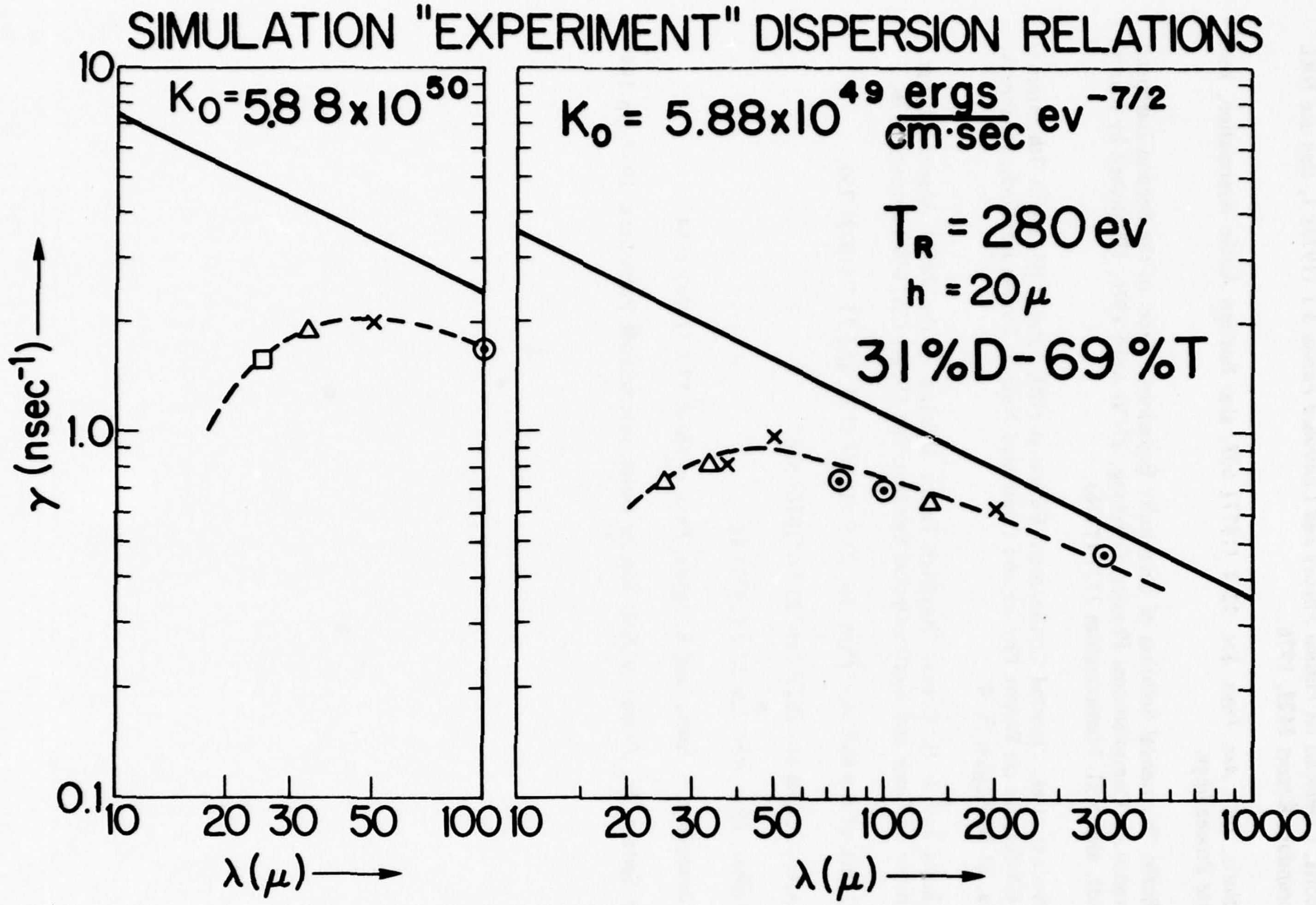

Figure C2.1 Dispersion relations depicting growth rate γ versus wavelength λ for the external (ablation layer) Rayleigh-Taylor instability as computed by the FAST2D computer code. Two different values of the thermal conductivity are used.

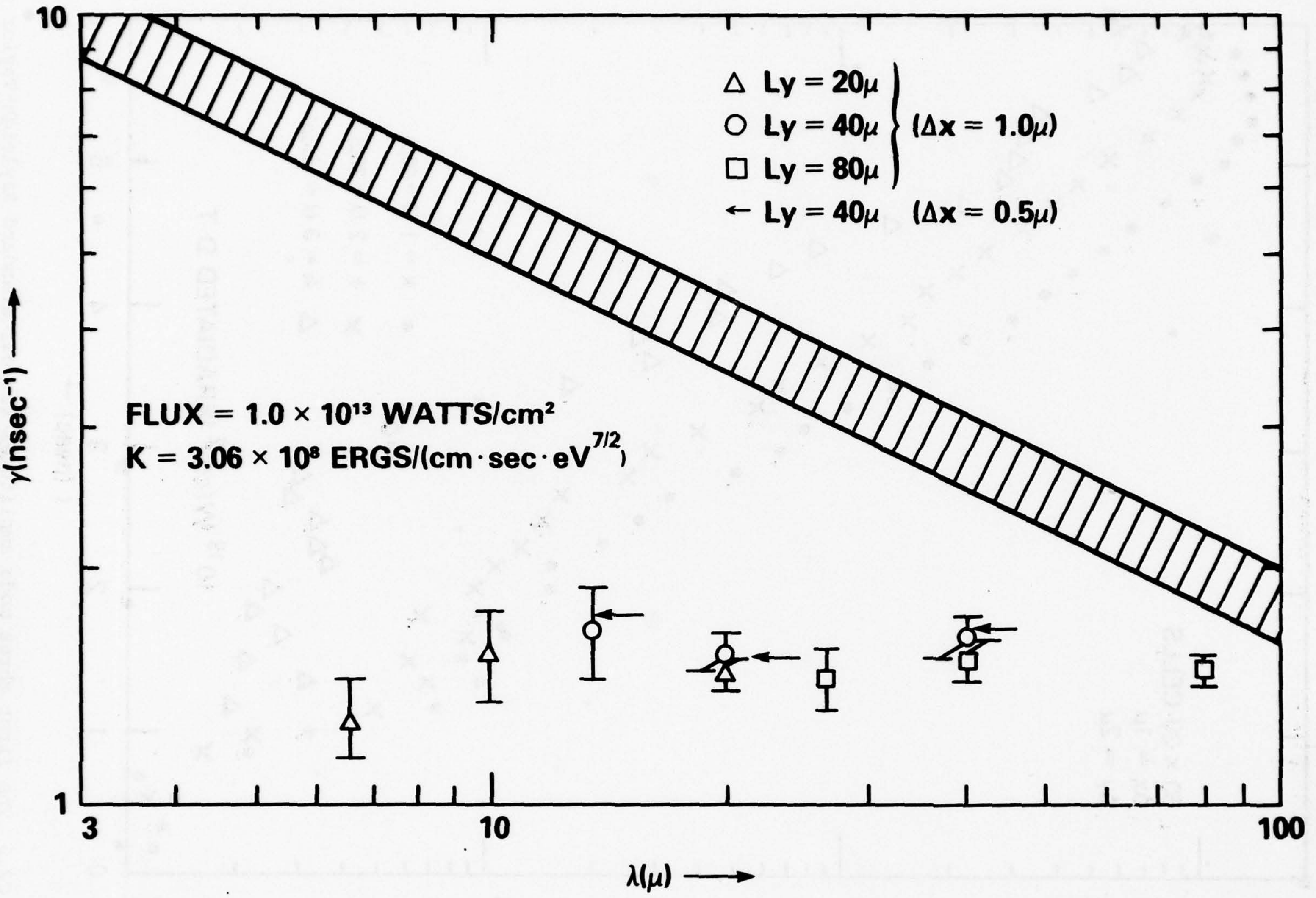

Figure C2.2 Convergence tests of the ablation layer Rayleigh-Taylor dispersion relation showing short wavelength cutoff and growth rates depressed below the classical value.

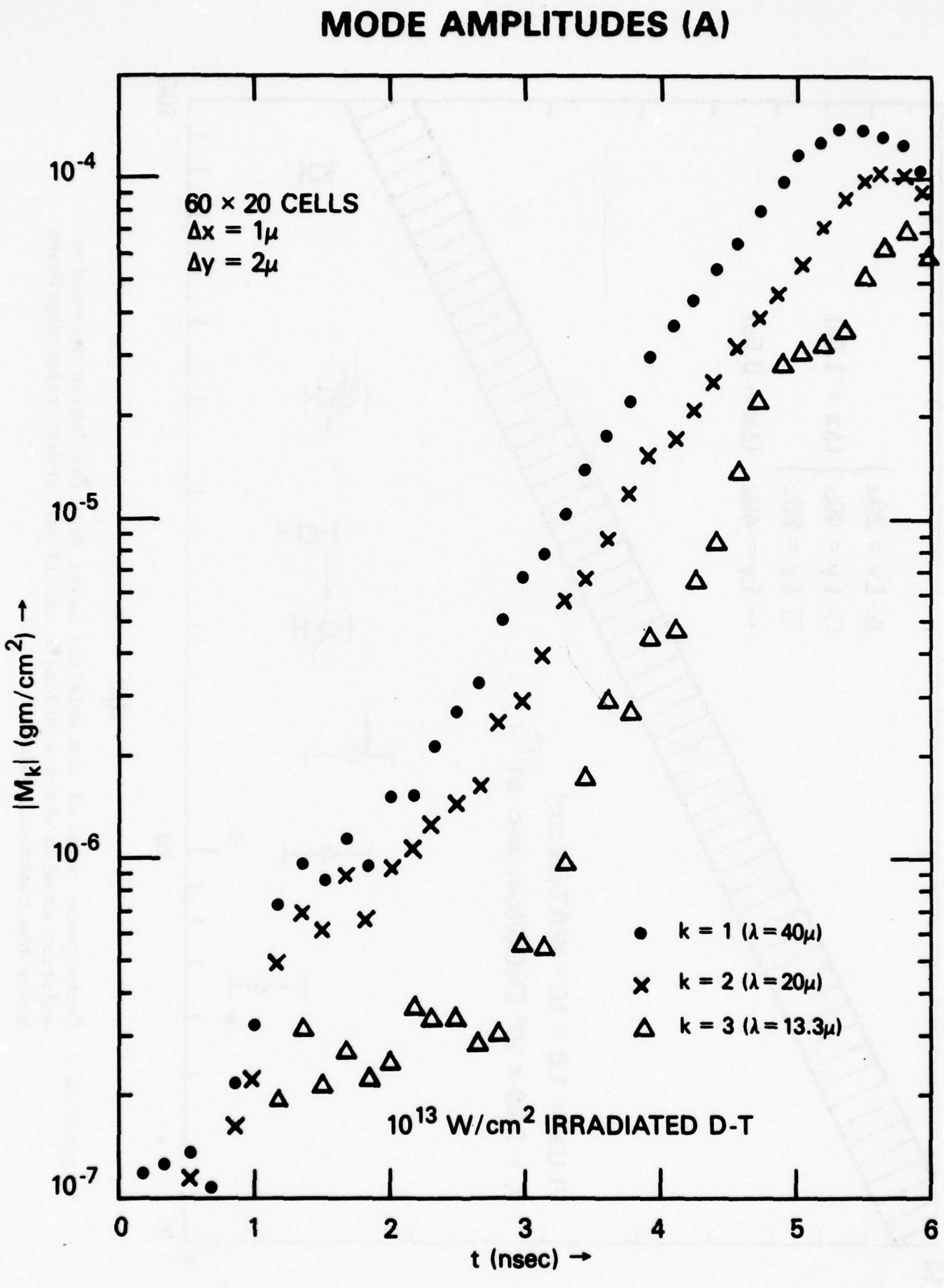

Figure C2.3 The first three mode amplitudes for our standard Rayleigh-Taylor case. Exponential growth occurs roughly in the region from 2-4 nsec. Straight line fits and hence approximate growth rates can be easily deduced here.

RAYLEIGH-TAYLOR INSTABILITIES GENERATED BY A SUPPORT WEB

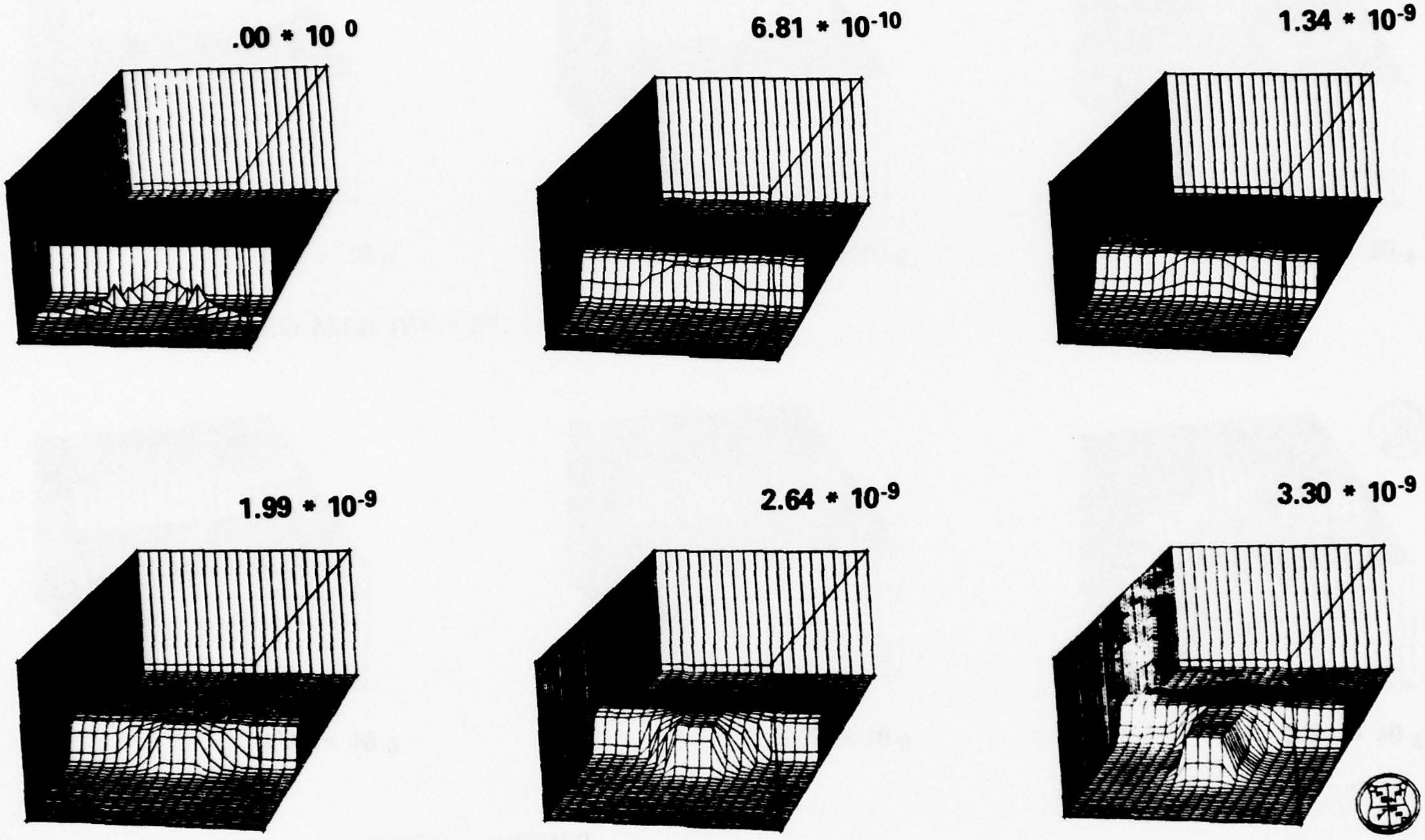

Figure C2.4 Time evolution of a D-T slab irradiated by 10^{13} w/cm^2 when an osculating support web is present. The maximum slab density is .315 g/cc and the maximum web density is .125 g/cc.

SUPPORT WEB (CONT.)

REDUCED WEB ($\varrho_{MEM} = \varrho_{MEM/5}$)

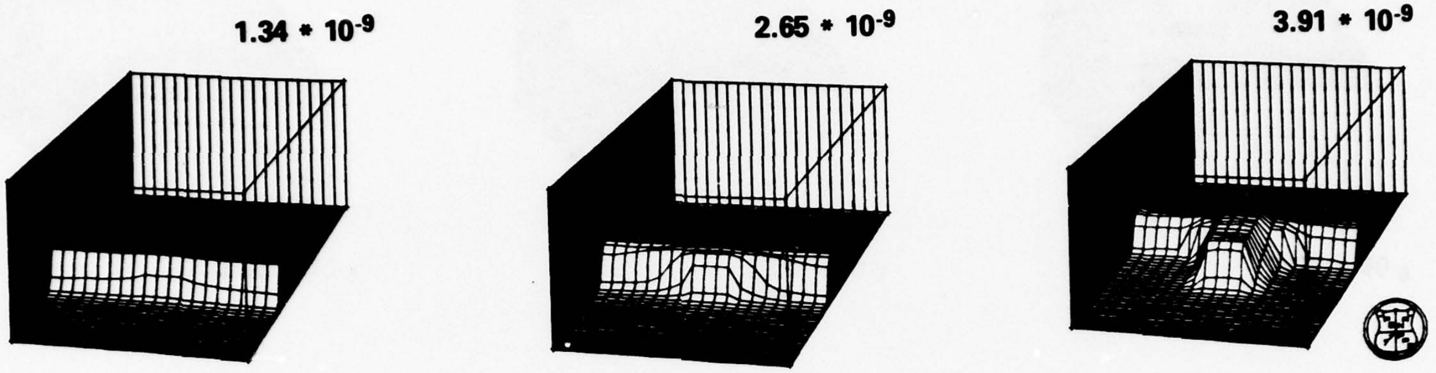

DISPLACED WEB ($\Delta x = 5\mu$)

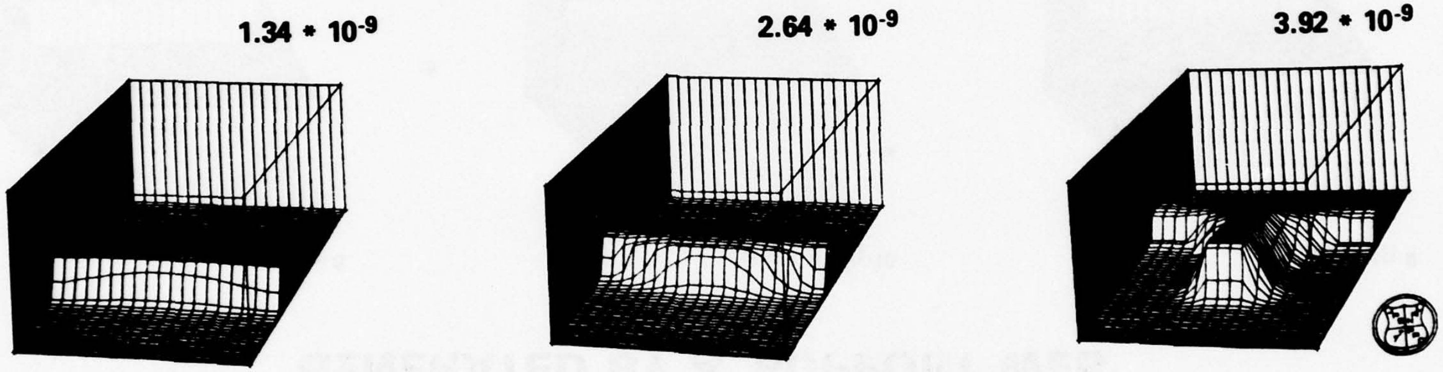

Figure C2.5 Same as Fig. C2.4 except that for the top sequence the web density has been reduced by a factor of 5, and in the bottom one, the web has been displaced by 5μ.

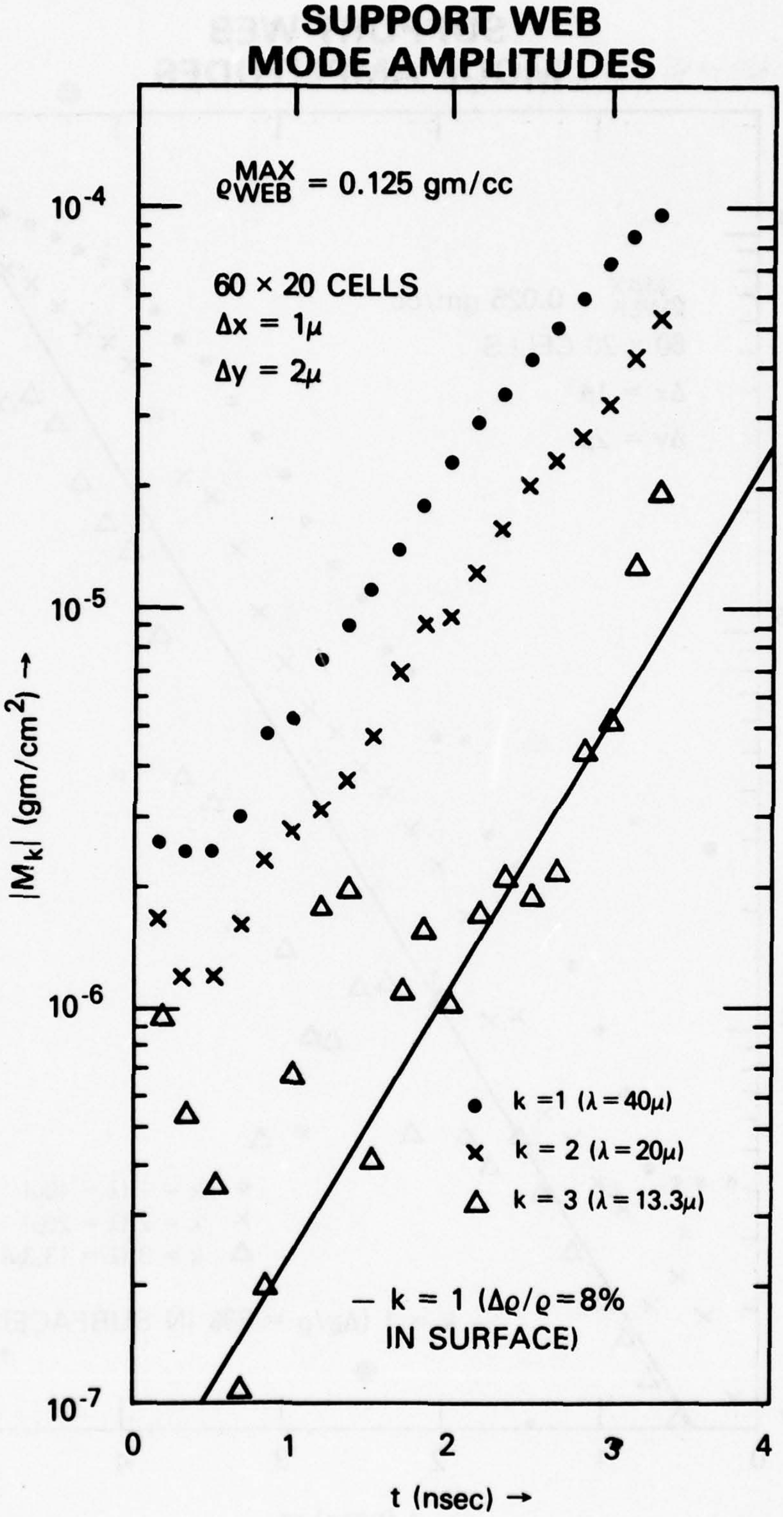

Figure C2.6 Growth rates from our standard support web simulation. Note the linear growth for t ≳ 1 nsec. The k = 1 amplitude of Fig. C2.3 is represented as the straight line for comparison.

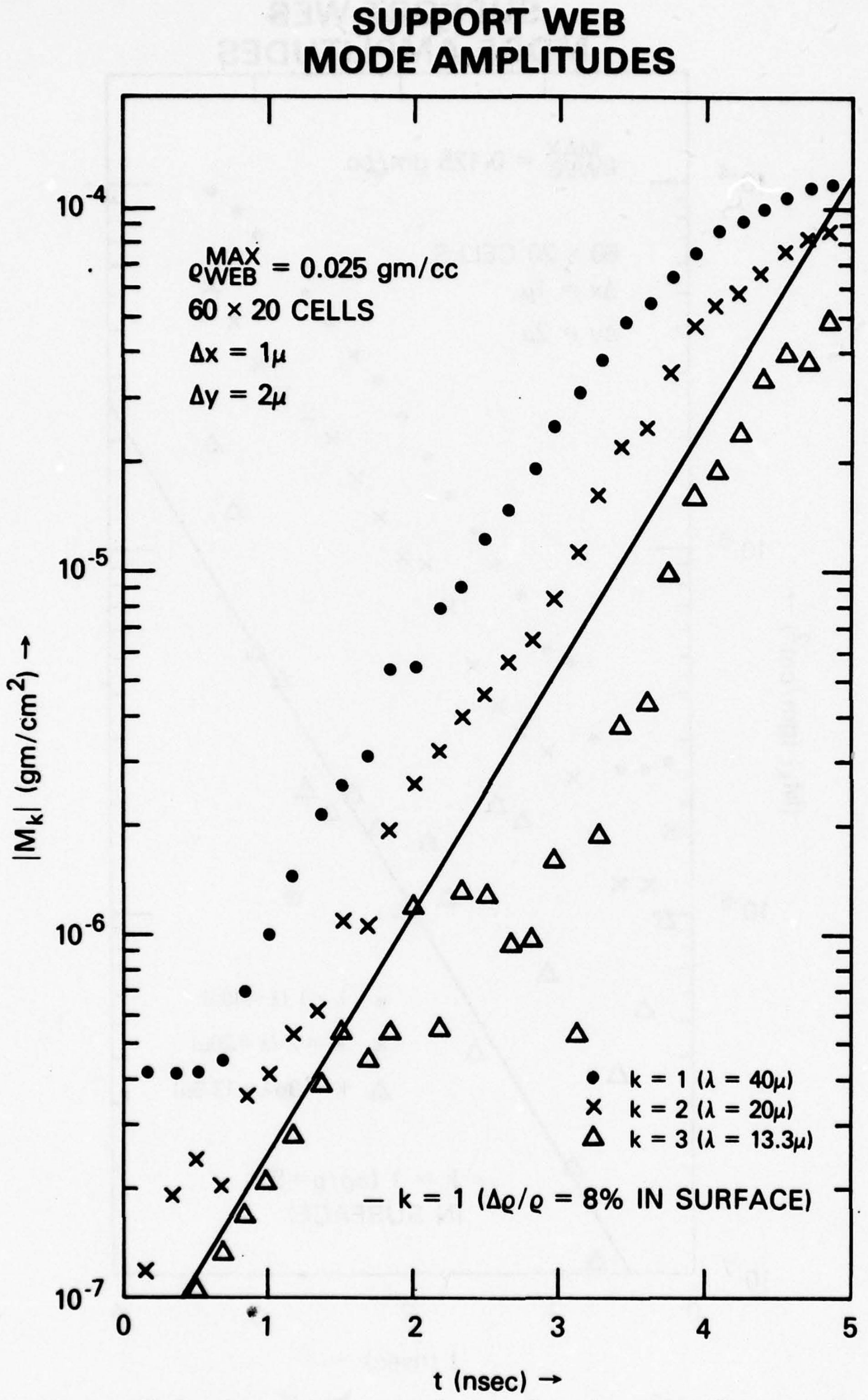

Figure C2.7 Same as Fig. C2.6, but for the reduced membrane. Here $\rho_{web}^{max} = \rho_{web}^{max}/5$.

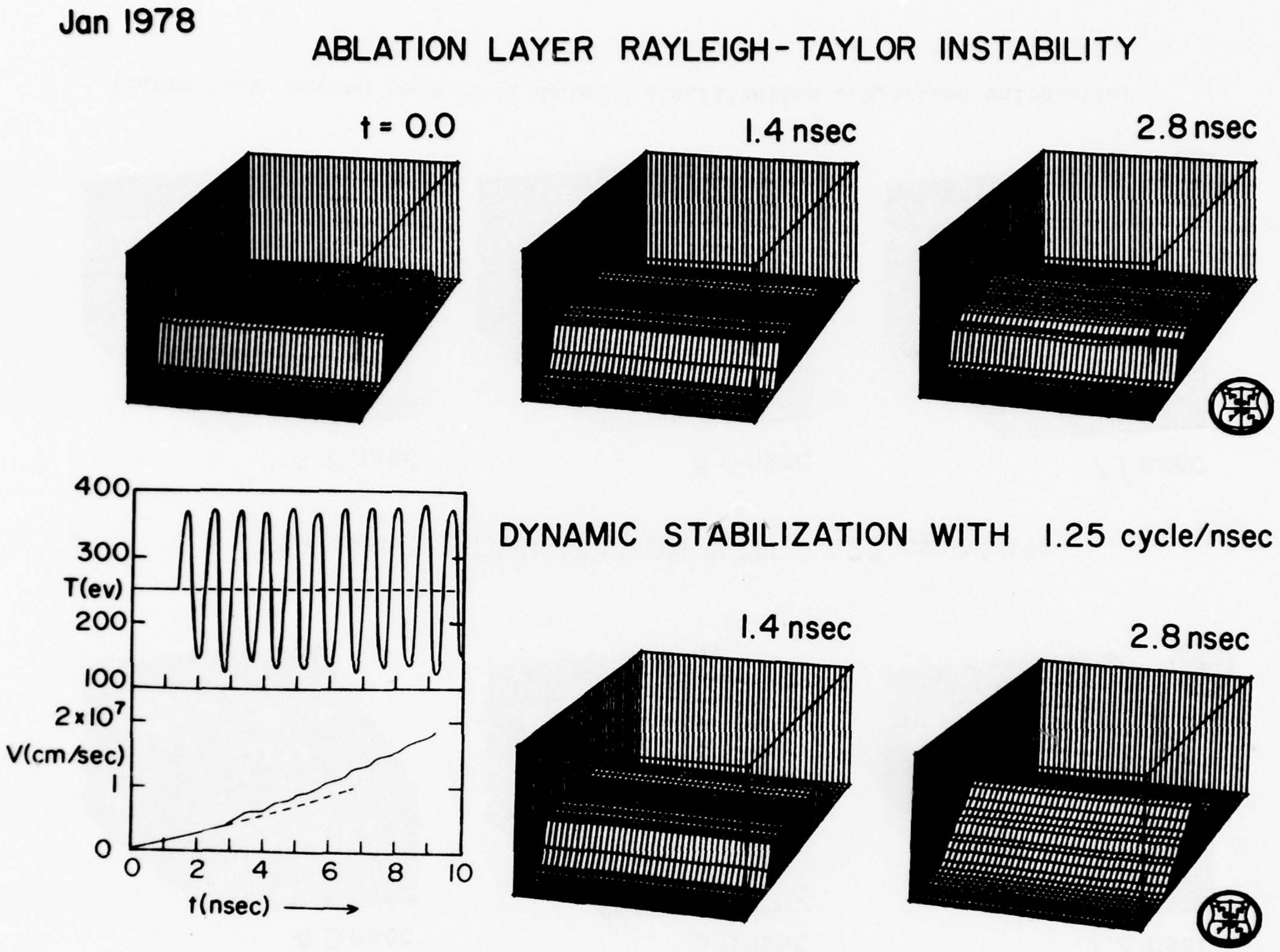

Figure C2.8 First segment of a comparison between a dynamically stabilized implosion and an otherwise identical unstabilized one. Roughly twice the useable shell velocity was obtained in the dynamically stabilized case.

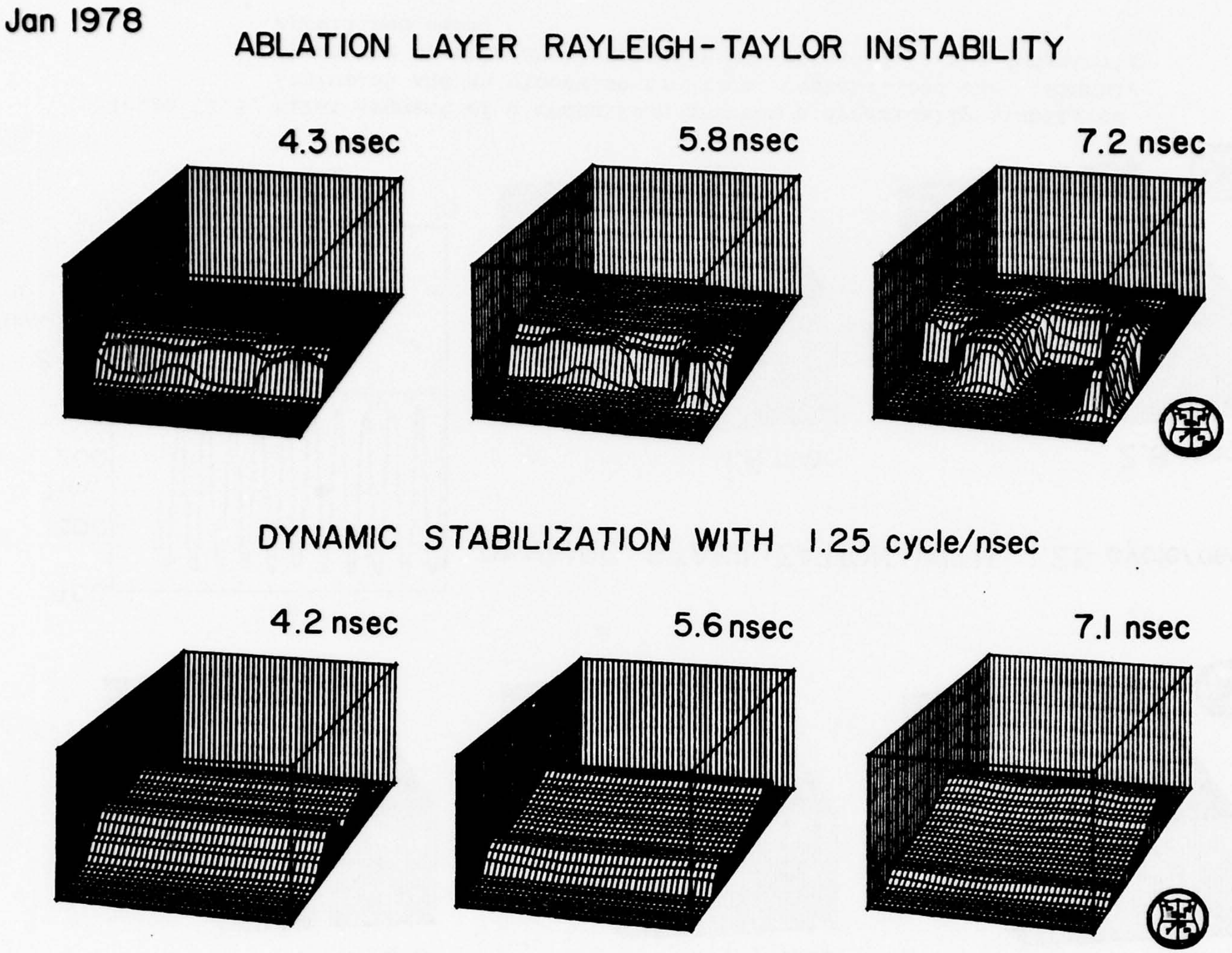

Figure C2.9 Second segment of dynamic stabilization comparison calculation.

Jan 1978

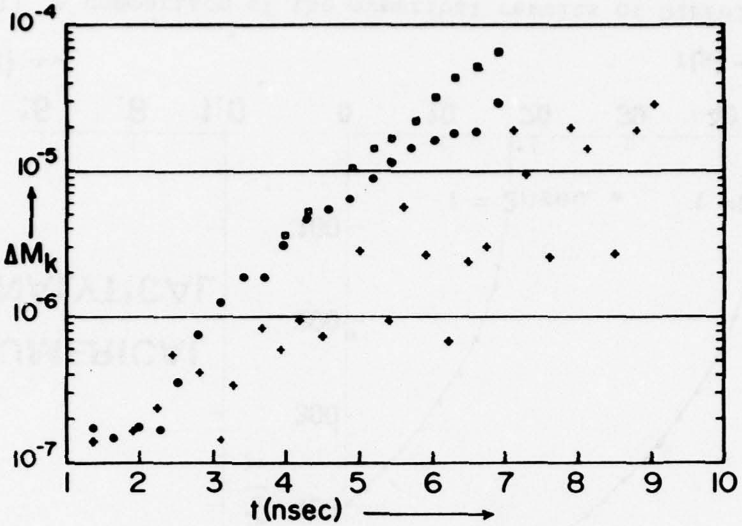

DYNAMIC STABILIZATION WITH 1.25 cycle/nsec

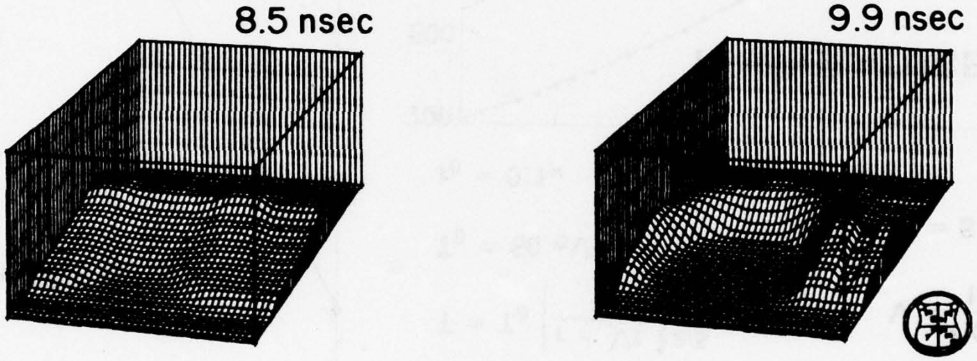

Figure C2.10 Final segment of dynamic stabilization comparison calculation.

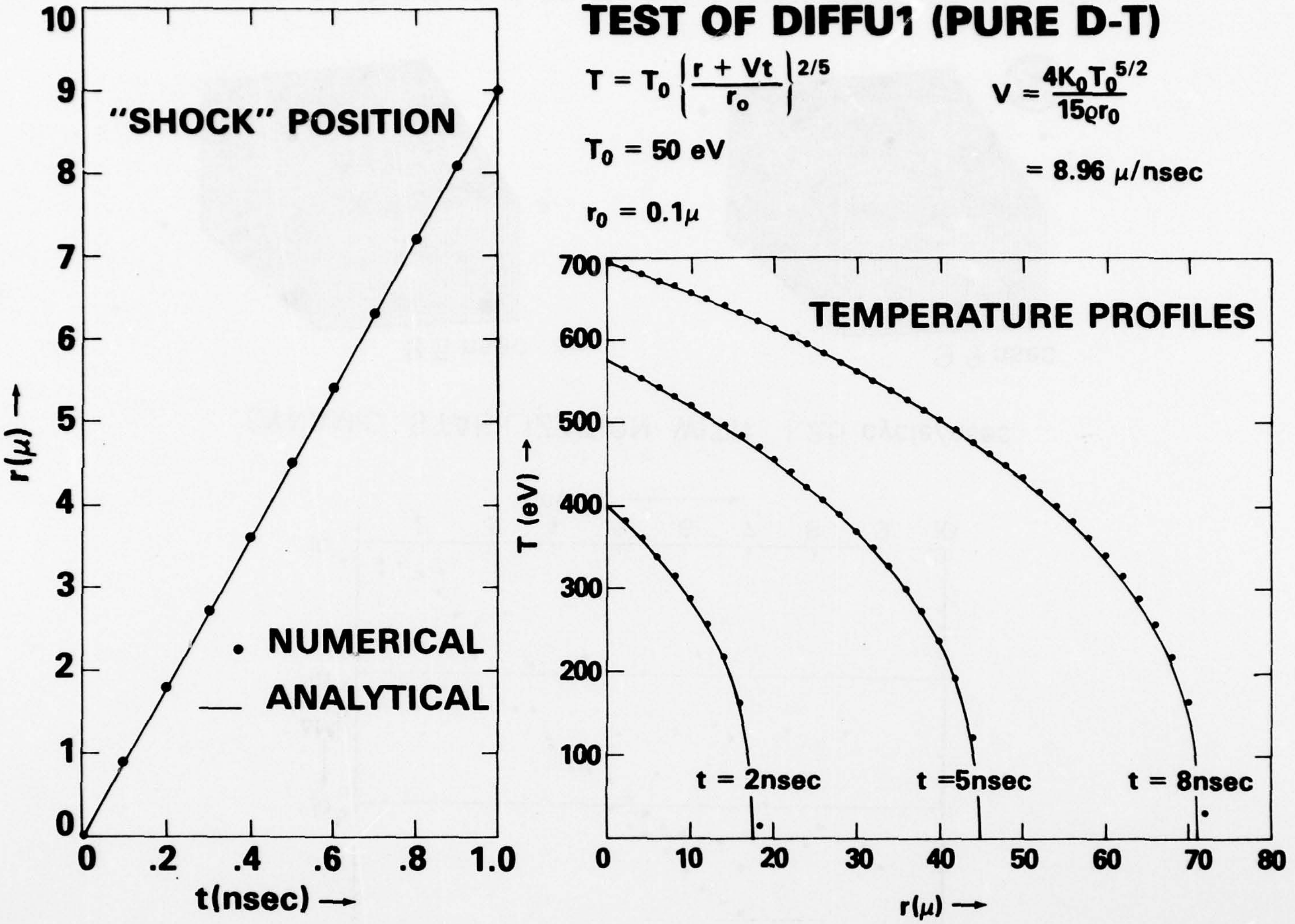

TEST OF DIFFU1 (PURE D-T)

$$T = T_0 \left\{ \frac{r + Vt}{r_o} \right\}^{2/5} \qquad V = \frac{4K_0 T_0^{5/2}}{15 \varrho r_0}$$

$T_0 = 50$ eV

$= 8.96\ \mu/\mathrm{nsec}$

$r_0 = 0.1\mu$

Figure C2.11 A comparison of the numerical results of DIFFU1 with the analytical solution for the test calculation described in the text.

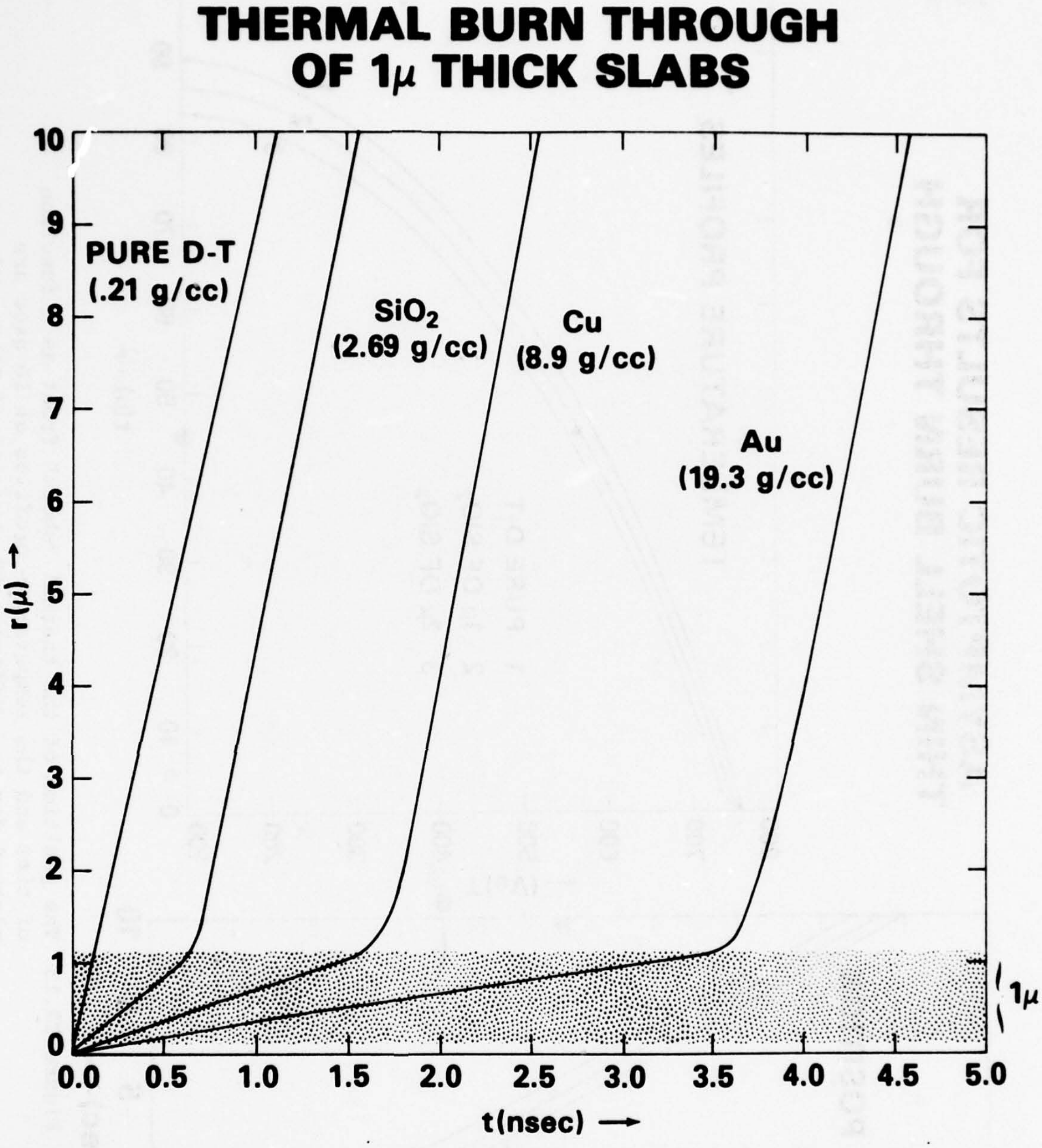

Figure C2.12 The "shock" position as a function of time similar to Fig. C2.11, except that a 1μ thick slab of different materials has been introduced (shaded area). The materials used and their densities are as labelled.

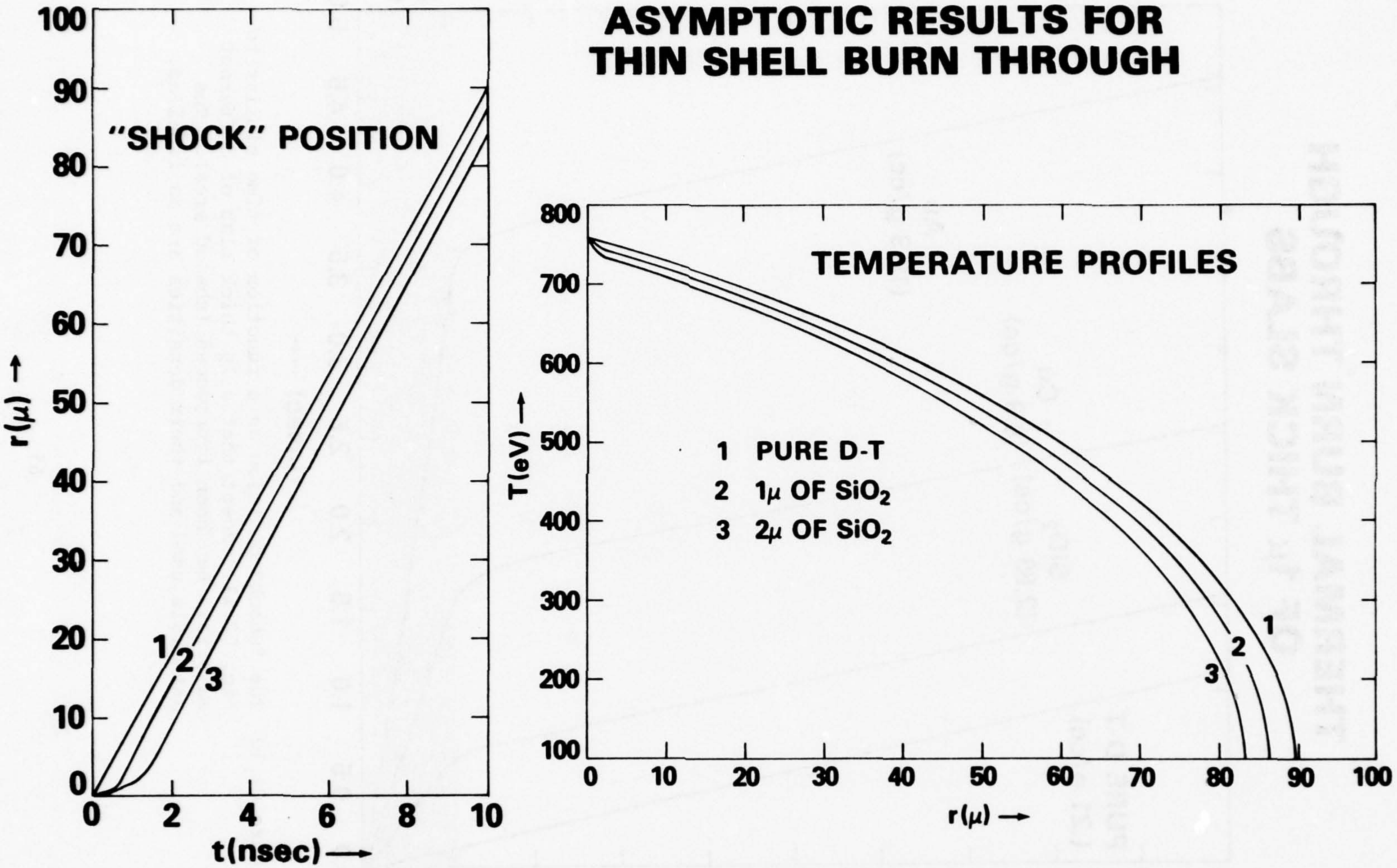

Figure C2.13 The position of the thermal "shock" front as a function of time and the temperature profiles at 10 nsec are plotted for two different thicknesses of glass and compared to the pure D-T case.

D. Rayleigh-Taylor Instability at Internal Material Interfaces

Realistic numerical calculations of the Rayleigh-Taylor instability at interior material interfaces require accurate advancement of the material interfaces. This requirement favors the use of a Lagrangian formulation because Eulerian techniques must either employ special procedures to locate an interface or use excessively fine gridding to resolve it. Unfortunately these procedures are not only cumbersome and time consuming, but result in a numerical diffusion which can grow large enough to mask the physical motion of the interface.

The price that is paid for ease in locating an interface in a Lagrangian treament is a distorted or skewed grid in all but the simplest of flows. As shown in Figure D1, even simple shear must result in grid distortion. Figure D1a illustrates the initial grid to either side of a shear layer. In the simplest case all the zones on either side of the shear layer are moving with a uniform relative velocity with respect to the zones on the opposite side. Figure D1b shows the grid at a slightly later time when the distortion has become appreciable. Difference equations for derivatives at interface vertices no longer involve the closest neighbors of a vertex since its former neighbors have been shifted by the shear. An orthogonal grid could be recovered at this time by replacing all skewed grid lines by vertical lines. However, reconnecting any one grid line results in one triangular cell and one pentagonal cell instead of two quadrilateral ones as indicated by the dotted reconnected line. Therefore, successive grid line reconnections can result in a uniform quadrilateral mesh in this case only for a infinitely long (periodic) mesh. In general this means that grid reconnections for a quadrilateral mesh must be global and can result in a quadrilateral mesh only for perodic grid anomalies.

In contrast, if a triangular grid is used, any reconnected grid line must result in two triangles as shown in Figures D1c and D1d. In other words grid anomalies can be resolved locally without recourse to global rezoning and cannot result in changing the character of grid zones. Vertices can also be added or deleted where required to maintain resolution with only local grid changes. In other words, it is possible to dynamically alter a triangular grid at a given location with the effects of the alteration being felt only by the vertices near that location.

This fact opens up the possibility of conserving physical variables locally even during grid restructuring. In the hydrodynamics code SPLISH this goal is attained through the use of conservation laws expressed as integrals over regions about each vertex and over triangles or pairs of triangles. Grid reconnections, vertex additions or vertex deletions result in the unambigious definition of new cell quantities through the use of these integral invariants. Regridding algorithms can therefore be formulated which are completely automated and local and which preserve conserved physical variables.

During the past year the regridding algorithms in SPLISH have been completely rewritten to accommodate material interfaces, since the original code was designed for a homogeneous fluid. This extension is not trivial since grid lines cannot be reconnected if they lie along interfaces. To preserve a regular grid, therefore, judicious use must be made of vertex addition and deletion routines to add or subtract vertices from the interface both to preserve resolution and to relieve local stretched triangles bounding interface grid lines. The routines necessary for this additional logic have been written and used in numerical simulations, which will be described below.

The tremendous flexibility gained through the use of a dynamically restructuring triangular grid also has its price. Global ordering was abandoned to allow reconnections, but it is precisely that ordering which is necessary in the fast Poission solvers available for quadrilateral grids. There has been virtually no effort made in the numerical community in constructing fast solvers for an irregular triangular mesh, and the triangle code suffers a corresponding decrease in computational speed. A potentially greater problem results from the loss of a one-to-one correspondence between mesh cells and vertices. As has been shown before[1], this results in a grid which can inhibit the physical flow if the grid variables are not properly positioned. Figure D2 illustrates the problem for the case of a simple vortex. A vertex at the center of the vortex has zero mean velocity as do vertices far removed from the vortex. Therefore there must exist a ring of vertices which have a maximum velocity and are therefore moving in a shear flow with respect to vertices radially displaced from it. In the figure a triangular cell is drawn for the grid. In standard quadrilateral difference schemes the divergence in the fluid is controlled by adjusting the pressure at the center of the quadrilateral. For an incompressible fluid the area of the quadrilateral is therefore maintained at a fixed value. In the triangular case there are more triangular cells then there are vertices. Using pressures centered in triangles results in having too many pressures which overdetermines the vertex advancement required to maintain triangle area. In Figure D2, a vertex having the maximum velocity is being forced toward a triangle side. Any attempt to maintain the triangle area *must* result in lowering the velocity of that vertex relative to the other two triangle vertices. This clearly perturbs the vortex motion which these Lagrangian vertices are supposed to model. Therefore placement of pressures at triangles centers in this formulation *must* numerically result in altering the physical flow. This unfortunate result can easily be avoided by placing pressures at vertices and instead maintaining a "vertex volume" as a measure of divergence. Attempts to use triangular grids with improperly positioned physical variables in the past have led to the labelling of triangular grids as "stiff" due to exactly this problem. In Figure D2, the vortex motion is modified into a flow more closely resembling rigid body rotation, since in this case only rigid body motion can maintain the triangle area exactly. The temptation to borrow from difference schemes formulated for quadrilateral grids remains very strong, however, to the extent that triangular codes are presently being used and constructed in the DOE community which employ this improper positioning of physical variables.

The fact that care in defining the numerical algorithms can result in the physically correct generation of vorticity is best shown by a current simulation using the updated SPLISH code. As shown in Figure D3, the restructuring grid makes it possible to follow the Rayleigh-Taylor modes well into the turbulent regime.

The calculation, shown for two fluids of density ratio 2:1, is patterned on the situation of an ablator (below) accelerating a heavier pusher (above). The free surface above the pusher models the gas region at the center of filled microballoons. During implosion these interfaces are generally quite cold so the thermal conduction smoothing effects should be small. Convective stabilization, as it occurs in the ablation layer, is absent and the density changes in time will be small as well. Thus the classical Rayleigh-Taylor problem is a good starting place and the turbulent mixing theories[2] should be applicable here if anywhere.

Figure D3a shows the initial grid of triangles with a small sinusoidal perturbation of the interface at $t = 0$. The initial velocities (in the accelerating frame of reference) were all taken to be zero. Figure D3b shows the flow field as the instability enters its nonlinear phase. The vertex locations are plotted at successive timesteps to give streaks whose length is proportional to the local fluid velocity. Shear flow is established as the interface steepens, giving rise to vortices centered on the interface in a flow which has been likened to the onset of the Kelvin-Helmholtz instability.[3] In Figure D3c the two fluids are beginning to mix in the Rayleigh-Taylor vortices and by Figure D3d the vortices have entrained enough lighter fluid to form "bubbles" which are about to be completely enveloped by the heavier fluid.

Figures D3a and D3d illustrate the computational grid being used at the timesteps shown. Near the end of the calculation (Fig. D3d) most of the grid carried by the lighter fluid has flowed out from below the downward jetting heavier fluid. Similarly, verticies in the heavier fluid have been deleted above the upwelling lighter fluid. A reasonable resolution has been maintained by adding other vertices, particularly along the interface. Originally the interface was resolved with 10 vertices, but 46 were required by the end of the run. New regridding routines are still needed to permit the attachment of fluid through an intervening thinned layer, as shown in Fig. D3d. The heavier fluid has not touched the bottom but rests upon extremely thinned and skewed triangle in the lighter fluid. The presence of these near-zero area triangles has terminated the calculation due to violation of the Courant condition. Similar problems will soon arise at the free surface near the upwelling lighter fluid and at the "bubbles" which are about to be formed in both vortices.

Figures D3c and D3d also illustrate a potential jetting problem which occurs in thin layer Rayleigh-Taylor systems. In Figure D3c the motion of the heavy fluid into the downward jet from both sides creates a dynamic pressure maximum jetting fluid upward as well. This motion is stable in the sense that in Fig. D3d the jet is collapsing, creating large amplitude waves at the free surface. The stability of this surface perturbation is sensitive to the thickness of the layer of heavy fluid and may become unacceptable for thinner layers. Alternatively, the perturbation shown here may become unstable at a later time when the profiles or the acceleration have changed.

Larger, more finely resolved calculations will be performed to evaluate the rate of progression of heavy fluid through the light fluid and the quasilinear effect of average interface broadening on the growth of longer, potentially more disruptive modes. We will also try to identify flow regimes in which jetting may contaminate the fuel.

Work was also begun during the past year in the formulation of a compressible Cartesian code using the same integral invariant techniques used in SPLISH. The most attractive method involves the evolution of the divergences about a vertex through the continuity equation with the densities determined from the equation of state. Once again vertex pressures are used to advance vertex positions required to obtain those values of vertex divergence. The method in particularly attractive because the pressure is well behaved across material interfaces, whereas the densities are discontinuous. Standard numerical lore obtains densities from an updated continuity equation and derives the pressures from the equation of state. Our approach is therefore opposed to standard techniques, but offers considerable incentive in terms of stability and ease of formulation for the triangular grid. Because of its radicalness, a one-dimensional code, the ADINC module discussed in Section C, has been written to test the concept before implementing it on the triangular grid.

Section D. References and Footnotes

1. M. J. Fritts and J. P. Boris, Solution of transient problems in free surface hydrodynamics, accepted for publication in *J. of Comp. Phys.* An early version appears as NRL Memorandum Report 3446, 1977.
2. S. Z. Balen'kii, and E. S. Fradkin, Proc. Lebedev Inst. 29 (1965) 197.
3. S. Chandrasekhar, *Hydrodynamic and Hydromagnetic Stability*, Clarendon Press (1961) 428.

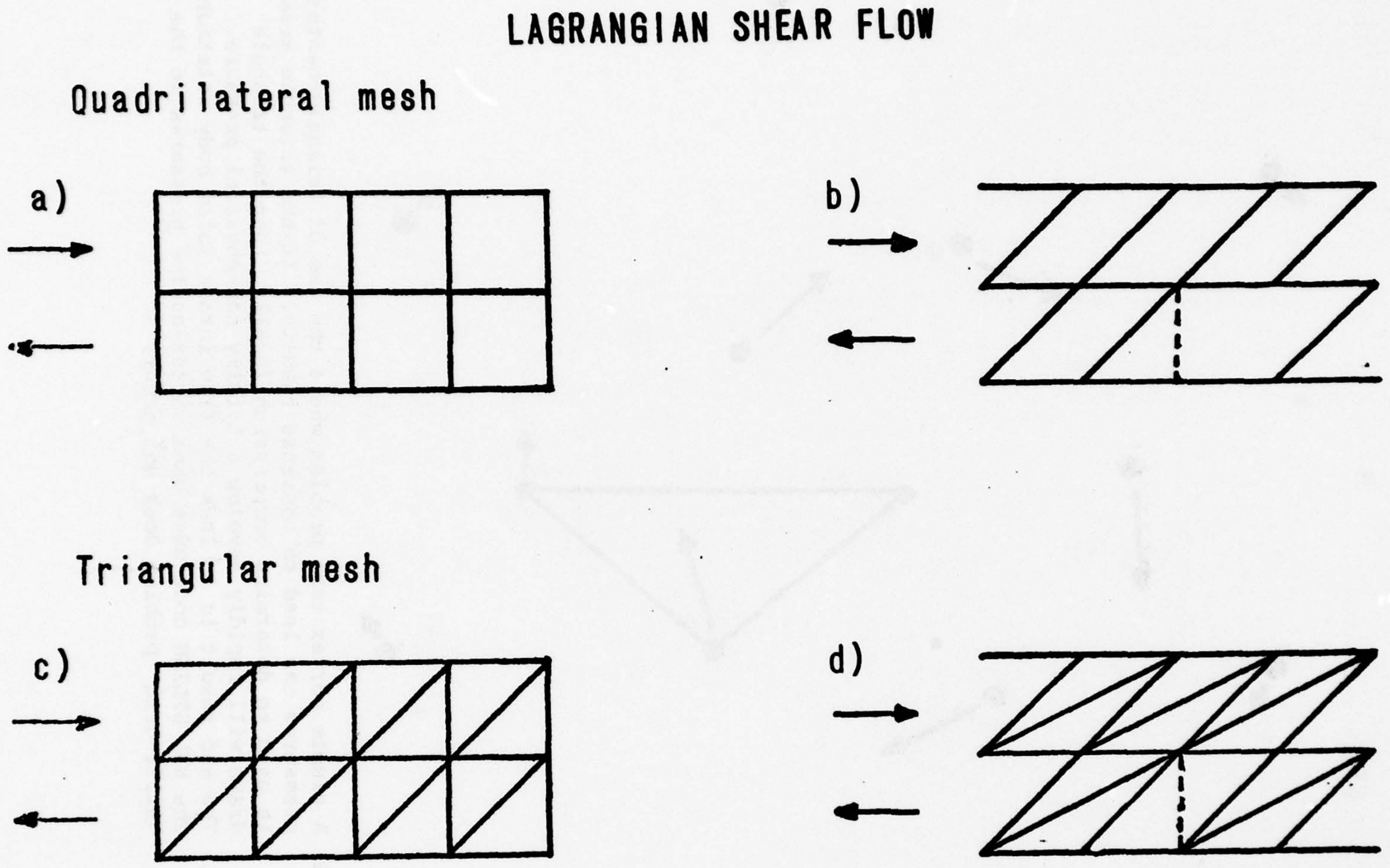

Figure D1 Comparison of possible reconnection procedures for a rectangular mesh and a triangular mesh in strongly sheared flow. Triangle reconnection is always possible. Rectangular reconnection leaves one triangle and one pentagon--an undesirable configuration.

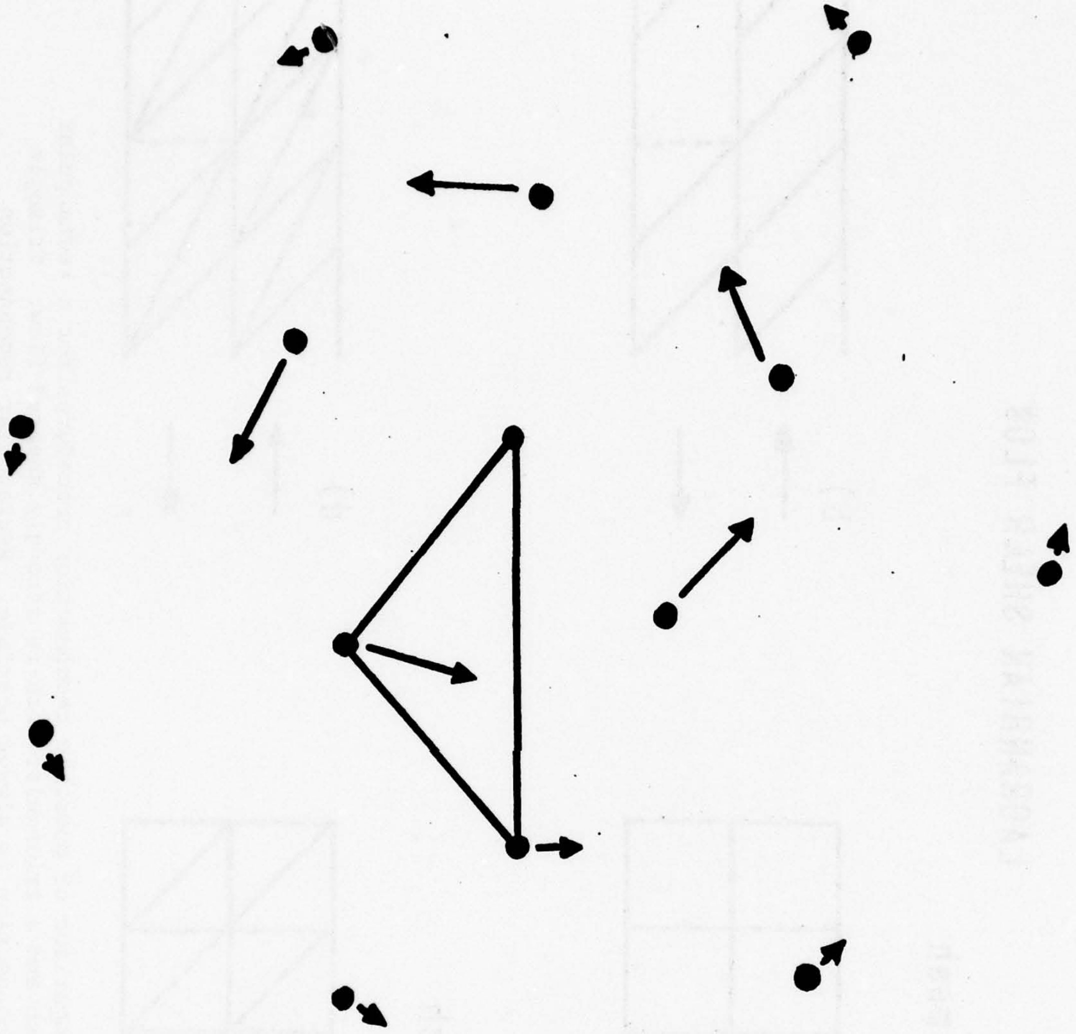

Figure D2 A simple vortex test problem where the use of triangle-centered pressures can lead to nonsense results. If the triangle area is used to determine compression locally, then the triangle drawn will rapidly develop a totally non-physical pressure. The end result is to lock the flow into a solid body rotation. The NRL SPLISH code uses uses vertex-center pressures so the "stiff grid" problem does not occur.

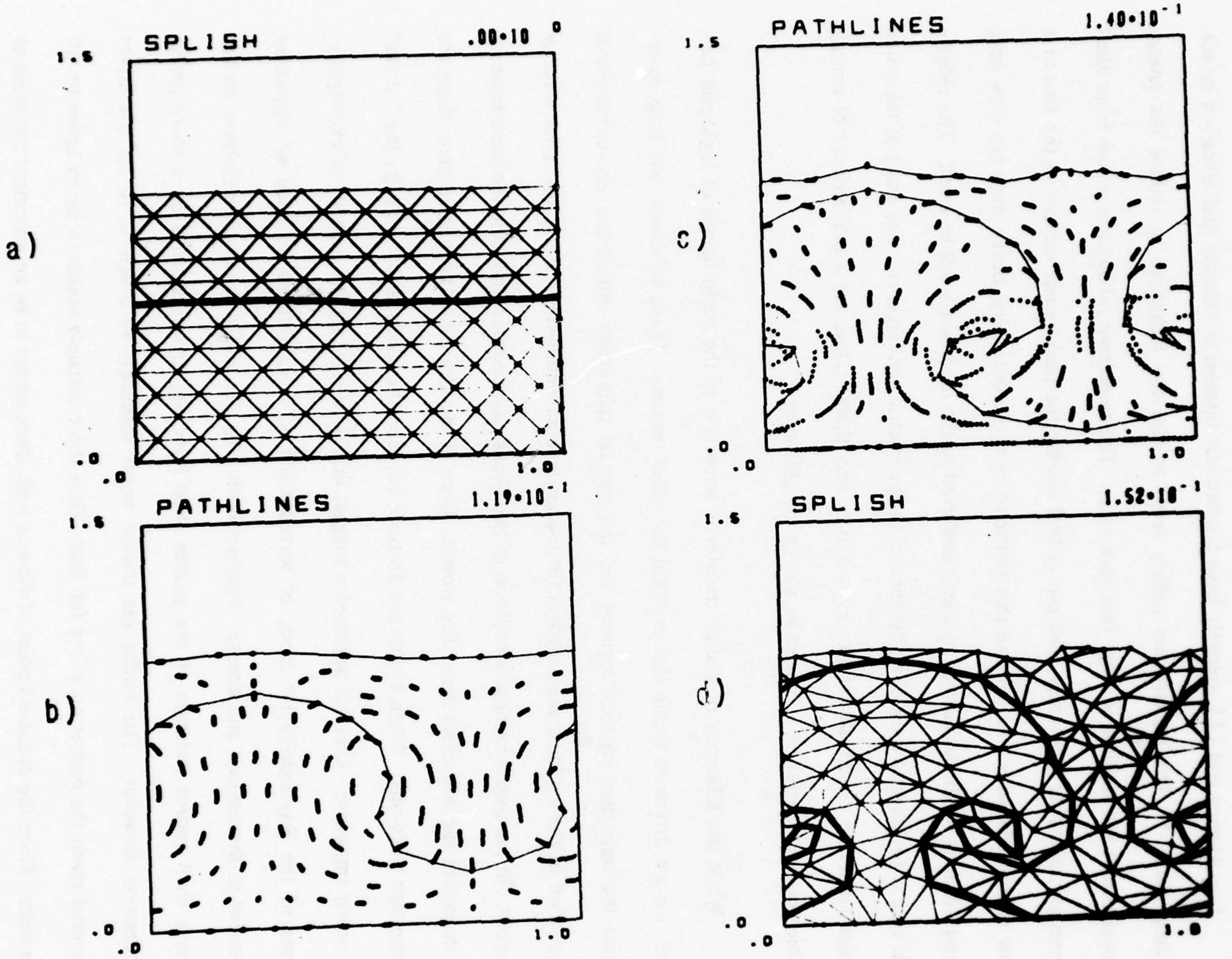

Figure D3 Flow patterns, interface location and grid structure of the internal interface Rayleigh-Taylor instability as computed by the SPLISH computer code.

E. Instability and Symmetry Issues in Colliding Shells

Los Alamos and LLL recently have kindled our interest in velocity multiplication by colliding shells[1,2,3] The highest-gain pellets seem to use the technique to reduce the energy requirement for ignition of large fuel reservoirs. The impulsive rebound of a low mass shell from an imploding high mass shell can at best double the heavy shell velocity at the cost of a low energy efficiency. To achieve this factor of two, the onrushing heavy shell can slow only insignificantly so the amount of energy transferred to the inner shell will be small. The spherical case is particularly interesting because of the geometric convergence. The mass of the outer shell cannot be effectively infinite even if it is very thick. Thus the actual amount of energy which can be transferred is limited as well as the efficiency.

While the efficiency of energy transfer is important to the performance of high gain pellets, we are driven to tackle this problem for other reasons. These solutions will help determine the important physical regimes and the general spherically symmetric, one-dimensional evolution of the colliding shell profiles for use as dynamic equilibria in Rayleigh-Taylor stability studies. In the nearly impulsive collision of two shells, compression effects in the shell material is important and will affect instability growth. Even in the idealized limit treated here, there are important trade-offs. When buffer gas pressure between the shells is low initially, the " strike" is nearly impulsive. Classical arguments suggest that $\int \sqrt{kg(t)\,dt}$, the number of exponentiations of the Rayleigh-Taylor mode of wavenumber k, is minimized by such an impulsive transfer of momentum and energy. Symmetrization by the buffer gas of perturbations on the driver shell and/or isolation of the pusher shell from the driver depends on a more gentle interaction however. The buffer gas should never compress so much as to let the driver material reach the pusher on a free fall line. Thus there certainly seems to be an optimum fill pressure. From the dynamics point of view as well, there seems to be an important optimum to be determined. As a function of buffer gas fill pressure and other parameters such as pusher aspect ratio and material densities, what is the optimum energy transfer configuration?

To transfer the maximum energy the inner shell wants to be thick enough and massive enough to bring the outer shell to rest. To transfer the maximum energy density the velocity should double, hence the amount of energy transferred will be far below maximum. At issue is the appropriate quantity to optimize and the meaningful parameter space over which to optimize it. By making the inner shell thin the velocity doubling can be achieved even though the shell is dense and hence the energy density can be maximized. If the velocity of a dense pusher is to be doubled, it cannot be too thick. Therefore, thin shell stability problems may be expected to accompany configurations which simultaneously try to achieve efficient energy transfer with high energy density. With the possibility of using the high thermal velocity buffer gas to symmetrize the implosion, an additional set of important considerations is added. An initial buffer of relatively high pressure will keep the two shells well separated in transmitting the "strike" but will not get as hot as the initially lower pressure buffer. Thus a hotter, nominally better symmetrizing buffer gas necessarily allows the two shells to get closer together. Furthermore, if the buffer gas gets hot enough, the possibility exists of more than velocity doubling by layering the outside of the inner shell with an ablator. Thermal conduction will then transfer excess kinetic energy from the outer shell to the inner shell.

To work on some of these questions a very idealized model has been developed and programmed. Figure E1 shows the simple, idealized model being treated by the SHLINT code. The spherical volume of interest is divided into five shells. The first shell on the inside is an ideal gas satisfying an adiabatic compression law. This shell encompasses the origin and is of low enough mass that the kinetic energy is negligible. The third and fifth (outermost) shell are low mass adiabatic gases also. The density and pressure are assumed to be constant throughout these three gas regions. The values of density and pressure are determined by the volume of the shell at any instant. The fifth shell is bounded on the outside by a rigid impermeable wall. The second and fourth shells are incompressible fluids with separate but constant densities. These shells are heavy compared to the three gas shells. This system corresponds to the simple mechanics course problem of a series of weights coupled by massless springs. Here, however, the spherical convergence adds an essential complication and the linear problem of small displacements is of no interest. Despite the complications, some analytic results are possible and a simple computer program was developed to integrate the resulting ordinary differential equations in other situations. A typical calculation involves specifying an inward velocity for the outer shell and then solving the coupled system of four ordinary differential equations for the position and velocity of the two incompressible shells. The system is not dissipative and no provision is made (currently) for internal energy in the heavy shells or kinetic energy in the light shells.

This problem is a useful and instructive generalization of a problem originally treated by Lord Rayleigh, the pressure developed in a liquid during the collapse of a spherical cavity.[4] Zel'dovich and Raizer discuss this problem from the viewpoint of similarity theory and summarize some of the non-ideal effects for the special case of a bubble in water.[5] Robson has considered pseudo-spherical and cylindrical implosions of liquid metal liners for the purpose of adiabatically compressing a magnetically insulated thermonuclear plasma.[6] Current interest in the ICF program now encompasses multiple shell pellets and colliding shell pellets[1-3] as concentration on exploding pushers subsides. This added degree of complexity permits the consideration of all sorts of new twists on pellet design.

There are only four independent equations, two positions and two velocities, so the system is fourth order. There are many more parameters, however. There are five shell densities, positions and energies. Including three gas constant parameters gives a total of eighteen. This is far too big a parameter space to investigate — at least initially. To trim it down some we can set the gas constants to 5/3 and ignore the mass of the three gaseous shells. By assuming that the fourth driver shell is thick when the "strike" on the inner pusher shell occurs, the two outer radii and the outer shell pressure can also be ignored. This leaves nine parameters. To examine the momentum and energy transfer from the driver to the pusher through compression of the buffer gas we can also ignore the initial energy of the two inner shells. The remaining seven parameters are the initial position, density, and thickness of the second shell, the initial position, density and velocity of the fourth shell, and the initial pressure in the third buffer shell. These seven parameters are reduced to four if the driver shell inner edge position, velocity, and density are used to non-dimensionalize the equations. The remaining four parameters are the aspect ratio, relative position and density of the pusher shell and the initial ratio of energy densities in the buffer and driver shells when the calculation is begun.

Figure E2 shows the results of calculations initialized which the driver density, initial driver inner radius, and initial driver inner surface velocity can be taken as 1.0, 1.0, and -1.0, respectively, without loss of generality. The driver is assumed to be very thick during the time when the pusher is being accelerated appreciably and the final adiabatic region is given low enough pressure that it does not influence the driver shell dynamics.

The location r_3 of the outer surface of the pusher was taken as $0.1 * r_4$. This choice is also quite general for small fill pressures since a different ratio of radii can be made to correspond to 0.1 by varying the fill pressure appropriately and scaling to the velocity the driver would have at $r_4(0) = 1.0$. This approximate similarity of solutions was tested and the results are indicated as "0" in the figure. The $\frac{\Delta R}{R} = 0.1$ case was re-run for $r_4 = 2.0$ with initial velocity and fill pressure scaled to correspond at $r_4 = 1.0$ with the values used in deriving the given curves.

The pusher density can be similarly scaled, at least for relatively thin shells. Velocity multiplication in planar geometry depends only in the mass per unit area. To the extent that convergence doesn't enter, the same situation will hold for spherical coordinates. The "xxx" points in Figure E2 were performed with $\rho_{23} = 2$, $\Delta/R = 0.05$. These values are nearly identical to the $\rho_{23} = 1$. $\Delta R/R = 0.1$ case.

At low buffer pressure the transfer of energy is essentially instantaneous on timescales of interest for the subsequent implosion. As the initial buffer pressure is increased, however, the interaction time increases because substantial momentum is transferred from the outer to the inner shell at greater separation distances. If the initial buffer pressure gets too large, the pusher will implode prematurely. For initial pressures in excess 5×10^{-4} of $\rho_{45} V_4^2$, the figure shows poor energy transfer ($\eta_c \leqslant 0.1$) even for rather thick or dense pushers which do not tend to run away before collision.

The result of these calculations is to focus attention on the relatively sharp maximum at about 50% for modest aspect ratio shells (10-20:1). Good energy efficiency is important, clearly, but so also is the original reason for colliding shell designs, velocity multiplication. The effective mass of the outer shell is always reduced severely by spherical convergence. Therefore, unless the inner shell is quite light, significant energy density concentration cannot be achieved. The next step is to set up one of these near-optimum configurations in the FASTID code to study the region near the idealized optimum when more realistic equation-of-state physics and finite thermal conduction is included.

Velocity multiplication in spherical coordinates has an interesting twist which arises from geometrical convergence. The outer shell is freely falling in the Rayleigh solution[4] before the buffer gas pressure becomes important. The inner surface is accelerating rapidly inward while the outer portions of the shell decelerate slightly to provide the momentum and energy flow required to feed this acceleration. If the inner pusher shell is quite thin, the nearly impulsive transfer of energy will generally cause the outer surface of the pusher shell to attain nearly twice the velocity that the inner surface of the driver shell had prior to the "strike". Velocity multiplication is a full factor of two only when the driver is not appreciably slowed. Immediately after the strike the buffer gas region expands and cools rapidly as the pusher moves radially inward faster than the driven shell.

At this point spherical convergence enters the picture with a vengeance. As soon as the shells have separated far enough for the buffer gas pressure to drop, the two shells are falling inward independently. The outer edge of the pusher starts decelerating right away to feed energy and momentum to the inner surface. The inner surface of the outer shell, on the other hand, starts to accelerate right away because of the convergence. Under a range of conditions the driver catches up to the pusher again before the pusher is forced to turn around. This subsequent "restrike" transfers energy from the outer shell to the inner again, increasing the real transfer efficiency over what is achieved on the first strike.

Figure E3. considers an idealized version of this phenomenon where the pusher remains thin until the accelerating driver restrikes it. The lower figure displays a series of idealized restrike trajectories and the upper figure plots the maximum aspect ratio versus velocity multiplication factor.

Let $r_d(t)$ be the inner driver radius and $r_p(t)$ the outer pusher radius as a function of time. If the shells collide at $t = 0$ with the thin pusher initially at zero velocity, after the collision the pusher is moving inward at $-\alpha V_d(0)$ and the driver at $-Vd(0)$. *Not much energy is* transferred to a thin pusher but the driver velocity can be doubled. As long as the pusher stays thin it follows the trajectory

$$r_p(t) = r_p(0) - \alpha V_d(0) * t.$$

If the pusher thickens, the outer surface actually decelerates but the inner surface also rebounds sooner because of convergence. Therefore recompression of the buffer and restrike is more likely with a thin pusher than a thick one.

The initial shell collision is indicated by the • at $t = 0$ in the lower figure. A number of straight lines indicating thin pusher trajectories have been drawn for $V_p(0) = \alpha V_d(0)$ with $\alpha = 1.4, 1.6, 1.8$, and 2.0. The smaller • points in the lower figure indicate restrike locations where the driver catches up to the pusher for each of the pusher velocities chosen. Under the ideal circumstances of a thick driver and a relatively light pusher, an analytic expression for the driver trajectory is also possible. When the buffer gas is again at sufficiently low pressure after the initial collision, the driver will free fall with $V_d^2(t)\ r_d^3(t) = \text{const}$. This driver equation of motion can also be integrated analytically to give

$$r_d(t) = r_d(0) \left[1 - \frac{5}{2}\, r_d^{-1}(0)\ V_d(0)\ t \right]^{2/5} .$$

Since $r_p(0) = r_d(0)$ to define the collision, recompression of the buffer occurs when $r_p(\tau) = r_d(\tau)$ where $\tau \equiv V_d(0)t/r_p(0)$ is a non-dimensional measure of the closure time. The velocity doubled pusher reaches the origin at $\tau = 0.5$ in the absence of a restrike. The driver reaches the origin at $\tau = 0.4$ in the absence of the pusher. Clearly the restrike occurs before $\tau = 0.4$ when the accelerating driver surface overtakes the constant velocity or decelerating pusher. The upper figure is a plot of maximum aspect ratio computed by finding solutions to the restrike radius $r_p(\tau) = r_d(\tau)$ numerically. The volume inside this restrike radius, when distributed uniformly over the surface of the initial pusher radius sphere, defines a maximum aspect ratio. Thicker pushers must rebound before restrike occurs.

A possible ramification of this restrike phenomenon is the use of an ablator on the outside of the inner shell. The tendency of the outer shell to "dog the tracks" of the inner shell might possibly be used to keep the buffer gas hot and the inner shell ablatively accelerating due to electron thermal conduction. To make this effective the inner shell would have to start out relatively thick so convergence could be expected to decelerate the outer surface before appreciable implosion has occurred. Another application of the restrike might be to ensure that peak compression of the main fuel reservoir in the driver during restrike is timed to coincide with ignition in the core to optimize fuel utilization.

These arguments all ignore the effects of compressibility in the heavy shells and the effective loss of energy that goes with it. Shock heating can be expected to be a major contributor if the buffer gas is sufficiently low density that the strike is impulsive. If a softer strike is attempted by increasing the buffer gas pressure, the inner shell tends to run in an rebound off the origin before much energy has been transferred.

Two further applications of this simple model are worthy of mention. To perform dynamic stabilization calculations of ablators layered with light and heavy material to alter the shell acceleration periodically, this model will clearly prove useful. Applications are also planned in the analysis of thin foils being accelerated by deposited laser and light ion energy. In the next section calculations on core density and temperature profiles will be presented which were driven by the incompressible pusher shell of this idealized model as an outer boundary condition.

Section E. References and Footnotes

1. E. Lindman, Jr. and R. Mason, Los Alamos Scientific Laboratory presentations at APS and Gordon Conferences.
2. J.D. Lindl, "Low Aspect Ratio Double Shells for High Density and High Gain," paper THC7, Technical Digest of the Topical Meeting on I.C.F., San Diego, Feb 7-9, 1978.
3. A.J. Toepfer and W. Tiffany, "Stability of Multiple Shell ICF Capsules," paper ThC2, Technical Digest of the Topical Meeting on I.C.F., San Diego, Feb 7-9, 1978.
4. Lord Rayleigh, *Philosophical Magazine S.6*, Vol. 34, No. 200, Aug. 1917.
5. Zeldovich and Raizer, *Physics of Shock Waves and High Temperature Hydrodynamic Phenomena,* Vol. II, Chapter 12 (Academic Press, New York, 1967).
6. A.E. Robson, U.S. Naval Research Laboratory Memorandum Reports 2616, July 1973; 2692, December 1973; and 3472, April 1977.

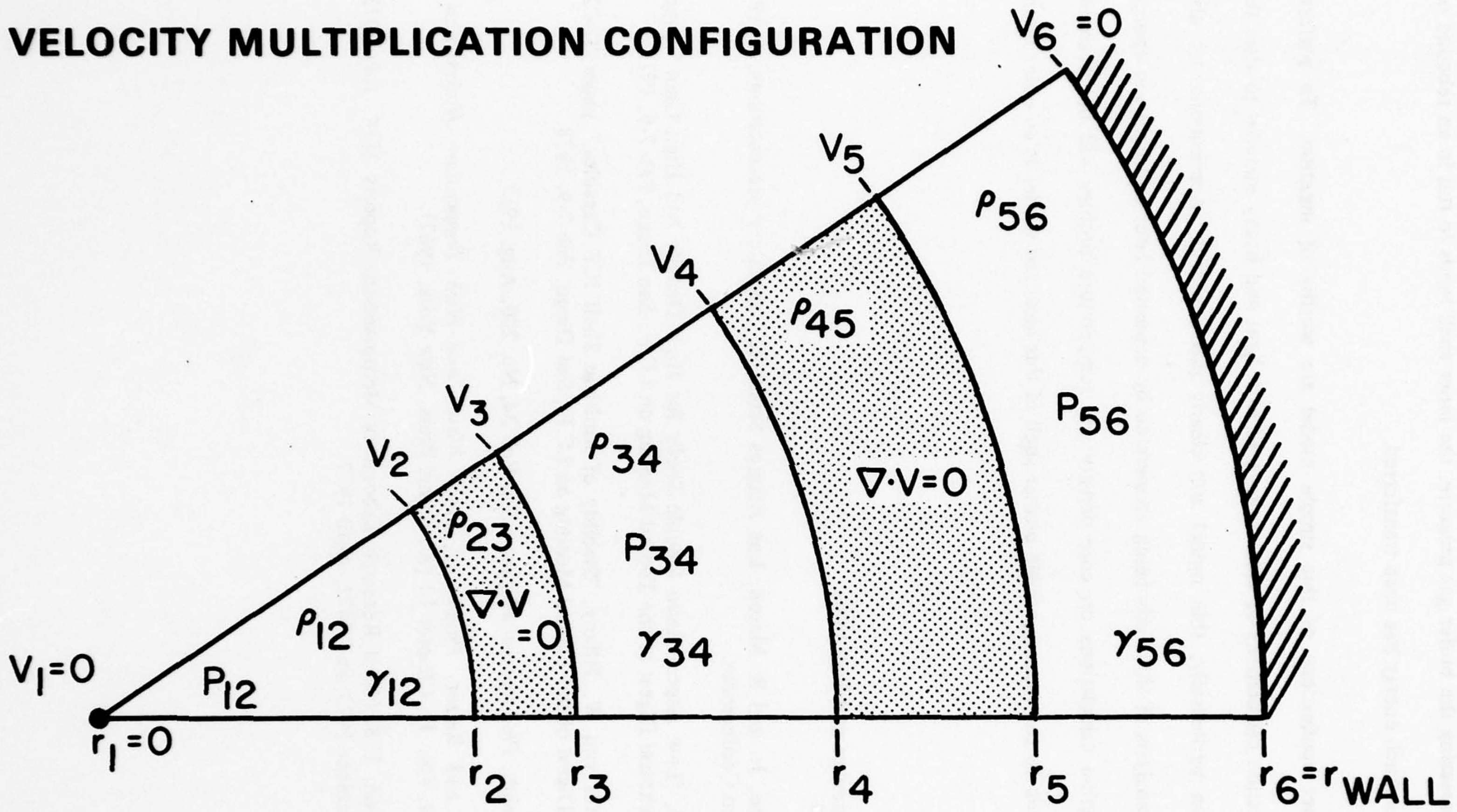

Figure E1 The idealized, five-shell velocity multiplication configuration programmed into the SHLINT code for simple estimates of colliding shell dynamics and energy transfer efficiency.

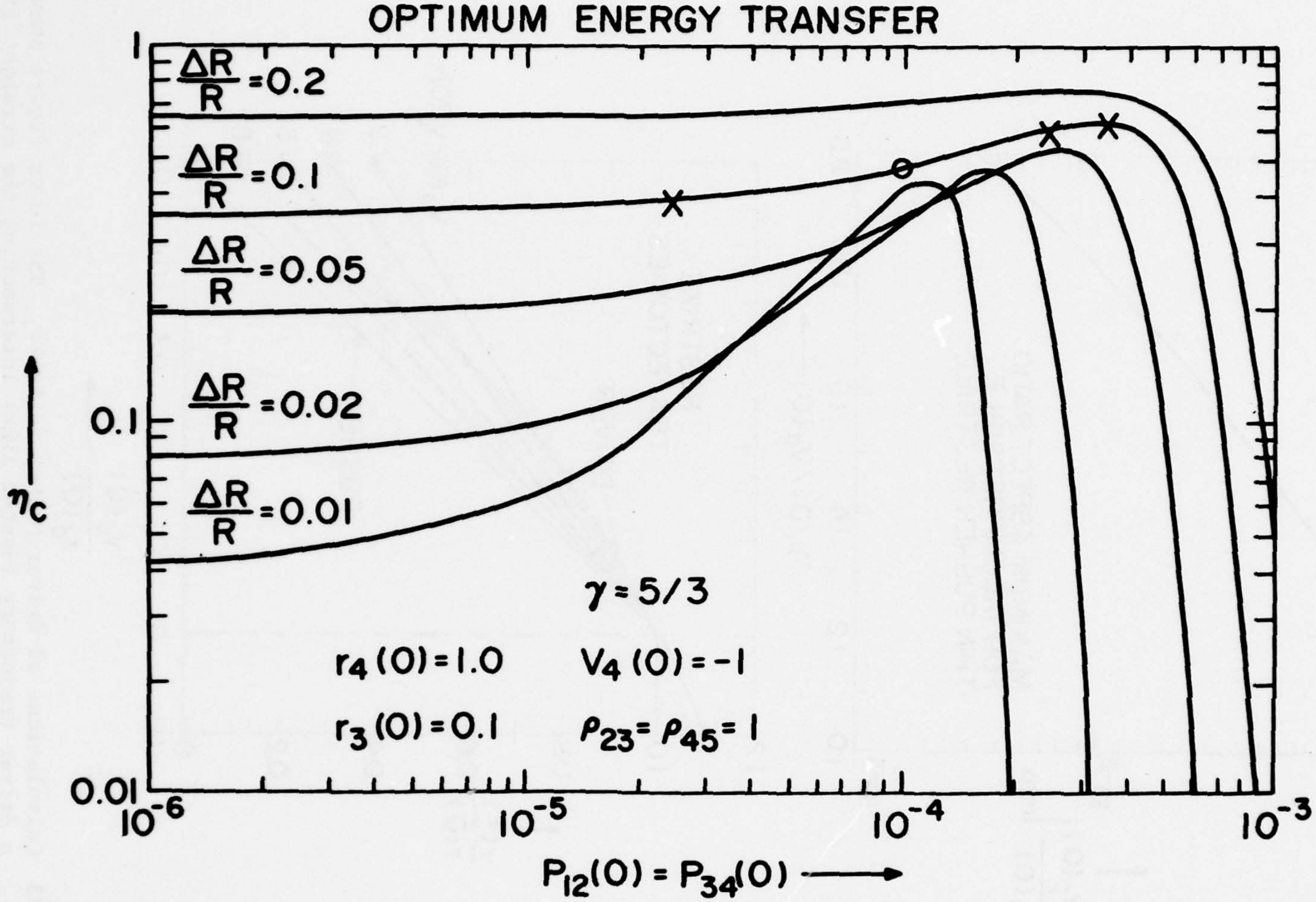

Figure E2 The idealized SHLINT adiabatic-incompressible model is used to compute the efficiency of energy transfer from the outer driving shell to the inner "pusher" shell as a function of buffer gass fill pressure.

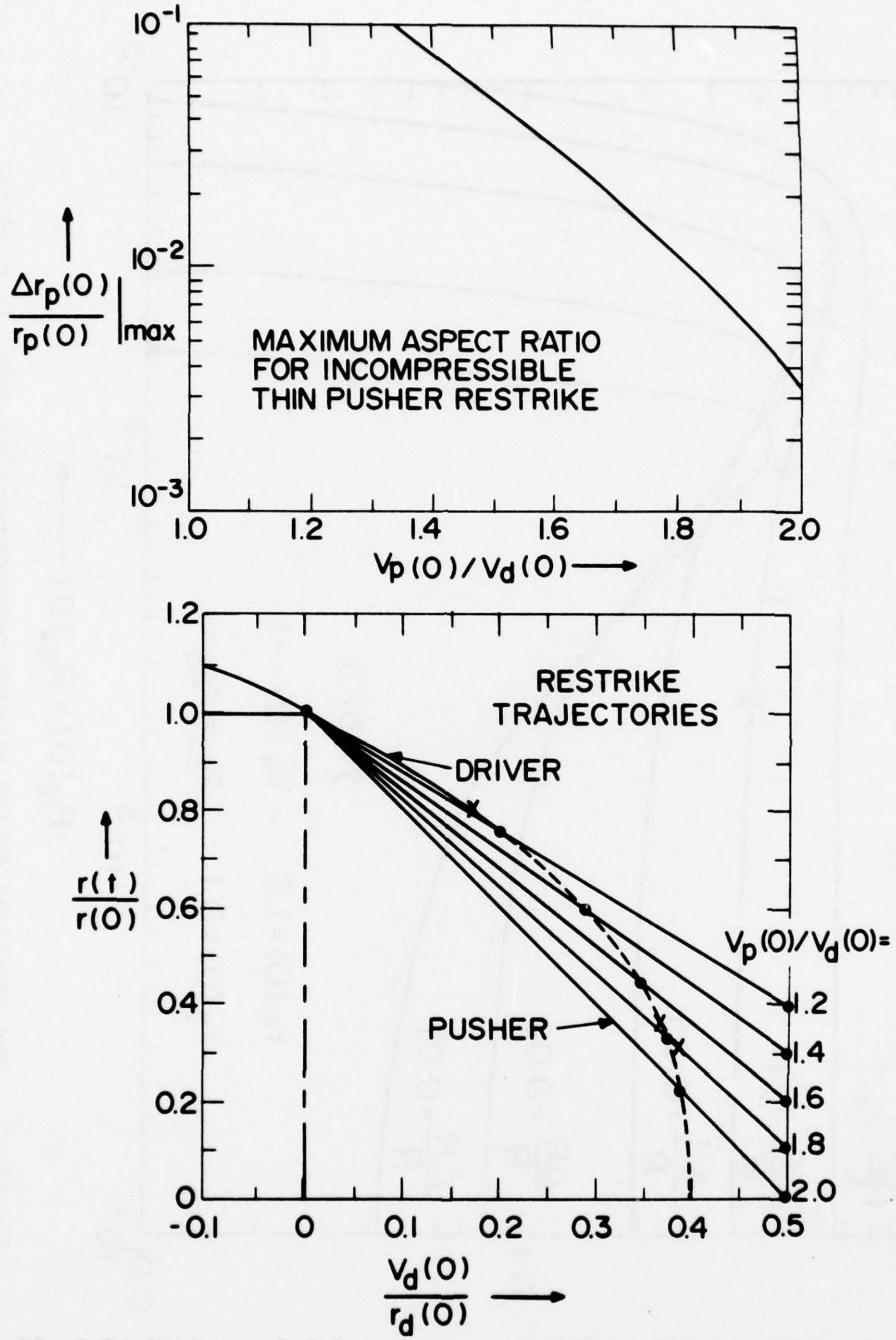

Figure E3 Calculations of driver-pusher restrike. The lower figure shows a driver trajectory (dashed line) intersecting the straight line trajectories of very thin pusher shells. The upper figure shows the maximum aspect ratio (thickness) the pusher could have and still undergo restrike as a function of the velocity multiplication ratio.

F. Rayleigh-Taylor Stability and Central Core Dynamics

The symmetry of the void closure during collapse of the pusher will be critical in determining the temperatures and compressions that can be achieved in the central "ignitor" region. Growth or damping of Rayleigh-Taylor instabilities when core shocks interact with the density gradients formed in front of the pusher or with the pusher interface itself will play a large role in determining the degree of symmetry that can be achieved during void closure. Multiple shock reflection from the central core and the pusher interface potentially give several growth opportunities to the Rayleigh-Taylor instatiblities. On the other hand, these multiple shocks reflections are needed to achieve a high temperature in the central core region. Clearly we must determine optimum ways of compressing the core region to high temperatures while avoiding disasterous Rayleigh-Taylor instabilities which may destroy the symmetry of the implosion and the resulting geometric convergence. The timing of the shocks will be determined by a combination of fill gas density, temperature, initial void radius and pusher velocity as a function of time.

There are two regimes of core density receiving about equal attention in the search for a viable ICF ignitor. In the first the core density is so low and the temperature so cold that the fuel mass and pusher are effectively imploding on a vacuum. In the second regime a fluid of sufficient mass and energy fills the core that unopposed implosion of the fuel is impossible. We have diercted our attention to this second regime in the conviction that behavior of an ignitor with a fluid or gas fill will be more reproducible and predictable than one based on ideal vacuum implosion. Spall from initial shocks might introduce an unignorable amount of material to the void, for example. Another case would be non-cryogenic, gas-filled targets.

We hope to perform numerical simulations of the central "void" closure problem with a focus on stability and symmetry issues. The final calculations will be performed on FAST2D and the new linear/non-steady equilibrium code.

In order to address some of these symmetry and stability problems, we have begun by looking at the dynamic equilibrium problem in one dimension. Preliminary calculations are being performed in 1D using the fully conservative FCT code FAST1D.

The simplest problem to study first is the spherical collapse of a shock wave. Using a constant pressure boundary condition on the surface of a fluid sphere which is moving radially inward leads to the formation of a spherically convergent shock wave in the gas filled core region. Since the shock wave is accelerating due to spherical convergence as it approaches the core, it moves faster than a limiting characteristic so that information from the boundary condition becomes lost. Under such circumstances a self-similar solution is established for the case of a constant core fill density. At sufficiently small radius, when the shock has become strong enough that the core fill pressure can be neglected compared to the shock strength, a self-similar solution due to Guderley exists.[1] This solution allows us to check the accuracy of our numerical solution in the immediate core region at the time of the first shock collapse.

The three conservation equations for perfect gas with $\gamma = 1.4$ are solved using the fully conservative FCT code FAST1D. The calculations were preformed in spherical symmetry using 100 zones on a variably spaced grid. The grid moves dynamically to follow the most important region of the flow; however, the calculation is still basically Eulerian. The first 20 zones contain a region in which the grid spacing expands by a constant percentage (~ 5%). The remaining 80 zones are spaced using a power law $R_i = R_b + \Delta R \left(\frac{i-20}{80} \right)^P$ with the exponent P chosen to match the grid spacing at R_b, the interface between the two regions. The outer boundary R_{max} is allowed to move inward with the boundary flow velocity in a Lagrangian fashion to model the moving pusher interface. The boundary between the two grid regions R_b is allowed to move inward with the flow as the shock passes over it. This allows the gridding in the central region to improve as the shock moves inward without having to pay the full price of the numerical CFL conditions except when the shock is near the origin. The problem is started at an initial radius of 1 cm with a zone size of ~ 37μ at the origin. A minimum resolution of ~

4μ is used at the origin at the time of collapse when the outer boundary is at about 0.5 cm.

The outer boundary is held at a fixed pressure and alowed to move freely with the fluid at the boundary. The initial conditions at the boundary are set up to satisfy Rankine-Hugoniot shock with a pressure ratio of $P_2/P_1 \sim 10^3 (M \approx 30)$.

The self similar solution due to Guderley[1] predicts that the ratio of the pressure behind the reflected shock to the pressure behind the incident shock at a fixed location is a constant $(P_r/P_i = 26)$. In addition it predicts that $P\frac{|t - t_c|^2}{R^2} = \text{const}$ where P is the pressure behind the shock at radius R and time t, t_c is the time of collapse of the shock to the origin.

The pressure ratio is almost independent of the final resolution at the origin. Varying this resolution from 4μ to 16μ gives approximately the same result $(P_r/P_i \approx 20)$ although the peak pressure at the origin varies by over an order of magnitude. This is to be expected since the numerical problem is also self similar and is independent of grid size. The lower pressure ratio measured numerically results from a slight delay in the reflected shock leaving the origin due to the finite thickness of the numerical shock. This pressure ratio can never be corrected by an increase in resolution since the problem is self similar. The delay can be reduced to zero by improving the resolution however.

If a hard sphere with radius of order the numerical shock thickness is placed at the origin, it forces the shock to be reflected sooner. At several radii the size of this sphere is negligible and the self-similar solution is again recovered. Using spheres radius of 30μ and 50μ with minimum zone size of 4μ both give a similar pressure ratio $(P_r/P_i \approx 26)$. A radius of 10μ (dudding out two or three zones in effect) gives a lower value of ~ 22. There thus appears to be a threshold radius, proportional to the grid spacing at the origin, above which the analytic solution can be recovered. This dudded-out sphere, for our FCT calculation, seems to play the role that adjustable Von Neuman coefficients do in other calculations.

The size of this sphere and the gridding needed will be determined by the influence of thermal conduction which destroys the self similar solution at the origin in any case. A sphere radius of less than the dimensions of the thermal boundary layer will have a negligible influence on the final solution. Determining the size of this region is the next step in this investigation.

Shown in Figure F1 is a plot of the parameter $P\frac{|t-t_c|^2}{R^2}$ for the inward and outward shocks. The inward value has a theoretical value of 4.3×10^{-4} given by $P\frac{|t-t_c|^2}{R^2} = \frac{2}{\gamma-1}\rho_o\alpha^2$ (the limiting value for a strong shock). Until the shock reaches the central hard sphere the solution for the converging shock is the same for runs with and without the hard core and lies very close the theoretical value of $.43 \times 10^{-3}$. For the diverging shocks there is a considerable difference in the two runs although both reach an asymtotic form of the similarity solution. The case without the hard sphere center always has too low a pressure. This results from the shock getting too late a start reflecting from the origin. Since it starts late, it will always be moving into a region of higher density and pressure than it would have with an earlier start and therefore never catches up in the similarity sense even though the delay is very small.

The case of an actual pusher collapse is much more complicated than the simple self similar Guderley solution we have been discussing. Unfortunately the Guderley solution is a limiting one valid in at most a small region of the real problem. The solution rapidly becomes contaminated by the influence of the boundary which destroys the self-similar solution unless a self-similar boundary condition is used. Thus this soution will tell us very little about the behavior of the core region except near the instant of the collapse of the first shock wave. It will give us little guidance as to the nature of the solution after multiple reflections of the shock from the core and the driving pusher which in this case is the outer boundary.

It is the multiply reflected shocks of the nonideal case that are of primary interest in determining the core conditions for ignitor design. Since the pusher will move at a velocity supersonic with respect to the fill gas, shocks will be driven in toward the origin. Upon reflection these outward moving shocks will rebound from the density gradients in front of this pusher and from the pusher interface itself. Each of these reflections, when transmitted to the pusher, will slow it down, transferring part of its energy to this reflected shock. The number of reflections and strengths of these shocks will depend upon the velocity of the pusher interface, initial radius, fill density and temperature of the interior core material. For a sufficiently cold fill, the initial core temperature ceases to be a parameter and only the fill density and mass will be important.

If the density of the pusher is much larger than the fill gas density and the pressure in the fill region sufficiently lower than ρC_s^2 in the pusher, the pusher may be reasonably modeled by an incompressible fluid. A more realistic driving boundary condition than the constant pressure used for the Guderley problem is obtained by surrounding the compressible core fluid with an imcompressible spherical shell which can be used to represent a pusher for the core fluid. For a sufficiently thick pusher with a large kinetic energy compared to the initial energy in the core fluid, the concepts of a similarity motion of the pusher discussed earlier in term of the Rayleigh problem[2] are valid. In this case the motion of the pusher is characterized by the density of the pusher and its kinetic energy. As the pusher moves in, it transfers part of its energy to the core fluid which in turn slows the pusher down.

The question is to find some optimum transfer of energy from the pusher to the core region and optimize the temperature in the core. This optimum configuration is then a prime candidate for Rayleigh-Taylor analysis. Clearly one can either heat the core region uniformly to a lower temperature or obtain a very hot central core with a surrounding denser and cooler region. Such considerations may lead to a variety of interesting ignitor concepts but our primary interest is to obtain the dynamic equilibrium profiles for such configurations to perturb about. Rayleigh-Tarlor instability is likely in as the reflected shocks slow down the pusher and the density gradients generated in front of the pusher.

Calculations are done using the incompressible model for the pusher acting on a perfect ($\gamma = 5/3$) fluid as the fill. The FAST1D code is used to compute the motion in the fluid core. The problem is started with a shell at a radius of 1000μ surrounding a fluid of density $\rho_{GAS} = 10^{-3}$ gm/cc at a temperature of 10^{-2} ev. This corresponds to a fill fluid energy of $2 \times 10^{-3}\pi$ joules. The pusher is given 20π joules of energy which gives an initial inner edge velocity of the incompressible shell of $V_a = -\sqrt{10} \times 10^5$ cm/sec. The incompressible shell serves as the boundary condition for the moving outer edge of the fluid region which is computed numerically using the fully compressible one-dimensional code. The velocity of the inner edge of the incompressible shell is computed self-consistently by subtracting from the kinetic energy of the pusher the energy transferred to the core fluid which can be computed at each time step. Initially due to geometric convergence, the inner edge of the incompressible shell accelates until it reaches a peak velocity of $V_a = 1.2 \times 10^7$ cm/sec at cycle 1150 and $t = 126.9$ ns. There after the transfer of energy to the core fluid takes place more rapidly than geometric convergence accelerates it and thus the pusher slows down.

In Figure F2 we show the temperature as a function of radius and the shell locations for several times in the calculation The radius is in microns and the temperature in units of cm^2/sec^2. The first plot at $t = 124$ ns corresponds to the situation just before the first spherically imploding shock reaches the center. The second plot at $t = 125$ ns shows the reflected shock before it has reached the pusher. The curve at $t = 126.8$ ns shows the shock after it has been reflected from the steep density gradient that has formed just inside the pusher. This curve is well after the Guderley solution has broken down due to the influence of the boundary at the pusher. A second spherical shock is launched by the pusher at this time which overruns the already heated core and heats it to a peak temperature of 1.8×10^4 ev shown by the 126.9 ns curve. Further heating by yet more reflections is shown by 127.16 ns when the pusher has moved inward to its furthest point. As can be seen, it is the second shock that is primarily responsible for heating the core region to very high tempratures. In Figure F3 we show the core density profile at the time $t = 127.16$ sec. The profile shows a low density region at the

AD-A068 470 NAVAL RESEARCH LAB WASHINGTON D C F/G 20/7
NRL INERTIAL CONFINEMENT FUSION THEORY PROGRAM 1978 ANNUAL REPO--ETC(U)
FEB 79

UNCLASSIFIED NRL-MR-3944 SBIE-AD-E000 293 NL

2 OF 2
AD
A068470

END
DATE
FILMED
6--79
DDC

center where the temperature is very high surrounded by a mass of higher density inside the pusher. It is this central core that will hopefully serve as the ignitor for a pellet design.

The density at the pusher inner edge has reached about 9 g/sec which is above the density of the incompressible pusher. This indicates a breakdown of the assumption of an incompressible pusher. The implicit ADINC model with a proper equation of state for solid or liquid densities would provide a more accurate pusher for the central region. Nevertheless, a great deal can be learned from these simple models about the behavior of the interior region. The next step is to include a realistic equation of state and include the compressibility in the pusher which will effectively absorb some of the energy that the pusher delivers to the core fluid.

The steep density gradient formed in front of the pusher will suffer from Rayleigh-Taylor instability when it is decelerated by the reflected core shocks. By appropriate timing of the formation of this gradient and the reflected shocks the damage caused by these instabilities may be minimized. The ultimate temperature achievable and the density obtainable may depend on how well these instabilities can be controlled and the degree of symmetry obtainable in this core implosion.

References and Footnotes

1. G. Guderley, *Luftfarhtforschung 19(9)*, pp. 302-312, 20 October 1942.
2. See the discussion and references in section E on the self similar Rayleigh problem for the collapse of a spherical bubble.

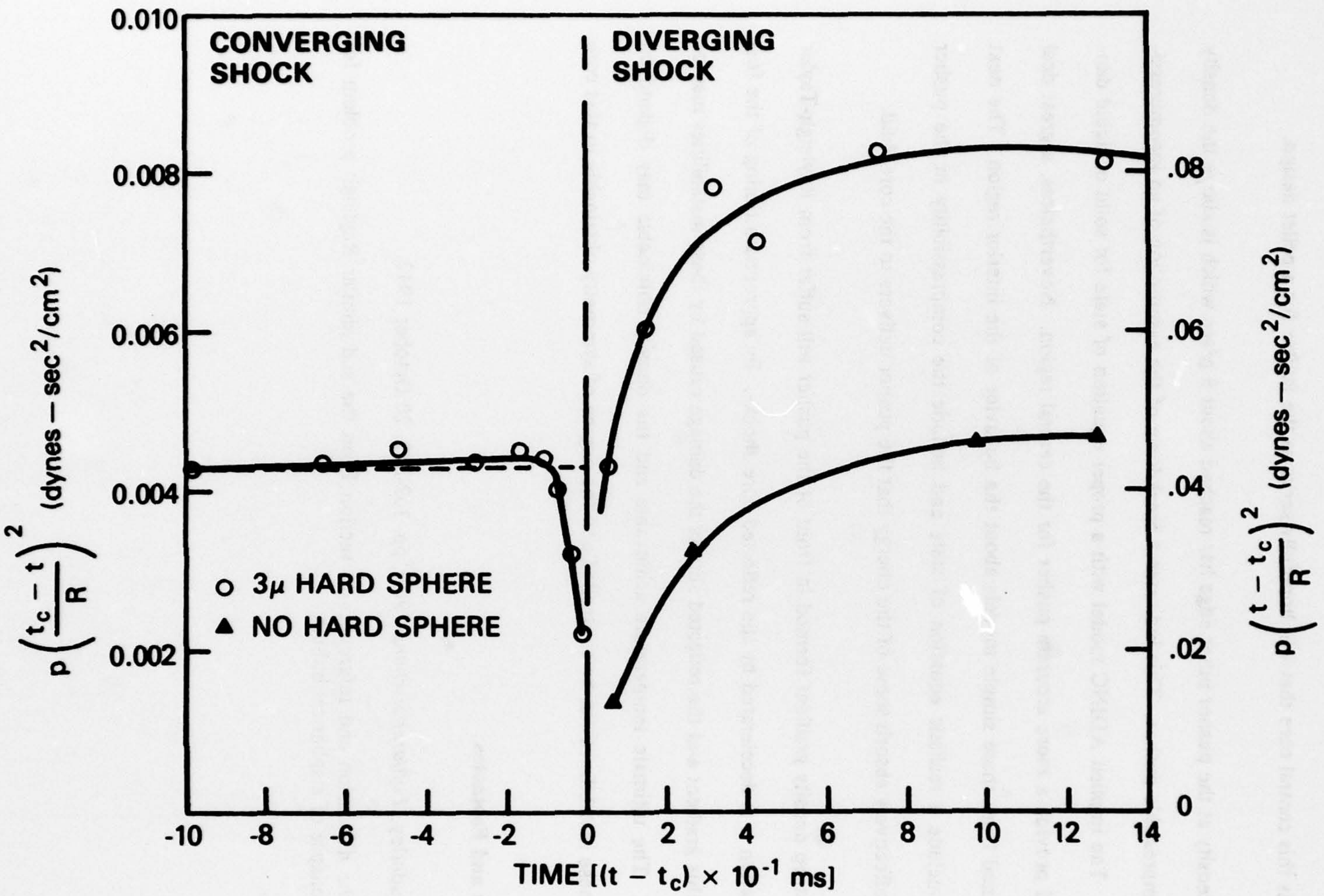

Figure F1 The similarity parameter $p \frac{(t-t_c)^2}{R^2} = \frac{2}{\gamma+1} \rho_o \alpha^2$ for the incoming (outgoing) shocks. The upper curve on the right is for the case with a hard sphere boundary condition at 3μ radius. The other case has zero inner radius.

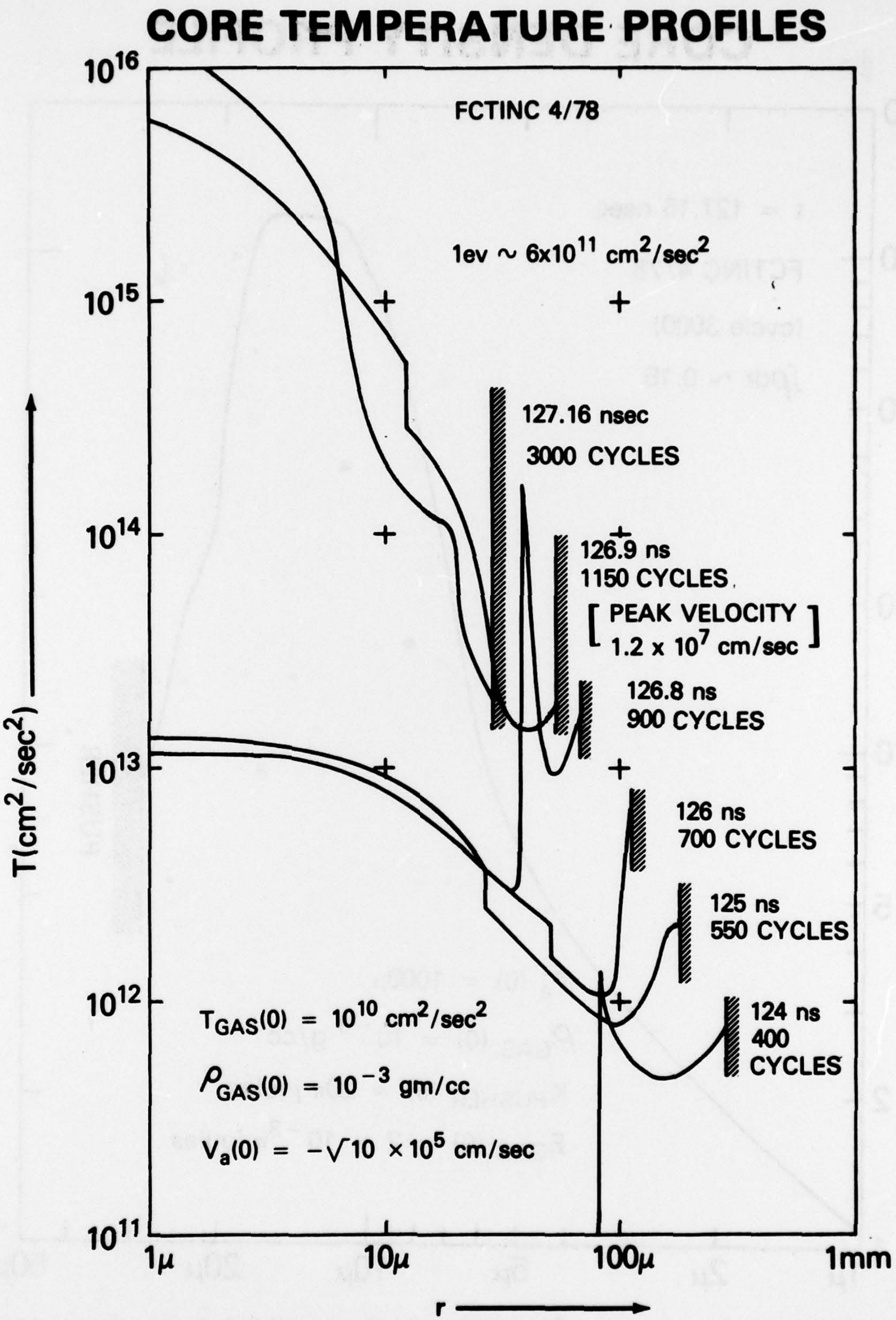

Figure F2 Temperature as a function of radius for several times for void closure driven by an incompressible pusher of large mass. The second shock wave does most of the heating.

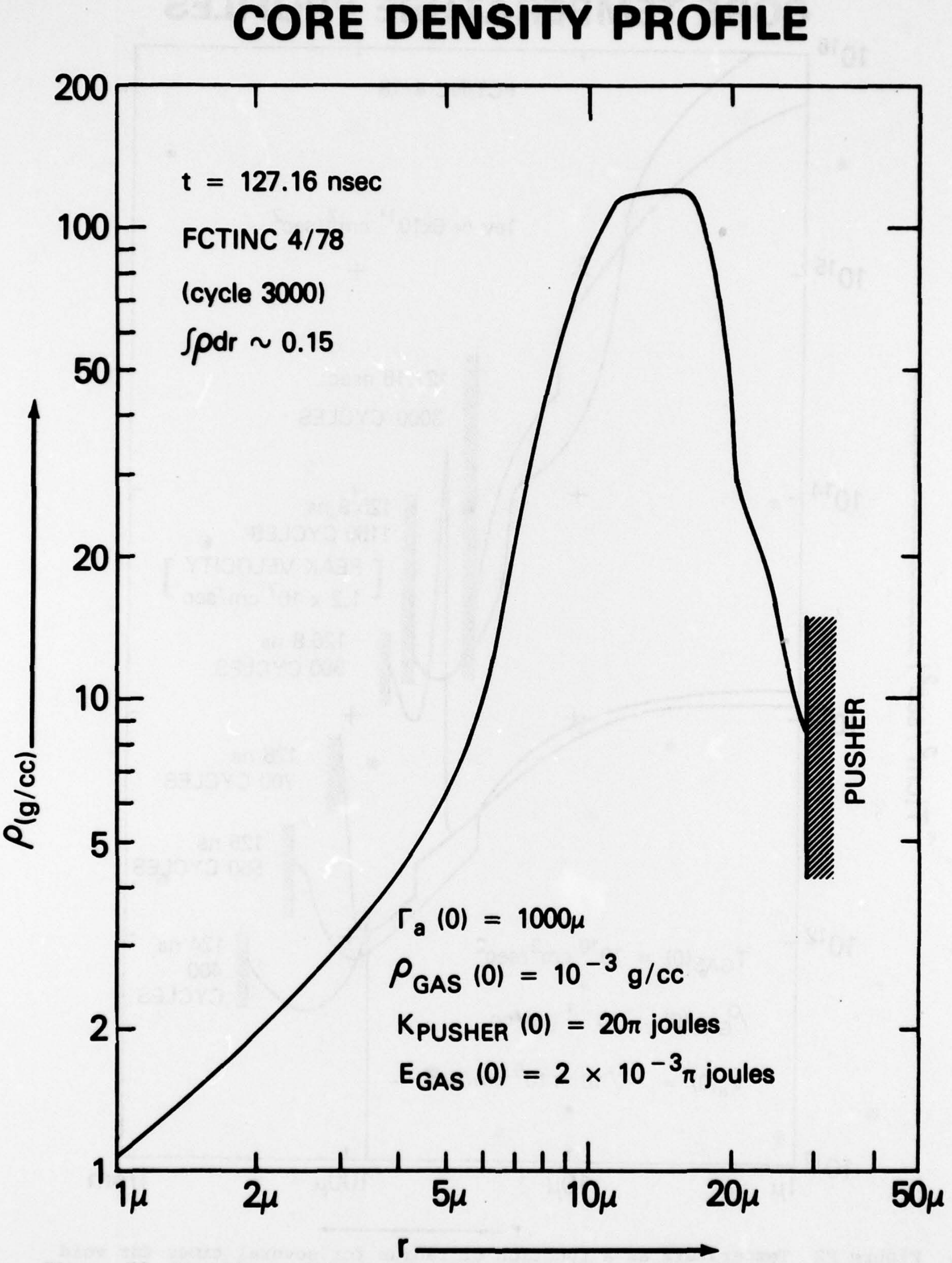

Figure F3 Density profile at the time of minimum radius for the problem shown in the previous figure. A hot low density core has formed surrounded by a cooler high density region.

PLANS

During FY78 our studies of heavy ion beam transport in quadrupole focussing systems have brought a number of useful and encouraging results to the HIB fusion program. The most important of these is the demonstration of conditions where space-charge limited beams can be propagated long distances with limited emittance growth. Because of the wide variety of phenomena which can be investigated and which are important for accelerator system design, the choice of research topics in the future depends on the directions taken in the heavy ion program. Several of these directions are apparent. First, the study of solenoidal systems is important because solenoidal, rather than quadrupole, focussing will be used in the lower energy sections of the accelerator. It is also important because experiments are being undertaken that will use solenoidal geometry to study the fundamentals of focussed transport. There experiments will need guidance and theoretical interpretation.

Second in importance is the study of axial heavy ion beam transport. Axial beam dynamics, as in bunching, introduces another potential set of instabilities which can degrade beam quality, transport, and focussing. Therefore our simulation efforts will concentrate on the two dimensional $r-z$ system where the shorter transverse time scales present the major numerical obstacle.

We also plan to continue our efforts on the related light ion channeling, bunching, and focussing. The advantages of light ion beams for their use as drivers in inertial confinement fusion are their ease and efficiency of production and focussing and their efficient coupling to matter. The major problems which remain to be solved lie in between, namely transport and bunching of the beam from source to target chamber. It is planned by the NRL ICF program to focus the ions first in a relatively short focussing chamber and then to transport them in a long plasma channel. We plan to investigate the physics occurring in the plasma channel as a result of the beam passage.

The absorption of high intensity laser light by matter remains a major emphasis of the DOE ICF research program. Absorption by return-current-driven ion acoustic fluctuations has been shown to be an efficient absorption mechanism which bridges the gap between experimental absorption measurements and resonant absorption theoretical predictions. Recent inclusion of the magnetic field effects on the ion acoustic absorption of laser light have brought encouraging quantitative success to our absorption predictions. Therefore, we plan to pursue the study of laser absorption by this mechanism somewhat further by beginning the work on the time dependent problem. We feel it is important to resolve the ambiguity encountered in the steady state solution: the fact that one of the boundaries had to be chosen near the critical density where the variables are not necessarily well known. Further, some of the complications existing in the steady-state solution are removed from the time-dependent solution so the work should also help to explain similar ambiguities encountered in our ablation layer modelling.

Our studies of Rayleigh-Taylor instability in laser ablation layers and associated physics have constituted the single largest component of our ICF theory effort. In the past our theoretical analyses, code development, and numerical simulations have been directed toward understanding and predicting the onset, growth and nonlinear "saturation" of these modes. This emphasis should continue into the future and will extend to related ablation layers driven by direct ion deposition. Experiments on foils driven by lasers, electron and ion beams throughout the ICF community are beginning to produce some experimental data on Rayleigh-Taylor growth in real situations. We plan to be in a position to analyze and interpret this data by a combination of one-dimensional and two-dimensional simulations and ad hoc theoretical analyses.

The main theoretical problem to be resolved is the presence or absence of accelerative stabilization in the low power regime. Numerical resolution in ablation-layer R-T calculations throughout the community has been too coarse to date to resolve the ablation layer structure. Theory, on the other hand, has proven up to suggesting a mechanism for greatly reduced R-T growth but has been helpless to prove the effect. We are marrying a piggyback linearized stability module to our implicit 1D Lagrangian hydrocode. In this way we should be able to provide the $5\times10^{-2}\mu$ resolution needed in the ablation layer to resolve the separated peaks of density and pressure profiles when the incident power is $\sim10^{13}$ watts/cm^2 without working with unacceptably short timesteps.

We also plan to merge the quasi-static, analytic ablation layer model (developed during FY77-FY78) with our implicit hydrocode directly in an attempt to demonstrate the feasibility of bypassing the expensive ablation layer and blow-off calculation altogether. We have found that the initial transients during prepulse and start-up pervade even the quasi-static solutions. They specify the effective adiabat of the shell and the shell momentum relative to the ablation layer. Spall, fluff, preheat, and start-up shocks all affect these conditions and thus will be the subject of some work during the coming year in an attempt to determine better "initial" conditions for fluid dynamic simulation.

All these studies and capabilities will be applied, as appropriate, to the possibility of using dynamic stabilization to limit the growth of R-T modes in the ablation layer. The piggyback module, on top of our implicit 1D Lagrangian model, should also pay important dividends in analyzing current and planned foil experiments and possible future applications include the analysis of Rayleigh-Taylor instabilities in realistic colliding shell configurations.

Our work on the stability of interior material interfaces has a rather clearly mapped out series of milestones which have to be accomplished. The major effort must be in the continued development of the method to include at least the physics which is currently in FAST2D. This will be a long term effort with very large potential payoffs for stability analysis of thin shells and layered material.

The existing code, used to perform the calculations shown in Section D, should also be applied to two outstanding problems in its current form. The first of these is the classic problem of an ideal heavy fluid over a lighter fluid where the short wavelength saturation results in a slow "turbulent" interpenetration of the two fluids. Our object would be to test the Russian theory by simulation in a simple idealized case before all the complications of heat flow, compressibility, and realistic equations of state have to be taken into account.

The second problem is the simulation of a local configuration which can be expected to occur in a number of ICF situations. The problem is the introduction of a thin, high density, layer between two otherwise stably stratified layers. Deformation of the interface as a whole involves moving the thin layer as a surface and consequently long wavelengths should be stable. At short enough wavelength the upper and lower surface of the thin heat shield should be able to decouple sufficiently to allow growth of Rayleigh-Taylor modes. Thus a cutoff is expected, a wavelength beyond which longer wavelengths are stable. The major application is to ~ 1 gm/cc ablator materials accelerating ~ 0.2 gm/cc fuel through a thin, ~ 20 gm/cc heat shield.

We also plan continued work on symmetry and stability aspects of colliding shells and pellet core dynamics but work in these areas will continue to receive low priority during the next year relative to our efforts on the ablation layer Rayleigh-Taylor modes and the material interface problems mentioned above. This is true for two reasons. First, the conditions which exist in the collision of two shells or the core collapse and void closure depend in a causal way on what goes on before. Not only the level of asymmetry and R-T mode amplitudes, but the dynamically evolving equilbria themselves also depend on the dynamics and stability of the ablator, the driver and/or the pusher shells. Second, our overall level of effort does not warrent concentrated effort on all aspects of Rayleigh-Taylor instability simultaneously. Nevertheless some work in these two areas is projected. The first step is to find meaningful one-dimensional equilibria. SHLINT and our implicit hydrodynamics code ADINC, described above, will be used to zero in on dynamic equilibria in colliding shells. FAST1D, our one-dimensional FCT shock code will be used to assess core density and temperature profiles. Simple calculations of the general type described earlier should be sufficiently well developed by the

end of the year to allow piggyback calculations of R-T modes in colliding shells. Our modest development program for the 2D Lagrangian and Eulerian simulation codes during this year should put us in position to perform a few useful simulations of void closure asymmetry (FAST2D) and growth of perturbations in shell collision (SPLISH) shortly thereafter.

RECENT NRL CONTRIBUTIONS TO INERTIAL CONFINEMENT FUSION THEORY

Publications and Reports

D.G. Colombant, et al., "Laser Target Model", *Physics of Fluids* **18**, 1687 (1975).

B.H. Ripin et al., "X-ray Emission Spectra from High Power Laser Produced Plasmas," *Phys. Rev. Letters* **34**, 1313 (1975).

D. Mosher, "Interaction of Relativistic Electron Beams with Fusion Target Blow-Off Plasmas," *Phys. Rev. Letters* **35**, No. 13, 1975.

D. Mosher and I.B. Berstein, "A diffusion Theory for the Interaction of Relativistic Electron Beams with Fusion Target Blow-Off Plasmas," *Proc. 7th Europ. Conf. on Controlled Fusion and Plasma Phys.* 1, Lausanne, Switz. (1975).

D. Mosher, "Ion-Stopping Power of Ionized Media," and "Current Neutralization in Beams Traversing Gas Backgrounds," in the report of the ERDA Summer Study of Heavy Ions for inertial Fusion, published by Lawrence Berkeley Lab. as LBL-5543, Dec. 1976.

D. Mosher, S.J. Stephanakis, G. Cooperstein and S. Goldstein, "Production of Intense Proton Beams in Pinched-Electron-Beam Diodes," *Phys. Rev. Lett.* 37, p. 1543, 1976.

J. Boris, "Dynamic Stabilization of the Imploding-Shell Rayleigh-Taylor Instability," *Comments on Plasma Physics and Controlled Fusion, Vol. 3, No. 1,* pp. 1-13, 1977. See also NRL Memorandum Report 3427, Dec. 1976.

D.G. Colombant and N.K. Winsor "Fast Ion Transport in Laser-Produced Plasmas", NRL Memorandum Report 3393 (1976)

D.G. Colombant, D.A. Tidman and N.K. Winsor "Magnetic Fields Due to Impurity Grains in Laser-Produced Plasmas", *App. Phys. Lett.* **29**, p. 401, (1976)

I. Haber, A.W. Maschke, "Saturation of Space-Charge Driven Instabilities in Beam Transport," Proceedings of the Heavy Ion Fusion Workshop, BNL 50769, Brookhaven National Laboratory, Oct. 1977

D.G. Colombant and N.K. Winsor, "Thermal Force Terms and Self-Generated Magnetic Fields in Laser-Produced Plasmas," *Phys. Rev. Lett.* 38, p. 697 (1977)

F.S. Felber, "Rayleigh-Taylor Instability in a Layered Laser-Driven Target," submitted to *Physics of Fluids*, July 1977.

J.P. Boris, "Dynamic Stabilization of the Rayleigh-Taylor Instability on the Surface of Imploding Pellets," invited paper, *B.A.P.S.* 22(4), p. 608, paper HD2, April 1977.

D. Colombant and D. Tidman, "Suprathermal Electrons and Peak Magnetic Fields," NRL Memorandum Report 3527 (1977).

W.M. Manheimer, D.G. Colombant and B.H. Ripin, "Efficient Laser Light Absorption by Ion Acoustic Fluctuations," Naval Research Laboratory Memorandum Report 3426, Dec. 1976,; *Phys. Rev. Letters* 38, p. 1135, (1977).

W. M. Manheimer, C. Max, J. Thompson, "Cross Field Thermal Transport Due to Ion Acoustic Waves in Magnetized Laser Plasmas, Naval Research Laboratory Memorandum Report 3593, submitted to *Physics of Fluids*.

F.S. Felber and S.E. Bodner, "Some Rayleigh-Taylor Stabilization Mechanisms in Thin Laser Targets," Naval Research Laboratory Memorandum Report Aug. 1977.

D. Mosher, G. Cooperstein, S.J. Stephanakis, S.A. Goldstein, D.C. Colombant, and R. Lee, Proc. 2nd International Topical Conf. on High-Power Electron and Ion Beam Research and Technology, Oct. 3-5, 1977, Ithaca, N.Y. Also NRL Memorandum Rpt. 3658, 1977.

P.J. Ottinger and D. Mosher, in Proceedings of the Heavy Ion Fusion Workshop, Brookhaven

National Laboratory, Upton, New York (1977).

W.M. Manheimer, "Energy Flux Limitation by Ion Acoustic Turbulence in Laser Fusion Schemes," *Physics of Fluids* **20**, 265 (1977).

D. Mosher and I.B. Berstein, "Magnetic Enhancement of Relativistic Electron-Beam Deposition," *Phys. Rev. Letters* **38**, 1483 (1977)

D.G. Colombant and D. Mosher, "Two-Dimensional Fluid Simulation of Relativistic Electron Beam — High Z Target Interactions," NRL Memorandum Report 3496, 1977.

F.S. Felber, "Steady-State Model of a Flat Laser-Driven Target," *Phys. Rev. Lett* **39(2)**, p. 84, 11 July 1977.

J. Davis and K. Whitney, *J.A.P. 47 (4)*, April 1976; J. Apruzese and J. Davis, NRL Memorandum Report 3277, May 1976; J. Apruzese, J. Davis, and K. Whitney, "The Importance of Photo Excitation to the Ionization Dynamics of a Laser-Produced Carbon Plasma", *J.A.P. 48(2)*, Feb. 1978.

S.E. Bodner, et. al., "Inertial Confinement Fusion at NRL", 23-30, August 1978, Innsbruck, Austria, IAEA-CN-37-B3.

D.L. Book, "Acoustic Amplification in Imploding Sperical Shells," (to be published in *Phys. Rev. Letters* (1978).

D.L. Book, "Linear Stability in Self Similar Flow: 3. Compressional Waves in Imploding Spherical Shells," NRL Memorandum Report 3799, 1978.

I. Haber and A.W. Maschke, "Steady State Transport of High Current Beams in a Focussed Channel," NRL Memorandum Report 3787, May 1978.

P.F. Ottinger, D. Mosher, S. Goldstein, "Microstability of a Focused Ion Beam Propagating

through a Z-Pinch Plasma," NRL Memorandum Report 3784, June, 1978. to be published in *Physics of Fluids*.

P.F. Ottinger, D. Mosher, and S.A. Goldstein, accepted Phys. Fluids. Also NRL Memorandum Report 3784, 1978.

I. Haber, "Computer Simulation of Space Charge Effects in Accelerators" NRL Memorandum Report 3705, Jan. 1978.

W.M. Manheimer and D.G. Colombant, "Light Absorption by Ion Acoustic Turbulence in Laser-Produced Plasmas", *Physics of Fluids*, **21**, p. 1818 (1978).

D.G. Colombant and N.K. Winsor, "X-Ray Emission from CH_2 Laser-Produced Plasmas at 10^{16}W/cm^2", NRL Memorandum report to be published.

I. Haber, "Collisional Emittance Growth in the Particle Simulation of Focussed Beam Transport," NRL Memorandum Report 3817, July 1978.

I. Haber, L.J. Laslett and L. Smith, "Comparison of Instability Theory with Simulation Results," Proceedings of the Heavy Ion Fusion Workshop, Argonne IL, Sept. 1978, to be published.

I. Haber, "High Current Transport of Non K-V Distributions," Proceedings of the Heavy Ion Fusion Workshop, Argonne IL, Sept. 1978, to be published.

PAPERS PRESENTED AT THE 1977 PLASMA PHYSICS MEETING OF THE AMERICAN PHYSICAL SOCIETY (ATLANTA)

Computer Simulation of Space Charge Effects in the Transport of High Energy Ion Beams. **I. Haber, T.F. Godlove, Naval Research Laboratory, and A.W. Maschke, Brookhaven National Laboratory.**

Light Absorption by Ion Acoustic Turbulence in Laser-Produced Plasmas. **S.M. Manheimer and D.G. Colombant.**

Influence of Ionization Dynamics on Derived Temperature of Laser-Heated Carbon Plasmas. **J. Davis and K. Whitney and J. Apruzese, Science Applications, Inc., Arlington, Va.**

Density Diagnostics for Spherical Shells of Laser-Generated Plasmas, **K. Whitney and J. Apruzese, Science Applications, Inc., Arlington, Va., and J. Davis.**

Accelerative Stabilization of the Rayleigh-Taylor Instability in Inertial Fusion Pellets, **J.P. Boris.**

Analysis of the Rayleigh-Taylor Instability in an Ablation Layer, **J.H. Orens, S. Layson, and J.P. Boris.**

PAPERS SUBMITTED TO THE TOPICAL MEETING ON INERTIAL CONFINEMENT FUSION

February 7-9, 1978 (San Diego, California)

Computer Simulation of Space Charge Effects in the Transport of High Energy Ion Beams, **I. Haber, and A.W. Maschke, Brookhaven National Laboratory.**

Tame Turbulence in Laser Abosrption, **D.G. Colombant and W.M. Manheimer.**

Temperature and Density Diagnostics for Spherical Shells of Laser-Generated Plasmas, **J. Davis, K.G. Whitney and J.A. Apruzese.**

Rayleigh-Taylor Stability in the Pellet Ablation Layer, **J.P. Boris and J.H. Orens.**

D. Mosher, Shyke A. Goldstein, P.F. Ottinger and W.W. Hsing, presented at the Topical Meeting on Inertial Confinement Fusion, San Diego, Calif. (1978).

Other Talks and Presentations

M.J. Fritts, "Lagrangian Calculation of Transient Flows Using A Triangular Grid," 8th Conference on Numerical Simulation of Plasmas, Monterey, California, 28-30 June 1978, Conf.-780614, Session OA-1.

D. Mosher, D.G. Colombant, S.A. Goldstein and R. Lee, "Fluid Modeling of Neutralization in Ion Beams Traversing Plasma Backgrounds", IEEE Plasma Science Meeting, Monterey, California, May 1978. 1978 EEE catalogue no. 78Ch1357-3 NPS.

R. Lee and S.A. Goldstein, "The Pinch-Reflex Diode — A High Efficiency Ion Source," IEEE Plasma Science Meeting, Monterey, California, May 1978. 1978 EEE catalogue no. 78Ch1357-3 NPS.

S.A. Goldstein, D.P. Bacon, D. Mosher, G. Cooperstein, *Proceedings 2nd* Int'l Topical Conference on High Power Electron and Ion Beam Research and Technology, Cornell University, Ithaca, N.Y., p. 71 (1977).

F.L. Sandel, G. Cooperstein, S.A. Goldstein, and D. Mosher, 1978 IEEE Cat. No. 78Ch1357-3 NPS, p. 114.

G. Cooperstein, S.A. Goldstein, R. Lee, D. Mosher, P.F. Ottinger, and A. Sternlieb, 1978 IEEE Cat. No. CH1357-3 NPS p. 112.